

STM investigation of model systems for atomic and molecular scale electronics

Dissertation

to achieve the academic degree **Doktoringenieur (Dr.-Ing.)**

submitted at the
Technischen Universität Dresden
Faculty of Mechanical Science and Engineering

Frank Eisenhut
Born on: 19. May 1989 in Stendal

First referee: Prof. Dr. Gianaurelio Cuniberti
Second referee: Prof. Dr. Angelika Kühnle
Submitted on: 11. April 2019
Defended on: 11. July 2019



Abstract

In this thesis, I explore model systems for planar atomic and molecular scale electronics on surfaces. The nanoscale systems are experimentally investigated by combining scanning tunneling microscopy (STM) with atomic and molecular manipulation. Furthermore, the on-surface chemical synthesis of molecules, as well as the construction of atomic wires on selected surfaces is applied. Polycyclic aromatic hydrocarbon (PAH) molecules play a key role in this work, as they can provide the functionality of the molecular scale devices.

In the first part of this work, I investigate different PAH's on the Au(111) surface. The precursor molecules form supramolecular assemblies and the on-surface synthesis approach to obtain the desired molecular products is used. In particular, bisanthene molecules *via* a cyclodehydrogenation reaction and the non-alternant polyaromatic hydrocarbon diindenopyrene after a thermally induced debromination followed by selective ring-closure to form a five-membered ring are obtained.

An interesting surface for future applications is the passivated silicon Si(001)-(2x1):H. I prepare this surface and characterize the substrate. The surface has a band gap and molecules are electronically decoupled from the semiconducting substrate due to the passivation layer. Furthermore, atomic defects on this substrate, so called dangling bonds (DB's), have defined electronic states. I show that it is possible to produce DB-defects controllably by applying voltage pulses using the tip of the STM and achieve with this method atomic wires with DB's.

The third part of this thesis deals with the investigation of molecular structures on Si(001)-(2x1):H. I present the generation of hexacene by a surface assisted reduction. This result can be generalized for the generation of PAH's after deoxygenation on passivated silicon and can open new routes to design functional molecules on this substrate. Secondly, one-dimensional chains of acetylbiphenyl (ABP) molecules are explored. They interact *via* its π -stacked phenyl rings that are considered as conducting channel. Finally, I demonstrate that a single ABP molecule acts as a switch, as one can reversibly passivate and depassivate a single DB by a hydrogen transfer.

In the last part of this work, I test the new low-temperature four-probe STM located at

CEMES-CNRS in Toulouse. This machine is constructed for the development of molecular scale devices. For this purposes an atomic precision is needed for all the different tips at the same time and a high stability of this scanning probe microscope must be achieved. I perform a manipulation experiment of molecules to test the necessary sub-molecular precision. For that reason, supramolecular assemblies of ABP molecules on Au(111) are imaged and manipulated by any of the four tips using the lateral manipulation mode as well as by voltage pulses. The stability of the system is shown, as all tips of the four-probe STM work independently in parallel.

Kurzzusammenfassung

In dieser Arbeit untersuche ich Modellsysteme für planare atomare und molekulare Elektronik auf Oberflächen. Die Systeme auf der Nanoskala werden experimentell durch die Kombination aus Rastertunnelmikroskopie (RTM) und atomarer sowie molekularer Manipulation untersucht. Moleküle werden durch die oberflächenchemische Synthese generiert und atomare Drähte auf ausgewählten Oberflächen hergestellt. Polyzyklisch aromatische Kohlenwasserstoff (PAK) Moleküle spielen bei dieser Arbeit eine Schlüsselrolle, da sie die passiven und aktiven Elemente auf molekularem Maßstab darstellen können.

Im ersten Teil dieser Arbeit untersuche ich verschiedene PAK's auf der Au(111)-Oberfläche. Die Präkursoren bilden dabei supramolekulare Anordnungen und ich nutze die Oberflächensynthese, um die gewünschten molekulare Produkte zu erhalten. Im Speziellen habe ich Bisanthen-Moleküle über eine Zyklodehydrogenationsreaktion und das nicht-alternierende PAK Diindenopyren erzeugt. Dieses entsteht nach einer thermisch-induzierten Debromierung gefolgt von selektivem Ringschluss, sodass ein fünfgliedriger Ring gebildet wird.

Eine interessante Oberfläche für zukünftige Anwendungen ist das passivierte Silizium Si(001)-(2x1):H. Ich habe diese Oberfläche erfolgreich präpariert und das Substrat charakterisiert. Die Oberfläche hat eine Bandlücke und Moleküle sind elektronisch von dem halbleitenden Substrat durch die Passivierungsschicht entkoppelt. Desweiteren haben atomare Defekte dieser Oberfläche, sogenannte Dangling-Bond's (DB's), definierte elektronische Zustände innerhalb der Bandlücke. Ich habe DB's kontrolliert durch Spannungspulse mithilfe der Spitze des STM erzeugt und stelle so atomare Drähte mit DB-Defekten her.

Der dritte Teil dieser Arbeit befasst sich mit der Untersuchung molekularer Strukturen auf Si(001)-(2x1):H. Die Erzeugung von Hexacen auf passivierten Silizium durch eine oberflächenunterstützte Reduktion wird gezeigt. Dieses Ergebnis ist eine neue Strategie für die Herstellung von PAK's nach der Deoxygenierung und eröffnet neue Wege um funktionelle Moleküle auf diesem Substrat zu entwerfen. Zweitens zeige ich, dass Acetylbiphenyl (ABP) Moleküle eindimensionale Ketten auf dieser Oberfläche bilden.

Diese interagieren über ihre Phenylringe, welche als leitender Kanal gesehen werden können. Zudem kann ein einzelnes ABP Molekül wie ein Schalter genutzt werden, da es reversibel einzelne DB's durch Wasserstoffübertragung passivieren und depassivieren kann.

Im letzten Teil dieser Arbeit wird das neue Tieftemperatur Vier-Sonden RTM, welches sich in CEMES-CNRS in Toulouse befindet, getestet. Diese Maschine ist für die Herstellung und Untersuchung von Geräten im molekularem Maßstab konstruiert worden. Zu diesem Zweck ist eine atomare Präzision für die verschiedenen Spitzen zur gleichen Zeit erforderlich und eine hohe Stabilität des Rastersondenmikroskops muss gewährleistet sein. Ich führe ein Manipulationsversuch an Molekülen durch, um die notwendige submolekulare Präzision zu testen. Dafür werden supramolekulare Anordnungen von ABP-Molekülen auf Au(111) abgebildet und die Strukturen mit jeder der vier Spitzen im lateralen Manipulationsmodus und durch Spannungspulse bewegt. Damit habe ich die Stabilität des Systems getestet und konnte zeigen, dass alle Spitzen des Systems unabhängig voneinander parallel arbeiten.

Contents

1	Introduction	7
2	Fundamentals of scanning tunneling microscopy	9
2.1	The working principle	9
2.2	Scanning tunneling spectroscopy	12
2.3	Manipulation modes	13
2.4	Modeling	15
3	Experimental setup, materials and methods	17
3.1	The scanning tunneling microscope	17
3.2	The Au(111) surface	20
3.3	Further experimental details	22
4	On-surface synthesis of molecules	25
4.1	Introduction	25
4.2	Generation of a periacene	27
4.3	Investigating a non-alternant PAH	32
4.4	Conclusion	39
5	The passivated silicon surface	41
5.1	Introduction	41
5.2	Preparation of passivated silicon	42
5.3	Characterization of Si(001)-(2x1):H	46
5.4	Tip-induced formation of dangling bonds	50
5.5	Conclusion	55
6	Organic molecules on passivated silicon	57
6.1	Introduction	57
6.2	Hexacene generated on passivated silicon	58
6.3	Acetylbiphenyl on passivated silicon	65

6.4	Conclusion	71
7	Testing a low temperature four-probe STM	73
7.1	Introduction	73
7.2	The four-probe STM	75
7.3	Performance test of the four-probe STM on Au(111)	77
7.4	Manipulation of ABP assemblies	80
7.5	Conclusion	86
8	Summary and outlook	89
9	Appendix	93
9.1	Dibromo-dimethyl-naphtalene on Au(111)	93
9.2	Epiminotetracene on Au(111)	95
	Bibliography	97
	Curriculum vitae	121
	Scientific contributions	123
	Articles	123
	Talks	124
	Posters	125
	Outreach	126
	Acknowledgement	127
	Statement of authorship	129

List of figures

Figure 2.1	-The tunneling principle.	11
Figure 2.2	-The operation principle of an STM.	12
Figure 2.3	-Manipulation modes of an STM.	14
Figure 3.1	-Setup of the vacuum system.	19
Figure 3.2	-The STM scanner head.	20
Figure 3.3	-The Au(111) surface.	21
Figure 4.1	-On-surface synthesis approach for an unimolecular reaction.	26
Figure 4.2	-On-surface approach for the synthesis of a bisanthene-derivative.	28
Figure 4.3	-B ₂ Me ₄ Chr adsorbed on Au(111).	29
Figure 4.4	-Supramolecular assemblies of B ₂ Me ₄ Chr on Au(111).	30
Figure 4.5	-B ₂ Me ₄ Chr on Au(111) after annealing to 170 °C.	31
Figure 4.6	-Br ₂ Me ₄ Ph ₂ Py molecules adsorbed on Au(111).	33
Figure 4.7	-Self-assembled structures of Br ₂ Me ₄ Ph ₂ Py on Au(111).	34
Figure 4.8	-Debromination of Br ₂ Me ₄ Ph ₂ Py molecules on Au(111).	35
Figure 4.9	-Images after annealing the sample to 160 °C for 5 min.	36
Figure 4.10	-Imaging of single DIP molecules adsorbed on Au(111).	37
Figure 4.11	-Spectroscopic measurement of single DIP molecules.	38
Figure 5.1	-Scheme of the production of a DB-wire on Si(001)-(2x1):H.	42
Figure 5.2	-In-situ preparation of Si(001)-(2x1):H in UHV.	44
Figure 5.3	-Packaged passivated silicon surfaces.	45
Figure 5.4	-Overview STM images of passivated silicon Si(001)-(2x1):H.	46
Figure 5.5	-Defect-free Si(001)-(2x1):H.	48
Figure 5.6	-Predominant defects on the prepared passivated silicon surface.	49

Figure 5.7	-I-z spectroscopy on top of a hydrogen atom on Si(001)-(2x1):H.	50
Figure 5.8	-Tip-induced dangling bond production.	51
Figure 5.9	-Erasing of dangling bonds using a hydrogenated tip.	53
Figure 5.10	-Electronic structure of DB's on passivated silicon.	54
Figure 5.11	-Creation of long dangling bond wires on Si(001)-(2x1):H.	55
Figure 6.1	-Organic molecules on passivated silicon.	58
Figure 6.2	-Overview image of the surface after the different preparation steps.	59
Figure 6.3	-The precursor HnO ₃ and the intermediate HnO ₂ on Si(001)-(2x1):H.	60
Figure 6.4	-Hexacene on passivated silicon.	61
Figure 6.5	-Hexacene interacting with a single DB on Si(001)-(2x1):H.	63
Figure 6.6	-Hexacene detached from a DB-defect.	64
Figure 6.7	-Scanning tunneling spectroscopy of hexacene.	65
Figure 6.8	-Acetylbiphenyl on passivated silicon.	66
Figure 6.9	-Isolated ABP on passivated silicon.	67
Figure 6.10	-ABP chains grown on Si(001)-(2x1):H.	68
Figure 6.11	-Adsorption and switching of ABP on Si(001)-(2x1):H.	70
Figure 7.1	-Scheme of a proposed setup of an interconnection machine.	74
Figure 7.2	-Setup of the vacuum system of the LT-UHV four-probe STM.	75
Figure 7.3	-The head of the four-probe STM	76
Figure 7.4	-The tips of the four-probe STM.	79
Figure 7.5	-The Au(111) surface measured on the four-probe STM.	80
Figure 7.6	-Supramolecular assemblies of ABP after sublimation.	81
Figure 7.7	-Lateral manipulation of selected supramolecular assemblies.	82
Figure 7.8	-Typical events of motion after voltage pulses on ABP assemblies.	84
Figure 7.9	-Reorganization of a supramolecular assembly.	85
Figure 8.1	-Graphical summary of the experimental results.	89
Figure 9.1	-Dibromo-dimethyl-naphtalene on Au(111) before annealing.	93
Figure 9.2	-Dibromo-dimethyl-naphtalene on Au(111) after annealing to 120 °C.	94
Figure 9.3	-The molecule Tn(NCH ₃) ₂ on Au(111).	95

List of abbreviations

ABP	Acetylbiphenyl
Ar⁺	Argon-ion
B₂Me₄Chr	Dibenzo-tetramethyl-chrysene
Br₂Me₄Ph₂Py	Bis(bromo-methylphenyl)-dimethylpyrene
CMOS	Complementary metal-oxide-semiconductor
CO	Carbon monoxide
DB	Dangling bond
DFT	Density functional theory
DIP	Diindenopyrene
fcc	Face-centered cubic
FFT	Fast-fourier transformation
H	Atomic hydrogen
H₂	Molecular hydrogen
hcp	Hexagonal close-packed
He	Helium
HnO₂	Diepoxyhexacene
HnO₃	Triepoxyhexacene
HOMO	Highest occupied molecular orbital
HOMO-1	Second highest occupied molecular orbital
LT	Low temperature
LUMO	Lowest unoccupied molecular orbital
LUMO+1	Second lowest unoccupied molecular orbital
MD	Molecular dynamics

N₂	Nitrogen
PAH	Polycyclic aromatic hydrocarbon
SEM	Scanning electron microscopy
STM	Scanning tunneling microscopy
STS	Scanning tunneling spectroscopy
TEMPO	Tetramethylpiperidinyloxy
Tn(NCH₃)₂	Diethylaminotetracene
UHV	Ultrahigh vacuum

1 Introduction

Microelectronics has a huge impact in our every day's life. It influences almost every human activity, not only the information and communication technology, but also science, sports, music, health, safety, or even the wellness sectors. This implies that more and more transistor-based electronics is used, with a trend towards miniaturization of the components. The rate of the miniaturization is predicted by Moore's law. According to that law the number of transistors on an area doubles at least every 24 month [1]. In 2017, IBM demonstrated that it is possible to produce a transistors with a size down to 5 nm using extreme ultraviolet lithography [2]. However, the transistor size is reaching its limitation and the miniaturization started to stagnate within the last decade. A further reduction of the size does not only requires great technological effort, but can also lead to short channel effects within the device [3].

Therefore, new approaches and technologies are required to overcome the size barriers of conventional complementary metal-oxide-semiconductor (CMOS) devices [4]. As the complete replacement of the CMOS devices is improbable, a possible scenario is the implementation of molecular electronics in addition to the proven technology, which would be called hybrid molecular electronics [3]. Concepts to use single molecules as active elements have been already proposed in the 70's of the last century, where researchers showed that a single molecule act as a rectifier [5]. Following this approach, molecules can function as active or passive elements, like rectifiers, switches, diodes or wires [6–13]. For the realization of these devices, standard lithographic methods cannot be used, as the resolution of the top-down produced structures is limited. Hence, functional molecules or highly organized molecular structures need to be achieved in a bottom-up approach using smart designed precursor molecules on surfaces [14–16]. In particular, complex molecules, that cannot be obtained in solution, can be synthesized on-surface. These molecules could for example act as single molecular logic gate with atomic inputs [17, 18].

The concept of molecular electronics has been accompanied by the development of scanning tunneling microscopy (STM). STM is an important tool that can image surfaces, atoms and molecules with sub-molecular precision [19, 20]. In addition, in ultrahigh

vacuum (UHV) conditions at low temperatures (LT) STM allows to manipulate single nano-objects and to investigate their electronic properties. The possibility of manipulating single atoms with the STM enables one to use the tip for the construction of structures on the surface and thus it provides a new lithography method at the atomic scale [21]. Therefore, STM is suitable for studying systems that can be used for molecular electronics. A possible further experimental technique to investigate nanoscale devices is the multi-probe LT-UHV STM, which represents the next generation of tools in this field.

This thesis is structured in the following way. Chapters 2 and 3 are introducing method and experimental details used during this thesis. In the chapters 4 till 7, the obtained experimental results are presented. In particular, chapter 2 explains the fundamentals of scanning tunneling microscopy (STM) and spectroscopy (STS) that are important methods for the investigation of surface structures and molecular materials. The experimental setup as well as the methods used in this work are described in chapter 3.

Chapter 4 is devoted to the investigation of different PAH's on the Au(111) surface. These precursors likely form supramolecular assemblies on this surface. The on-surface synthesis approach has been used to obtain desired molecules and the electronic properties of these products are investigated by using STS. Special attention is paid to the influence of the structure of the molecules to their properties. Further on-surface reactions are described in the appendix of this thesis.

Chapter 5 deals with the passivated silicon Si(001)-(2x1):H, which constitutes an appropriate substrate for hybrid electronic systems. I describe different preparation methods and the characterization of the surface, as well as the fabrication of atomic structures. The interest lies here in the preparation of a defect free surface and in the possibility to produce atomic structures with highest precision.

Chapter 6 describes the interaction of organic molecules with the passivated silicon surface. The aim of the chapter is to obtain molecules with designed properties that can function as electronic components. Thereby, one experiment is devoted to new strategies for the generation of PAH's on this surface and furthermore, the interaction with surface defects is explored. The adsorption of a second molecule, acetylbiphenyl, has been investigated. This molecule forms one-dimensional chains after assembling and a single molecule can switch a dangling bond.

In the last part of my work (chapter 7), I described the testing phase of a new low-temperature four-probe STM at CEMES-CNRS in Toulouse. I investigated the stability of each scanner on the Au(111) surface and performed manipulation experiments, to demonstrate a sub-molecular precision.

2 Fundamentals of scanning tunneling microscopy

In this chapter, I will focus on the main principles of scanning tunneling microscopy and spectroscopy. Furthermore, I will explain how the STM tip can be used as a tool for the manipulation of single molecules and will shortly describe the different modes of manipulation. Finally, I will present the theoretical methods used to describe molecules adsorbed on surfaces.

2.1 The working principle

Scanning tunneling microscopy is an experimental technique based on the quantum phenomenon of tunneling and was invented in 1981 by G. Binnig and H. Rohrer at IBM [19, 20, 22]. At that time, this technique opened a complete new field for studying the structure of matter in real space and the inventors were awarded with the Nobel prize only five years after in 1986.

To describe the tunneling effect, the simple model of tunneling through a one-dimensional finite barrier is presented in Fig. 2.1 a. In classical physics, an electron would not be able to pass over this barrier. However, as an electron can be considered as a quantum object with wavelike properties (region I and III), the transmission probability of an electron decreases exponentially within a finite barrier (region II). This effect is referred to as tunneling. The potential energy depends on the work functions Φ of tip and substrate, as presented in Fig. 2.1 b. When applying a small bias voltage between the two electrodes, a net current is flowing through the barrier (Figs. 2.1 c and d). The transmission coefficient, which means the probability of an electron to tunnel from region I to III, can be determined by solving a time-independent Schrödinger equation [23, 24].

In a first approximation, the transmission coefficient can be directly related to the tunneling current resulting in:

$$I \propto e^{-2\kappa d} \text{ with } \kappa = \frac{\sqrt{2m\phi}}{\hbar}, \quad (2.1)$$

where m is the mass of an electron, Φ the average work function of the two electrodes and \hbar the reduced Planck constant.

Bardeen developed a theory based on time dependent perturbation and Fermi's golden rule [25], obtaining the following expression for the tunneling current:

$$I = -\frac{4\pi e}{\hbar} \int_{-eV}^0 |M|^2 \rho_t(\epsilon) \rho_s(\epsilon + eV) (f(\epsilon) - f(\epsilon + eV)) d\epsilon, \quad (2.2)$$

where ρ is the density of states for tip and sample, M is the tunneling matrix and f is the Fermi-distribution of the electron energy.

Eq. (2.2) can be further simplified assuming that the tunneling matrix reflects the probability of the electron to tunnel from one electrode to another (from region I to region III in Fig. 2.1 a). Thus, the tunneling matrix M can be approximated as the exponential function presented in Eq. (2.1). Furthermore, as the tip is supposed to be a clean metal tip, its density of states is considered to be flat around the Fermi-energy and can be assumed to be constant. This reduces the complexity to

$$I = -\frac{4\pi e}{\hbar} e^{-2\kappa d} \rho_t(0) \int_{-eV}^0 \rho_s(\epsilon + eV) (f(\epsilon) - f(\epsilon + eV)) d\epsilon. \quad (2.3)$$

This equation reveals that the current is not only exponentially dependent on the tip-surface distance, but is also dependent on the integral of the density of states of the sample. As the Fermi-function has a sharp cutoff close to the Fermi-energy at low temperatures, an energy window is provided at that the electrons can tunnel elastically from the occupied state of one electrode to the unoccupied state of the other one.

This is shown in Figs. 2.1 c and 2.1 d. In Fig. 2.1 c a small positive bias is applied to the surface, resulting in the lowering of the Fermi-energy of the sample. Thus, the electrons tunnel into the unoccupied states of the sample. When applying a negative bias to the sample as shown in Fig. 2.1 d, it is vice versa and the occupied states of the sample is probed.

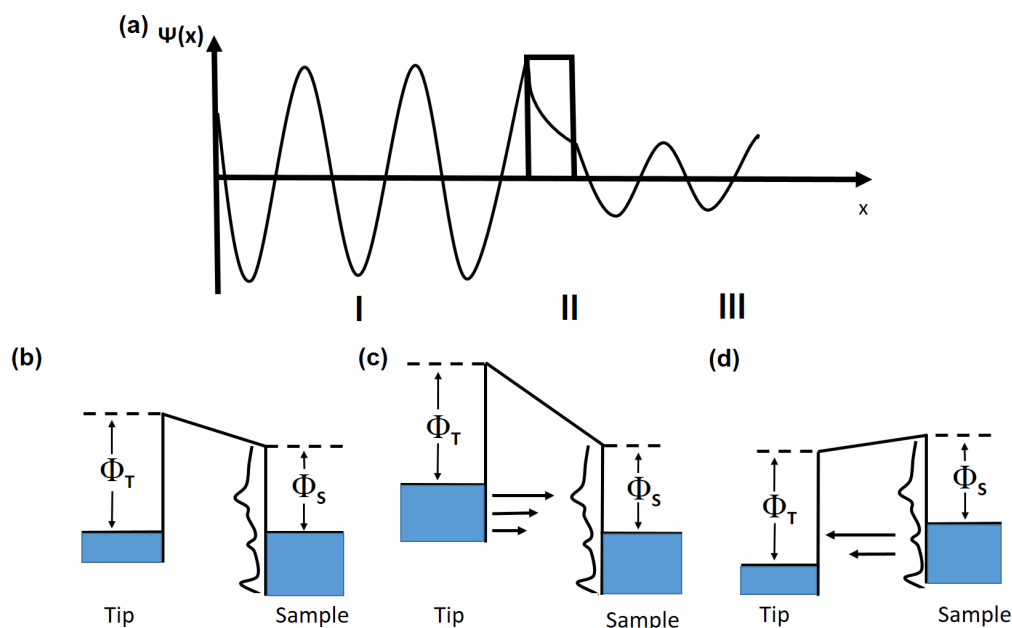


Figure 2.1 – The tunneling principle. (a) An electron tunneling through a one-dimensional finite barrier. (b)-(d) Energy diagrams of tunneling between a tip and a sample in the STM junction. In (b) no bias is applied to the sample. In (c) a small positive bias is applied to the sample, which results in lowering of its Fermi-level and thus tunneling from occupied states of a tip into unoccupied states of a sample. In (d) a small negative bias is applied to the sample, which results in increasing of the Fermi-level and thus tunneling from occupied states of the sample into the unoccupied states of the tip.

Scanning tunneling microscopy is based on these theoretical considerations. Its working principle is presented in Fig. 2.2 a. After approaching the tip to the surface to about 5 – 10 Å and applying a small voltage, a finite tunneling current in the range of 1 pA to 1 nA can be detected. Every irregularity of the surface has a huge influence on the current, as the current is exponentially dependent on the tip-surface distance. However, as shown in Eq. (2.3) the current depends also on the density of states of the sample.

When the constant-current mode is chosen (Fig. 2.2 b), a feedback-loop regulates the tip height, which is in this case the observable. The feedback-loop controls the current during scanning and retracts or advances the tip towards the surface when, for example, a step edge is approached. Piezoelectric actuators control the movement of the tip, while a computer records the signal.

The second possible measurement mode is the constant height mode. In this case, the observable is the measured current. No feedback-loop regulates the tip height during this measurement. However, the surface corrugation should be known before the measurement, as the tip can easily crash into the surface at steps or into molecular islands. Thus, in this thesis the constant height mode is only employed during high-resolution imaging of a single molecule with a CO-functionalized tip [26].

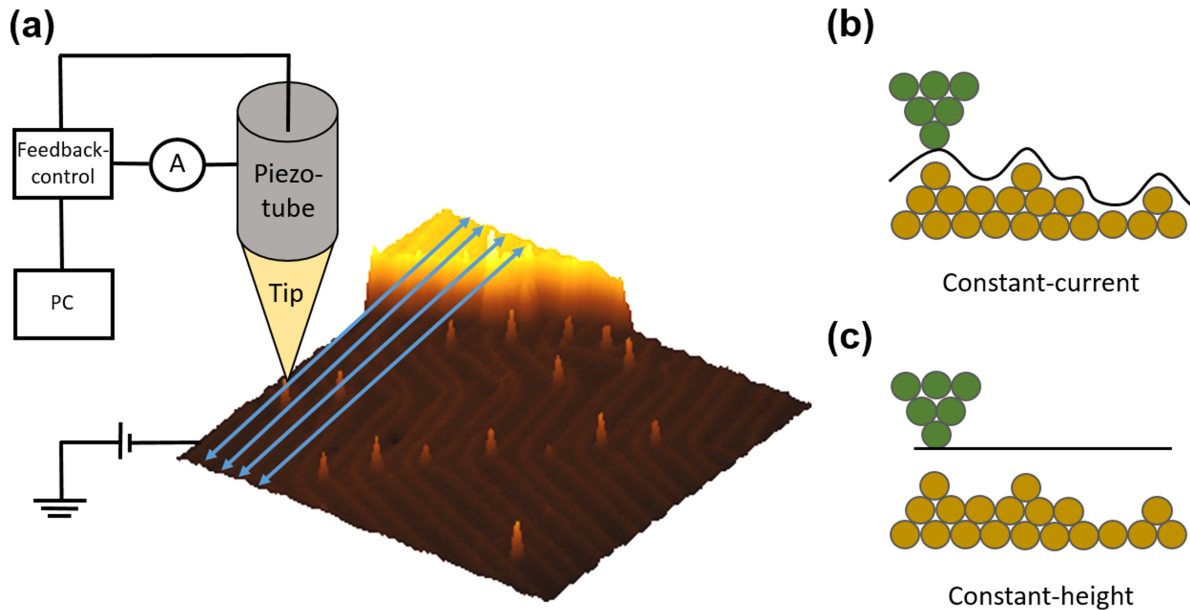


Figure 2.2 – The operation principle of an STM. (a) In the scheme, the tip is moved over the surface. In our setup, a voltage is applied towards the sample, while the current is measured at the tip. A feedback-loop regulates the tip height to achieve the set-point current. The tip height is displayed on the PC. This measurement principle is used in the so-called constant-current mode as displayed in (b). As a second possibility, the tip height can be kept constant, while the current is measured as presented in (c).

2.2 Scanning tunneling spectroscopy

As already discussed in the previous section (Eq. 2.3), the scanning tunneling microscope does not only provide the capability to image surfaces, but also to record the density of states of the sample. Thus, we can use scanning tunneling spectroscopy to identify resonant states of a molecular system. The differential conductance, that is proportional to the density of states of the system, is obtained by the derivative of the current with respect to the voltage [27]. It follows from Eq. (2.3) that:

$$\frac{dI}{dV} = -\frac{4\pi e^2}{\hbar} e^{-2\kappa d} \rho_t(0) \int_{-eV}^0 \rho_s(\epsilon + eV) \frac{\partial f}{\partial \epsilon} \Big|_{\epsilon=0} d\epsilon. \quad (2.4)$$

$\partial f/\partial \epsilon$ is a bell-curve function at $k_B T$, which explains that even at low temperatures the density of states is slightly broadened. The differential conductance dI/dV depends directly on the density of states of the sample.

Experimentally, STS measurements are realized in the following way. The tip is stabilized at the point of interest with a certain tip height (defined by the set point parameters current and voltage). The feedback-loop is then disabled and the bias is swept in the voltage range of interest. To obtain the first derivative of the current a lock-in detection

technique is used. The tunneling current can be then expressed in a Taylor series around the applied bias voltage:

$$I(V) = I(V_0 + V_{mod}\sin(\omega t)) = I(V_0) + \frac{dI(V_0)}{dV}V_{mod}\sin(\omega t) + \frac{d^2I(V_0)}{dV^2}V_{mod}^2\sin^2(\omega t) + \dots \quad (2.5)$$

The higher terms have a shorter periodicity in time, while the second term describes the current modulation with the frequency ω . As the lock-in amplifier is acting as a band-pass for the set frequency and the first term describes only the measured current of the unmodified signal, the current is proportional to the differential conductance dI/dV and can be directly detected with this technique.

The advantage of this technique is that the spectroscopic information can be well-resolved in the sub-nanometer regime. Despite the possibility of determining the resonances at a certain position above the sample, the spatial distribution of a resonance can be imaged by the so-called dI/dV -mapping. Thereby the area of interest is imaged at the bias voltage of interest (at the energy of a resonance). During this measurement, the modulation of the bias voltage is turned on and not only the topographical information, but also the dI/dV -signal is obtained at each point.

2.3 Manipulation modes

STM does not only allow to image conducting surfaces and molecular adsorbates with high spatial resolution, but provides a nanoscale probe able to manipulate matter at the atomic scale [21]. The STM tip can be used to induce chemical reactions [28, 29], to translate [30], rotate [31], and switch single molecules [7, 32], or to drive nanocars [33–35]. The different manipulation methods are presented in Fig. 2.3.

The first manipulation mode is the lateral manipulation mode and involves atomic forces that lead to the displacement of single adsorbates. Such forces are van-der-Waals forces and can be either repulsive or attractive. The tip is brought in close contact with the surface, which means that the tip-surface distance is in the range of 3-5 Å. The parameters usually used for moving a molecule are in the range of 1 nA and 10 mV ($R=10 \text{ M}\Omega$), while for moving a gold-atom 10 nA and 10 mV ($R=1 \text{ M}\Omega$) must be applied. It is important to note that for each system the parameters must be new adjusted, as it also can happen that instead of laterally move the molecule, one picks it up with the tip due to strong molecule-tip interactions. Different lateral manipulation modes are the pushing

mode, the pulling mode and the sliding mode [30]. Thereby the pushing mode involves repulsive interactions, while the pulling and the sliding mode involves attractive interactions.

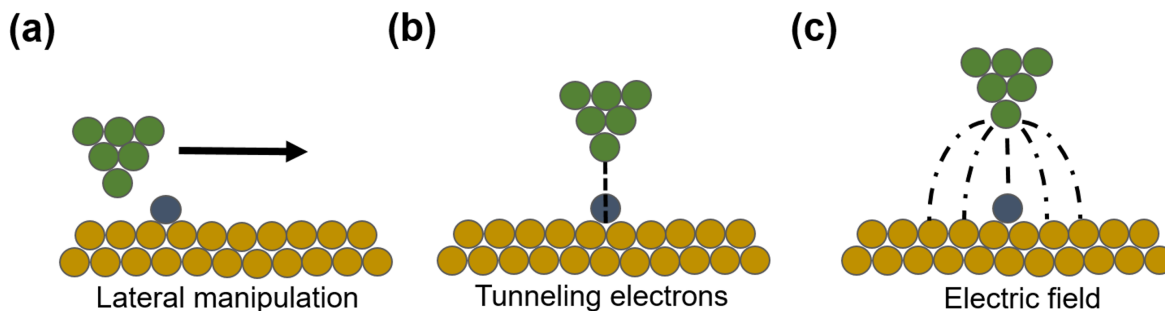


Figure 2.3 – Manipulation modes of an STM. (a) The tip-surface distance is reduced drastically during lateral manipulation. Consequently, the interaction between tip and object to be manipulated increases and the object can be moved. (b) Another option is to use tunneling electrons coming from the tip that have a certain energy. Thereby some objects can be excited and manipulated. (c) For some cases, the manipulation of an object can be triggered by an electric field that is applied.

While in the lateral manipulation mode the molecule-tip interaction is high due to the close distance between tip and adsorbate, there exist further possibilities of manipulating molecules and adsorbates with the STM at a larger tip-surface distance. In Fig. 2.3 b the use of tunneling electrons is shown. Inelastic tunneling electrons excite the molecule and can lead to its movement [34]. In the case of tunneling into resonances, the adsorbate undergoes an electronic transition into an excited state. During relaxation the adsorbate can dissipate the energy by hopping to another position on the lattice. Furthermore, it is possible that inelastic tunneling electrons vibrationally excite an adsorbate resulting in movement at voltages that are lower than the energy of the electronic resonance [35, 36]. As a third possibility, the excitation of a molecule *via* an electric field has been shown (Fig. 2.3 c). Due to the small distance between tip and surface, the electric field generated at the position of an adsorbate is huge (in the range 10^7 V/cm). If an adsorbate has a dipole moment within its molecular skeleton it can be moved by the electrostatic interaction or a conformational change can be induced [37]. Experimentally, a purely electric field origin of the motion can be proven by retracting the tip until it is completely out of the tunneling regime and to apply a voltage to obtain the same field strength, which would result in the same behavior of the adsorbate as before.

2.4 Modeling

The interpretation of the experimental STM data concerning the adsorption of molecules on surfaces can be enormously improved by using theoretical modeling. Thus, in this work the adsorption geometry of the relevant molecules on different surfaces have been achieved in collaboration with theory groups. The adsorption geometries were obtained with two different methods. Calculations using density functional theory (DFT) were performed by Seddigheh Nikipar and Thomas Lehmann under supervision of Dr. Dmitry A. Ryndyk, while molecular dynamics simulations were fulfilled by Dr. Xavier Bouju. DFT is a widely applicable general method to derive the properties of a many-body system in the ground state [38]. Based on a theorem from P. Hohenberg and W. Kohn [39], the electron density of interacting electrons determines the potential. The total ground state energy E_{tot} of the system of electrons and ions can be expressed as functional of the system [40]. The energy that must be minimized includes five terms: kinetic energy of the electrons, electron-ion energy, electron-electron Coulomb energy, exchange-correlation energy, and the classical electrostatic repulsion energy between the ions.

In practice, the ground state is obtained by solving in a self-consistent cycle the Kohn-Sham equations [41]. The adsorption geometry of the molecules is determined in this case by DFT calculations implemented in the quickstep code of CP2K [42]. The exchange-correlation is based on the Perdew-Burke-Ernzerhof functional [43]. The Au(111) surface is modeled by a periodic slab of six layers, while the Si(001)-(2x1):H substrate is modeled with boundary conditions representing an infinite passivated silicon surface, respectively and the three bottom layers being fixed at their bulk position during relaxation. The preferred adsorption geometries can be obtained by exploring the potential energy surface for several initial positions.

In contrast, molecular dynamics (MD) simulations are used when the size of a system is too large to be treated fully with quantum methods. Thereby the potential energy that must be minimized consists of bonded- and non-bonded terms. In the Universal Force Field that is used here, the total energy must be minimized and is a set of hybridization dependent atomic bond radii, a set of hybridization angles, van-der-Waals parameters, torsional and inversion barriers, and a set of effective nuclear charges [44]. Hence, the preferred adsorption geometry can be obtained after optimization of the substrate with the corresponding molecule.

3 Experimental setup, materials and methods

In this chapter, I will describe the vacuum system and the design of the STM that I used during the experiments performed in the main parts of my PhD thesis. Furthermore, I will give an insight into the Au(111) surface that I used as substrate (chapters 4 and 7). Finally, I will describe further experimental details important for this work.

3.1 The scanning tunneling microscope

The microscope described in the next section has been used in the experiments described in chapters 4, 5 and 6. The scanning tunneling microscope is a commercially available machine from the company Createc and can be seen in Fig. 3.1 a [45]. For single molecule investigations, the substrate must be hold in UHV, and at a temperature of 5 K (liquid He). The vacuum system is shown in Fig. 3.1 b. It consists of three vacuum chambers that can be separated from each other by metal valves. The first chamber is the load lock, which is evacuated *via* a turbomolecular pump. A combined ion-getter with a titanium-sublimation pump holds the preparation chamber as well as the STM chamber at UHV conditions. Together with the large cryostat in the STM chamber that acts as a kind of “cryo-pump”, the pump system enables us to achieve a pressure in the range of 10^{-10} mbar to 10^{-11} mbar. Hot-filament ionization gauges installed in each chamber can monitor the pressure.

The load lock chamber is used for a fast transfer of samples into the vacuum system and for differentially pumping the molecule evaporator, the manipulator and gas lines. All inserted samples can be transferred with the transfer rod into the preparation chamber. In that chamber the sample can be grapped with the manipulator (see Fig. 3.1 b).

The manipulator is wired and can be connected to a sample. This enables us to heat the sample and to read out its temperature. Furthermore, it is equipped with a diode to read out the temperature of the manipulator and it can be cooled down with liquid gases.

Hence, it is the tool of choice for the preparation of any substrate within the chamber. A storage is implemented in the preparation chamber, which has space to store five samples and six STM-tips. In addition, the storage has a built-in filament to be able to prepare oxidized tungsten tips by electron-bombardment and a blade to open special designed samples that will be described in detail in chapter 5. For the preparation of samples, the chamber is equipped with a sputter gun, a hydrogen cracker, as well as with a Knudsen cell molecular evaporator. For analyzing the gas composition, a mass spectrometer is available.

The third chamber is the STM chamber that has a two-stage cryostat and enables us to cool down the STM to 5 K (see Fig. 3.1 c). The outer cryostat is filled with liquid nitrogen and has a volume of 18 l, while the inner one is filled with liquid helium and has a volume of 8.5 l. This results in a consumption of 100 ml/h liquid helium, so that the cooled-down time is about 80 h before the next refilling. A shutter decouples the chamber from the STM-head and must be opened for the transfer of a sample into the STM. The cabling for the electrical feedthrough of the STM is led through the cryostats. Furthermore, to transfer a sample from the preparation chamber to the STM, the scanner must be pulled down onto the sample support by using a push-pull mechanism.

This mechanism is also used for hanging the sample free that is then held only by three springs. This system allows a high mechanical vibrational damping of the setup. Further noise isolation is obtained by four pneumatic feet, an eddy current damping system, as well as by a special vibration-isolated floor.

The scanner head can be seen in Fig. 3.2 a and schematically in 3.2 b. It has the Besocke beetle-type design [45]. After hanging free the sample with the push-pull mechanism, it is directly attached to the U-block. To do the coarse approach the scanner has three outer piezoelectric tubes. On top of these tubes are sapphire balls glued. A ramp is placed on these three outer tubes. Slip-stick motion of the tubes enables the coarse approach of the tip towards the sample. This coarse motion is possible because the ramp is not flat, but is formed by three segments with a slight angle. The complete stroke of the coarse approach is about 0.6 mm. In the center of the ramp the inner piezoelectric tube is placed. This tube regulates the fine approach and the STM tip is held by magnets on this tube. The tunneling distance between the tip and the sample is in the range of 5-10 Å. For a reduction of the noise level, the inner piezoelectric tube is responsible for the vertical movement, while the three outer tubes regulate the motion in the x,y-plane.

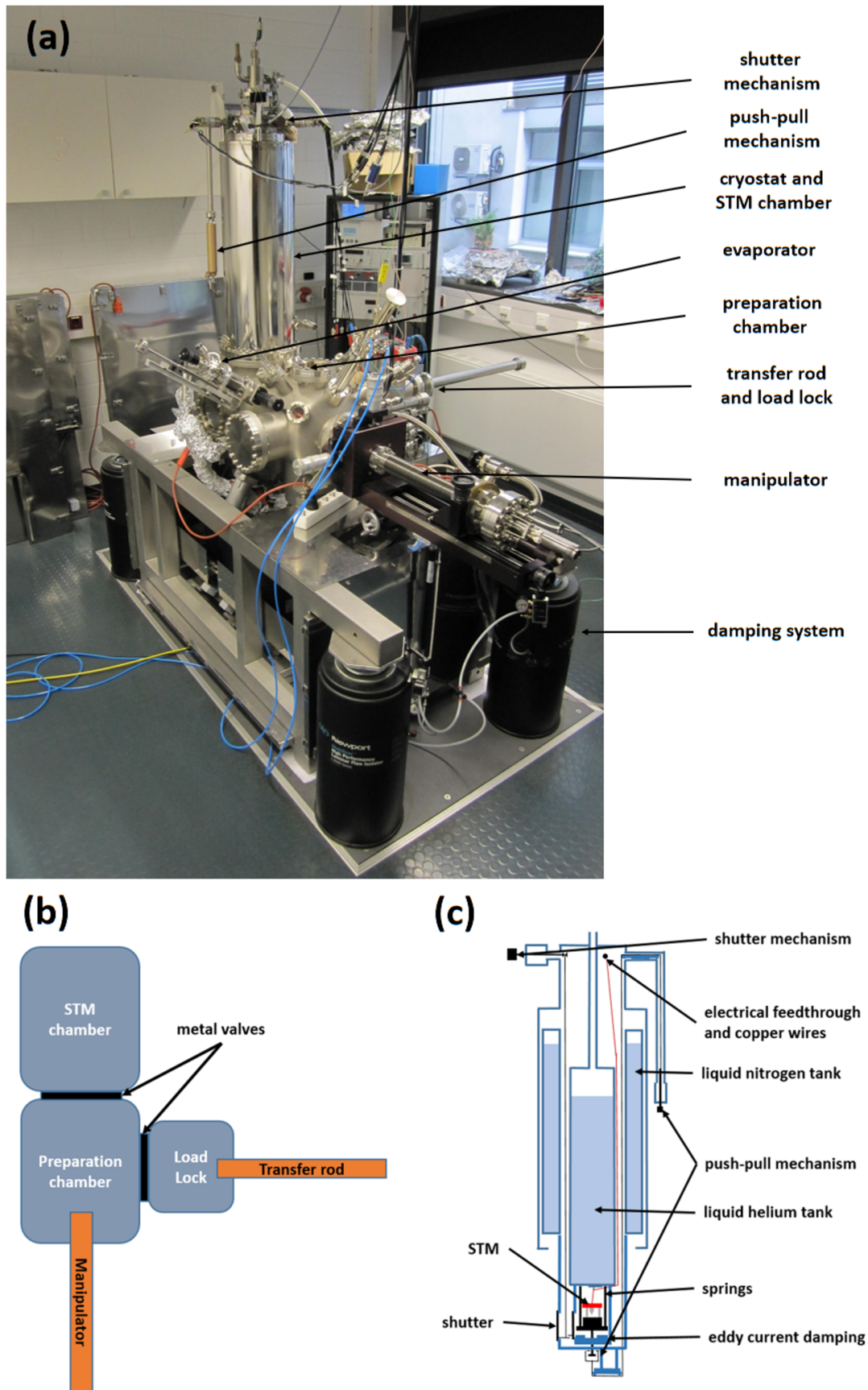


Figure 3.1 – Setup of the vacuum system. (a) Picture of the UHV system used during the work at the TU Dresden. (b) Corresponding scheme of the UHV system showing the three chambers: Load lock, preparation chamber and STM chamber. (c) A scheme of the setup of the cryostat with the STM head inside.

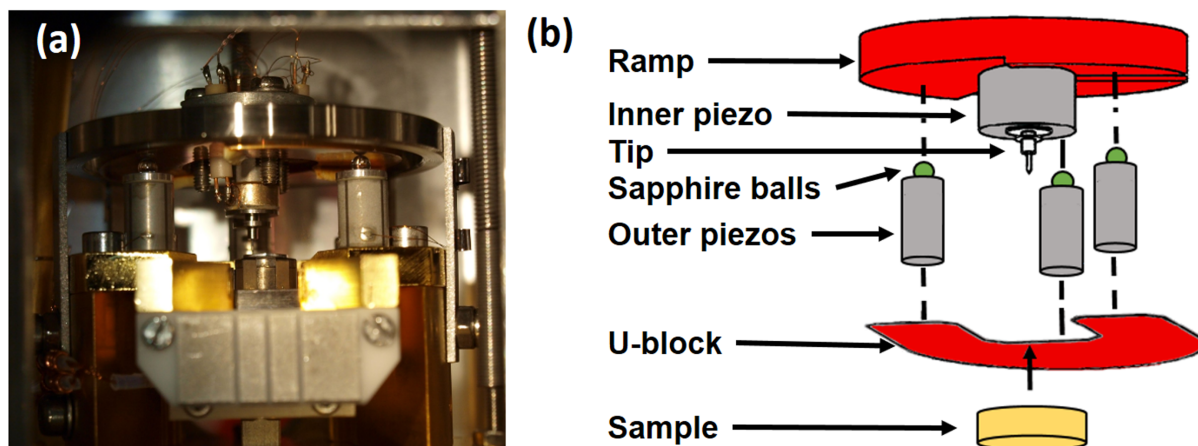


Figure 3.2 – The STM scanner head. (a) Picture of the STM scanner head with a sample inside. Visible in this photo are also the three outer piezoelectric tubes, the main piezoelectric tube, the ramp, sapphire balls as well as the tip. (b) Corresponding scheme of the scanner head.

3.2 The Au(111) surface

The Au(111) surface has been used as a substrate in this thesis in chapter 4 and chapter 7. The gold crystal, that is commercially available from the company “MaTeck”, is precisely cut along the (111)-facet. It is mounted on a specially designed sample holder. This mounted sample can be seen in Fig. 3.3 a. The metal surface is fixed on a heating oven and is tightly clamped with a star-shaped molybdenum sheet. The samples is resistively heated and is connected *via* two copper cables to the contact plate. The temperature is measured with a K-type thermocouple that is attached to two additional contacts on the contact plate.

Sputtering and annealing are performed in the preparation chamber, to obtain a clean and reconstructed Au(111) surface. To do that, the sample holder is grabbed with the manipulator and driven in front of the sputter gun. After sputtering the sample with Ar^+ -ions for 10 minutes at a pressure of $4 \cdot 10^{-5}$ mbar and an energy of 0.5 keV, the topmost layers of the gold surface are removed. The sample is than annealed for ten minutes to 450 °C. Finally, to heal and reconstruct Au(111), the sample is flashed to 500 °C for a few seconds. Afterwards, the sample can be transferred into the STM. To reduce the cooling down time within the STM chamber, the manipulator and consequently the sample can be cooled down with liquid N_2 to 77 K. With this pre-cooling, it is possible to cool down the sample to liquid He (5 K) within twelve hours.

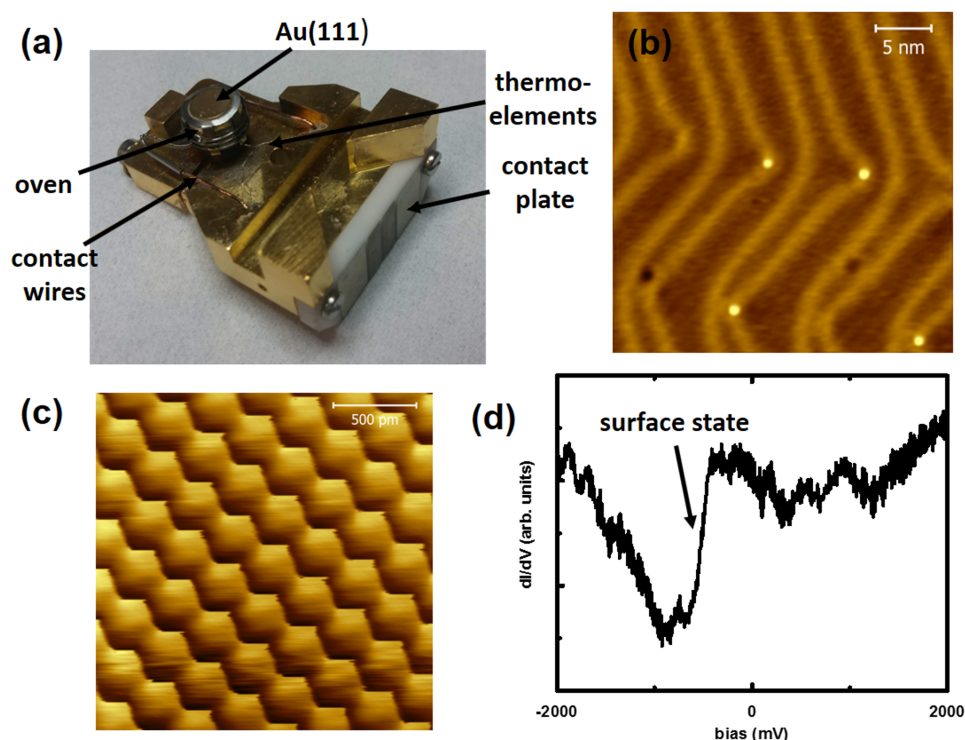


Figure 3.3 – The Au(111) surface. (a) The Au(111) surface on the sample holder. (b) Overview STM image of the Au(111) surface. (size: 30 nm x 30 nm; $I=50$ pA, $V=0.5$ V) (c) Atomic resolution STM image of Au(111). (size: 2 nm x 2 nm; $I=200$ pA, $V=0.2$ V) (d) Scanning tunneling spectra of clean Au(111).

An STM image of the Au(111) surface is presented in Fig. 3.3 b. As one can see, the surface forms the so-called herringbone reconstruction. In this reconstruction fcc- and hcp-domains are separated by soliton walls and thus a ridged structure is formed. The fcc-domains are wider than the hcp-domains and can be easily distinguished. The soliton walls have an apparent height of 0.22 \AA in an STM image [46]. Molecules likely adsorb at the kinks of the soliton walls and mostly favor the adsorption at the fcc-domain. This herringbone reconstruction is formed due to a strain release, as in the uppermost layer there is one additional gold atom as compared to the unit cell (23 atoms instead of 22 atoms), which results in the formation of the $(23 \times \sqrt{3})$ reconstruction. A step within this surface has an apparent height of 2.3 \AA [47,48].

In the STM image of Fig. 3.3 b, one can observe defects at the kink positions that can be commonly observed after sputtering and annealing. Furthermore, dark round protrusions are present on the surface, which can be identified as CO-molecules. A sub-monolayer coverage of CO-molecules is achieved by inserting the CO-gas in the preparation chamber with a pressure of $5 \cdot 10^{-8}$ mbar and opening the shutter of the STM for 30 seconds, while the sample sits on the base plate of the STM. These molecules can be used for the

functionalization of the tip, as further described in the next section.

An atomic resolution image of the clean Au(111) surface can be seen in Fig. 3.3 c. The six-fold symmetry of the surface is clearly visible. From these images it is possible to determine the lattice constant of 4.08 \AA and to calibrate the piezoconstants. Furthermore, the stability of the setup can be proven by scanning tunneling spectroscopy. An example of a dI/dV spectra is shown in Fig. 3.3 d. Noticeable, in the spectra is the characteristic enhancement of the differential conductance at -505 mV . This corresponds to the Shockley surface state of Au(111) [49].

3.3 Further experimental details

In the thesis, the vast majority of STM images have been obtained in the constant-current mode with the bias voltage applied to the sample. All the presented data have been post-processed using the software Gwyddion [50]. Typical tunneling currents are in the range of 1 pA up to 1 nA and are amplified with a preamplifier by a factor of 10^9 V/A . It is of importance to have a metallic tip with a single atom as probe. This is achieved by dipping the tip into the clean metal surface, until step edges are well resolved and circular protrusions at the kink sites are imaged circular. A tip can be used for spectroscopic measurements, if the surface state of the gold surface can be clearly observed.

To obtain high-resolution images with submolecular resolution, it is useful to functionalize the tip with a single CO-molecule. The effective tip radius is reduced when a CO-molecule act as apex. Thus, the lateral resolution is increased and chemical structures of planar molecules can be resolved, as recently reported by several groups [51–53]. There is still a debate about the increased contrast formation in these measurements. It is assumed that short-range forces act on the CO-terminated tip and lead to current changes during scanning. Thus, the tip can be considered as a force to current transducer, which enables us to obtain the atomic structure by STM images [54].

The functionalization of the tip can be obtained by using a purely metallic tip and placing it directly above a CO-molecule, which is imaged as round depression on the surface. The feedback-loop is disabled and the voltage is ramped to 2.0 V , leading to an attractive interaction between molecule and apex. Furthermore, the tip height is reduced by 1.5 \AA [55]. A successful functionalization of the tip can be directly determined by an abrupt increase of the tunneling current during the approach of the tip. The high-resolution images are obtained in the constant-height mode and with almost zero bias voltage applied. This is necessary because the energy of the tunneling electrons must be below any

resonance. Typically, the current during these images does not exceed 500pA, so that the molecule under investigation is not laterally manipulated during scanning.

All dI/dV spectra presented in this thesis have been carried out in constant-height mode. The tip is positioned with the chosen set-point parameters at the desired position. The bias voltage is then swept in the range of interest. To determine the dI/dV-signal, the lock-in technique is used. In this work, I used a modulation frequency of 833 Hz and a modulation amplitude of 20 mV. In contrary, during the dI/dV mapping at a certain voltage the constant-current mode was used. In this mode, the resonances are exactly at the same energy, with few minor differences in the spatial distribution [56].

4 On-surface synthesis of molecules

In this chapter, I will present the on-surface synthesis of molecular nanostructures and functional molecules. In particular, two strategies to self-organize molecules and two unimolecular reactions are presented. This chapter has been partially published in ACS Nano. Parts of the text and figures are reproduced from reference [57] with permission from the American Chemical Society.

4.1 Introduction

The control of supramolecular self-assembly has emerged as a powerful tool in nanoscience for the bottom-up fabrication of well-defined and long-range ordered molecular nanostructures at surfaces. It is an approach based on the chemical engineering of molecular building blocks [58–61]. It mostly consists of planar π -conjugated systems with peripheral functional groups that are able to form non-covalent interactions. Examples for those interactions are hydrogen bonding, metal-ligand, and van-der-Waals interactions [62–65]. The specifically designed building blocks adsorb on a substrate, diffuse on it, and their non-covalent coupling leads to the formation of physisorbed supramolecular structures that stabilize on surface by intermolecular interactions.

On-surface synthesis represents one possible strategy to tailor-make and precisely construct nanostructures, in which molecules form large covalent networks with atomic precision, or to synthesize molecules that are not achievable in solution [15, 16, 66, 67]. The two most investigated reactions in this field are the cyclodehydrogenation reaction and the Ullmann-coupling [68–73]. In the course of the last mentioned reaction, one or several halogen atoms are cleaved from the molecule thereby creating on-surface radicals, which can form covalent bonds either intramolecularly or intermolecularly leading to cyclization or polymerization. Exploiting the latter pathway, molecular wires [74, 75], 2D networks [72], as well as graphene nanoribbons have been obtained [76, 77].

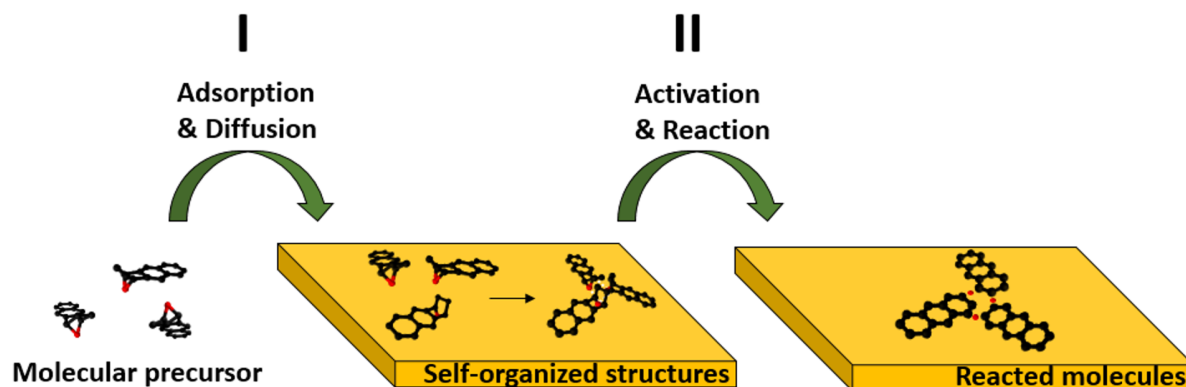


Figure 4.1 – On-surface synthesis approach for a unimolecular reaction. Exemplary the route towards on-surface synthesizing anthracene from an epoxyanthracene-precursor is illustrated [78]. The sublimated molecular precursor adsorbs on-surface and diffuses. Thereby the molecules form self-organized structures *via* hydrogen bonding. By thermal activation, the molecules are reduced and form the planarized anthracene molecule. (Colors: C-atoms: black; O-atoms: red; Au(111)-surface: yellow)

Despite the continuous drive to prepare large covalent structures from small molecular precursors on metal surfaces, the selective formation of specific non-polymeric molecules *via* surface-induced intramolecular reactions is of interest. The cyclodehydrogenation reaction is based on the cleaving of hydrogen atoms and the consequent activation of the molecules. This enables to perform intramolecular reactions leading to specially designed molecular scaffolds. Instead of using the dehydrogenation reaction, recently new molecular nanostructures have been generated by detaching halogen atoms. Some examples include the reversible Bergmann cyclization, the generation of arynes, the generation of anti-aromatic molecules, or molecules with an embedded azulene-moiety [28, 79–82].

Experimentally, the route towards new complex molecular nanostructures is given by the organization and transformation of precisely selected molecular building blocks on surface. One example of self-organized structures and unimolecular reaction is given in Fig. 4.1, showing the formation of molecular structures *via* hydrogen bonding and the conversion of epoxyanthracene to anthracene on Au(111). Those obtained results are discussed in detail in reference [78].

Firstly, the molecular precursors are sublimated in UHV from an ultraclean powder of molecules onto a metal surface held at room temperature. After adsorption on-surface the molecules diffuse and self-organize. This motion is frozen after cooling down the sample to liquid helium temperature (5 K) and thus the formed assemblies can be investigated using scanning probe techniques. In case of epoxyacenes, the molecules

tend to form non-covalently bonded structures, because there is an attractive interaction between them. For epoxyanthracene, hydrogen-bonded assemblies are formed with the bond originated between the oxygen of the epoxy-group and a hydrogen of another molecule, as presented in Fig. 4.1. With special designed precursors, it is then possible to generate supramolecular structures forming special sublattices.

To induce a chemical reaction, it is necessary to activate the molecules. This is shown as second step in Fig. 4.1. In the example of epoxyanthracene, the molecules are thermally activated, deoxygenated and planarized on-surface. Thus, they form upon annealing anthracene molecules. Hereby the molecules arrange in an unusual way for acenes (see the reacted molecules in Fig. 4.1). The cleaved oxygen that remains on surface stabilize the molecules as trimers and induce the ordering of the acene molecules. With clever designed precursors, it is then possible to form molecules that are not possible to synthesize *via* solution chemistry. In the case of acenes, the approach of deoxygenation lead to the formation of acenes with up to ten fused benzene rings, namely decacene [29,83,84]. The successful on-surface synthesis approach is normally obtained on coinage metal surfaces, as the reactivity of the molecules on these surfaces are known to be high. Even if the reactivity of the gold surface is lower in comparison to silver and copper, the diffusion barrier of the molecules is appreciably lower on Au(111) [85]. As most of the reactions do not only need an activation of the molecules, but also the intermolecular connection between the precursors, the gold surface is widely used. This balance between reactivity and diffusion of molecules persuades me, to take Au(111) as a substrate in the following experiments.

4.2 Generation of a periacene

Atomically defined nanographenes, or extended polyaromatic hydrocarbons (PAH's), like acenes or periacenes are of huge fundamental interest due to their expected physical properties, as for example decreased HOMO-LUMO gap and magnetic ground state with localized spin at the zigzag edges [86–89]. The confined structures of these molecules determine their properties. Periacenes for example are formed by two laterally fused acenes at the peri-positions, resulting in rectangular molecules. Exemplary, Fig. 4.2 a presents the chemical structure of an n-periacene. The molecules exhibit two parallel zigzag- and armchair-edges. However, it is only possible to synthesize the two smallest periacenes, perylene and bisanthene [90, 91]. Periacenes have a high reactivity with

4.3 e. To understand its appearance, the molecular structure is presented right beside the STM image in this Figure. Due to the repulsive interaction between the methyl-group and the neighboring hydrogen of the benzyl-moiety, the single molecule appears non-planar. Indeed, the methyl-group is facing away from the surface in this case.

Furthermore, the scanning tunneling spectrum of the precursor molecule taken in the center of the molecule is presented in Fig. 4.3 f. Similar spectra have been observed at other positions on the molecule. No differential conductance peak at positive bias is present in this energy range. Nevertheless, an increased differential conductance flank starts at about +2.0 V. At negative bias, two distinct resonances are visible at -1.3 V and -1.75 V.

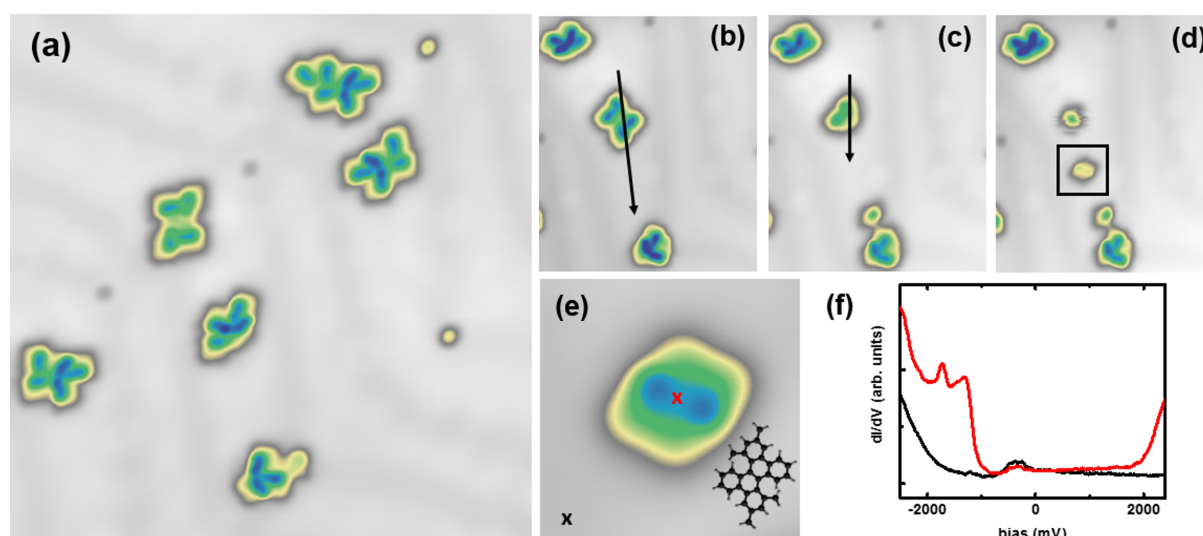


Figure 4.3 – B_2Me_4Chr adsorbed on Au(111). (a) Overview image of the molecules as-deposited on Au(111). (Parameters: $V=0.1$ V; $I=100$ pA; 20 nm x 20 nm) (b) – (d) Separation of a single isolated molecule *via* lateral manipulation (Parameters: $I=1.0$ nA; $V=0.04$ V) fulfilled along the black arrow presented in (b) and (c) (Parameters: $V=0.5$ V; $I=100$ pA; 12 nm x 14 nm). In (d) the isolated molecule is highlighted with a black rectangular. This segment is presented in (e) (Parameters: $V=0.5$ V; $I=100$ pA; 3 nm x 3 nm). Additionally, the molecular structure is inserted in (e). In (f) the differential conductance curve of Au(111) (black) as a reference and taken in the center of the molecule (red) as marked in (e) with the same color is presented.

The assemblies in Figs. 4.4 a and b are formed by four molecules. Those assemblies clearly consist of molecules that are non-planar on the surface, as they show an apparent height of almost 3.5 Å. These higher parts of the molecules can be assigned to benzene-moieties with introduced methyl-groups and the non-planarity originates from the steric

repulsion between two hydrogens. The strong interaction between the molecules results from a CH- π bonding. Also other organic molecules form supramolecular assemblies by this bonding type on metal substrates [96]. The same bonding motif can be seen for the second assembly type. The only difference between those two most frequently formed structures is that for the case of Fig. 4.4 a, all molecules have the same chirality on the surface, while for the case of Fig. 4.4 b the assembly consists of a mixture of both chiralities. To better understand the supramolecular assemblies, the chemical structures are superimposed in Figs. 4.4 c and 4.4 d.

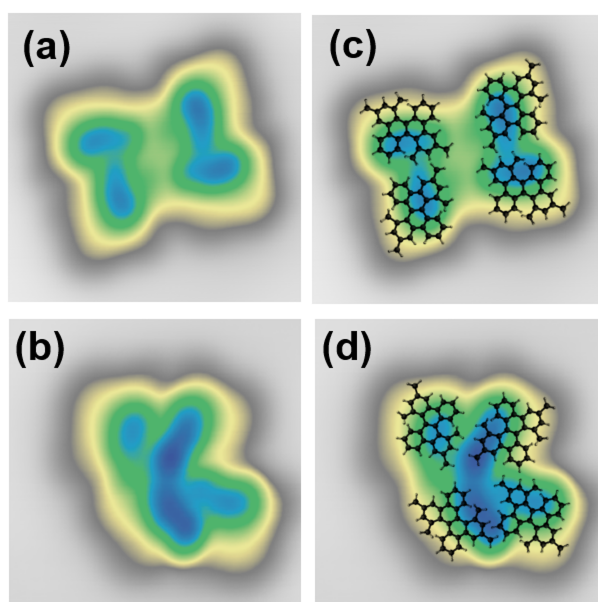


Figure 4.4 – Supramolecular assemblies of B_2Me_4Chr on Au(111). (a) Supramolecular assembly and (c) the same image with schematic overlay of the molecular structure (Parameters: $V=0.5$ V; $I=100$ pA; 3.5 nm x 3.5 nm). (b) Another often found supramolecular assembly and (d) the same image with schematic overlay of the molecular structure (Parameters: $V=0.5$ V; $I=100$ pA; 3.3 nm x 3.3 nm).

To investigate whether the molecule can be cyclodehydrogenated after activation on-surface, I annealed the sample at 170 °C in UHV for three minutes and cooled it down again. An overview STM image of the annealed sample is shown in Fig. 4.5 a. Some molecules are planarized or partially planarized upon annealing. The partially non-planar molecules can be clearly distinguished by the higher appearance of the molecular structure on one site of the molecule. As 170 °C is rather low for a cyclodehydrogenation, not a complete transformation yield is expected [76]. In this case, the yield for the

full transformation into bisanthene is about 20 %. The temperature could only be chosen in this range, as there is a competition between the reaction and the desorption of the molecules, and the complete desorption of the molecules must be prevented. However, some of the molecular structures appear flat and completely reacted, as shown in Fig. 4.5 b. Interestingly, in some cases no methyl-groups can be identified in the STM images. In this case, it can be concluded that the methyl-group is cleaved from the molecule and desorbs from the surface, while one hydrogen atom naturally existing in the vacuum chamber passivates this formed radical position. STS measurements of a single bisanthene shows a resonance at -1.7 V. The resonance at the positive bias starts with a flank at about 1.0 V.

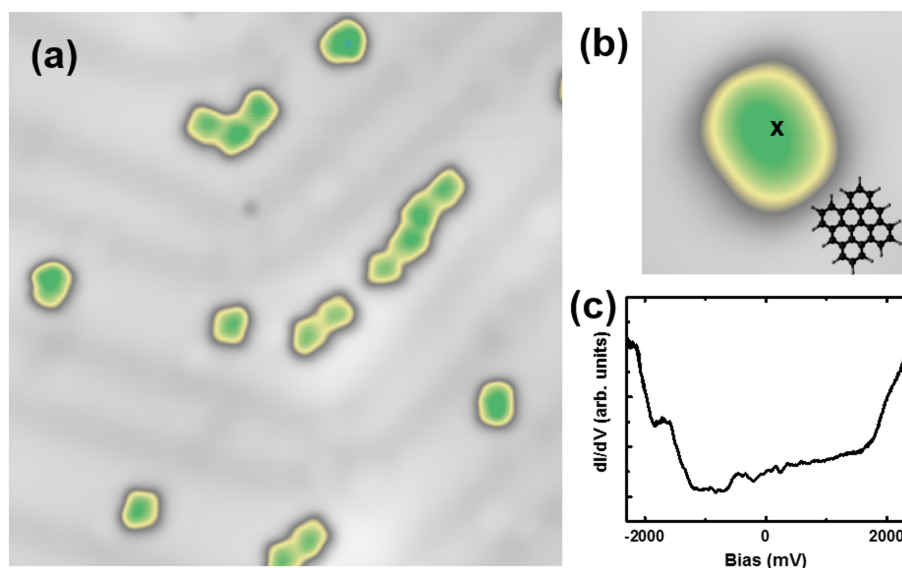


Figure 4.5 – B_2Me_4Chr on Au(111) after annealing to 170 °C. (a) Overview image of molecules upon annealing (Parameters: $V=0.5$ V; $I=100$ pA; 20 nm x 20 nm). (b) Single bisanthene molecule (Parameters: $V=0.5$ V; $I=100$ pA; 3 nm x 3 nm) and (c) spectra taken on top of the molecule as marked with the black cross.

This experiment shows that also all-carbon molecules are able to form supramolecular assemblies. Here, the driving force is probably the non-planarity, resulting in CH- π interactions. Furthermore, I demonstrated that the planarization of molecules *via* cyclodehydrogenation is also possible at the rather low temperature of 170 °C, resulting in the formation of bisanthene molecules.

4.3 Investigating a non-alternant PAH

A second on-surface reaction is obtained by the creation of radical sites in the molecule after debromination. This leads to the formation a non-alternant PAH. The investigation of these PAH's is of huge interest, since the presence of odd-numbered, such as five-membered, rings can be seen as a topological defect and have been shown to reduce the overall aromaticity [97]. Recently, five-membered rings have been achieved by surface-assisted cyclodehydrogenation or elimination of hydrofluoric acid [77, 98, 99]. In addition, other ways to synthesize non-alternant PAH's on surfaces have been presented by several groups [100–102].

I sublimated a submonolayer of the 4,10-bis(2'-bromo-4'-methylphenyl)-1,3-dimethylpyrene precursor molecules $\text{Br}_2\text{Me}_4\text{Ph}_2\text{Py}$ synthesized by Prof. S. Hecht (Fig. 4.6 a) on the Au(111) surface kept at room temperature. As one can see in the STM image of Fig. 4.6 b, one side of the molecule shows a larger conductance, *i.e.* appears higher than the other one, despite the symmetry of the molecular structure. To understand the adsorption conformation of the molecule, density functional theory (DFT) calculations were performed by Dr. D. A. Ryndyk, T. Lehmann and S. Nikipar. These calculations show that the carbon-carbon bond between the pyrene core and the lateral phenyl rings is rather flexible (Fig. 4.6 c). The $\text{Br}_2\text{Me}_4\text{Ph}_2\text{Py}$ precursor is mainly adsorbed in a non-planar conformation on the Au(111) surface with one of the bromine atoms pointing towards and the other bromine atom pointing away from the surface. This adsorption geometry explains the missing mirror symmetry and the significant apparent height difference within the molecule observed in the STM image.

At higher coverages, $\text{Br}_2\text{Me}_4\text{Ph}_2\text{Py}$ forms one-dimensional chains along the fcc domain and row-like ordered monolayers (Figs. 4.7 a and 4.7 c). In the one-dimensional chains, large apparent height differences are visible in the STM images, similar to the case of single molecules. Most of the $\text{Br}_2\text{Me}_4\text{Ph}_2\text{Py}$ molecules are symmetric in the self-organized structures. In these cases, the bromine atoms are probably pointing towards the surface, as their height is comparable with the bromine atom pointing towards the surface of a single isolated molecule. The unit cell contains four molecules and its dimensions are $a=51 \text{ \AA}$, $b=12 \text{ \AA}$ (see Fig. 4.7 c). A few molecules in the monolayer show also the asymmetric character of isolated molecules.

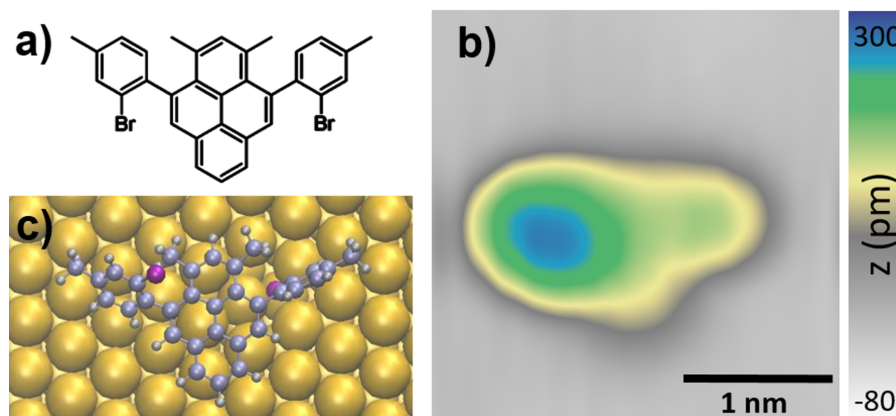


Figure 4.6 – Precursor molecule adsorbed on Au(111). (a) Molecular structure of the precursor molecule 4,10-bis(2'-bromo-4'-methylphenyl)-1,3-dimethylpyrene ($\text{Br}_2\text{Me}_4\text{Ph}_2\text{Py}$). (b) STM image of a single isolated precursor molecule. The STM scan ($V=+1.0$ V; $I=100$ pA) shows that $\text{Br}_2\text{Me}_4\text{Ph}_2\text{Py}$ molecules appear asymmetric after adsorption on Au(111). (c) Ball-and-stick model of the fully relaxed $\text{Br}_2\text{Me}_4\text{Ph}_2\text{Py}$ molecule obtained by density functional theory (DFT) (colors: C-atoms: blue; Br-atoms: purple; H-atoms: grey).

$\text{Br}_2\text{Me}_4\text{Ph}_2\text{Py}$ molecules interact non-covalently with each other, possibly by π - π interaction, as the phenyl-rings are perpendicular to the surface [103,104]. Furthermore, they form the supramolecular assemblies by weak interactions between bromine atoms and hydrogen atoms, so called X-bonding [105–107]. Superimposing the molecular structure in Figs. 4.7 b and c, one can see that the distance between neighboring molecules is below 5 \AA that is typical for these weak interactions.

To explore intramolecular on-surface chemical reactions using the $\text{Br}_2\text{Me}_4\text{Ph}_2\text{Py}$ precursor, I annealed the sample to $160 \text{ }^\circ\text{C}$ for 5 minutes in UHV. At this temperature, and as expected from the literature [101, 108–111], a partial debromination is induced on Au(111). Fig. 4.8 a shows a STM image after this annealing. Three main molecular species are visible at the kink sites of the Au(111) herringbone reconstruction. At these defect points, the molecules are isolated on the surface. These three, approximately triangular, molecular species show large differences in their relative apparent height in the STM images. They have either two maxima, one maximum, or are completely planar, as shown by the linescan in Fig. 4.8 b. I assign the molecule with two maxima to the unreacted precursor $\text{Br}_2\text{Me}_4\text{Ph}_2\text{Py}$. Molecules having one maximum are partially planarized and are therefore probably a reaction intermediate, while the fully planar molecule appears to correspond to a complete debrominated molecule. Beside the molecules at the kink sites, larger structures on the surface have been observed (discussion follows later). Further byproducts are not observed on the surface.

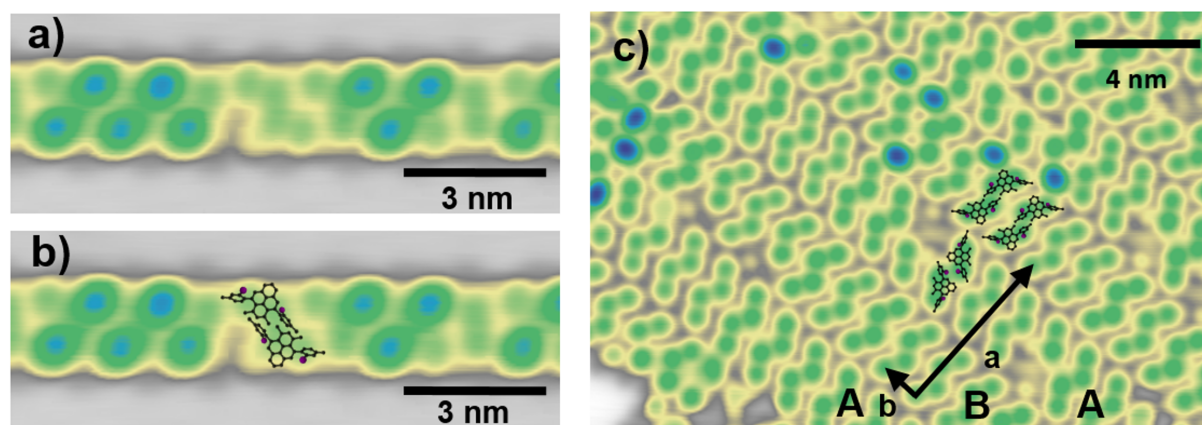


Figure 4.7 – Self-assembled structures of $\text{Br}_2\text{Me}_4\text{Ph}_2\text{Py}$ on $\text{Au}(111)$. (a) Close-up STM image ($V=+1.0$ V; $I=100$ pA) of a one-dimensional chain and (b) the same image with the molecular structure of $\text{Br}_2\text{Me}_4\text{Ph}_2\text{Py}$ superimposed in the chain. (c) A close-up STM image ($V=+1.0$ V; $I=50$ pA) of a formed row-like ordered monolayer. The rows are alternating between rows of A and B. The unit cell is marked with the black arrows. The molecular structures of $\text{Br}_2\text{Me}_4\text{Ph}_2\text{Py}$ are superimposed above molecules in A and B. (Colors of superimposed molecules: carbon: black; bromine: purple; for simplicity hydrogen atoms are left out).

After a further annealing step to 200 °C, all molecules are planar on the surface (Fig. 4.8 c). At this temperature, the debromination is expected to be completed on $\text{Au}(111)$ [101, 108–111]. I can therefore conclude that debromination causes the planarization of the molecules induced by an efficient unimolecular reaction.

In addition and after annealing, non-covalently bound dimer and tetramer molecular structures can be observed (see Fig. 4.9 a). To confirm that the enlarged structures found after annealing to 160 °C are not formed by covalently coupled molecules, I performed lateral manipulation. One typical example can be seen in Fig. 4.9 b. The direction of manipulation is marked with the black arrow. After this manipulation, two single, partially planar molecules are observed on the surface (Fig. 4.9 c). This proves that the molecules are not covalently coupled as it could be expected, but only supramolecular assemblies are formed. As proven by lateral manipulation, after partial planarization molecules form molecular assemblies consisting mainly of two or four molecules. The supramolecular structures are formed due to interactions between hydrogen-atoms and the bromine atoms (X-bonding). The chemical structure is superimposed for the assemblies in Fig. 4.9 d for a dimer and in Fig. 4.9 f for a tetramer.

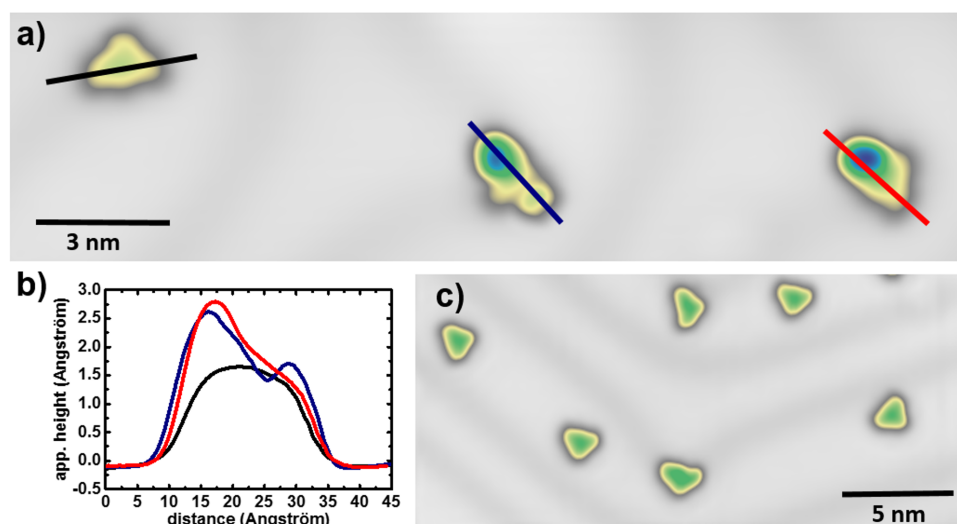


Figure 4.8 – Debromination and planarization of $\text{Br}_2\text{Me}_4\text{Ph}_2\text{Py}$ molecules on Au(111). (a) STM image of three single isolated molecules after annealing to 160 °C for 5 min. The STM image ($V=+0.5$ V; $I=100$ pA) shows that isolated molecules with different shapes adsorb at the kink sites of the surface reconstruction. In the linescans in (b), taken along the molecules (marked in (a) with the same color), one can directly observe that precursor molecules, partially planar and completely planar molecules are on the surface after annealing. (c) STM image of several molecules after annealing to 200 °C. The STM image ($V=+0.5$ V; $I=100$ pA) shows that all molecules have been planarized after the complete debromination of the molecules and no Ullmann-coupled structures have been observed.

To assign the molecular structure of the final product, I performed high-resolution STM imaging. Fig. 4.10 a presents a molecule measured with a metallic tip in constant current mode. By scanning this molecule with a CO-functionalized STM tip in constant height mode [26], a highly resolved image can be obtained as presented in Fig. 4.10 b. Two five-membered rings can be observed at the upper two bay regions of the pyrene core, giving rise to an indene formation. Since the planarity of the structure is maintained, the formed pentagons lead to a bending between the two upper arms of the molecule. Note that the methyl groups, initially present in the $\text{Br}_2\text{Me}_4\text{Ph}_2\text{Py}$ precursor, disappeared in the final reaction product, as it can be seen in the overlaid structure of Fig. 4.10 c. This on-surface synthesized, completely planar product can be assigned to a diindeno[1,2,3-cd:1',2',3'-mn]pyrene (DIP), a molecule which has not been reported so far.

Based on theoretical calculations from T. Lehmann and Dr. D. A. Ryndyk, the reaction path, starting from the $\text{Br}_2\text{Me}_4\text{Ph}_2\text{Py}$ precursor and ending in DIP on Au(111), is summarized in Fig. 4.10 d. After the debromination, which is favored on the Au(111) surface in comparison to the gas phase [112], the molecule cyclizes to form a five-membered instead of a six-membered ring (step 1). The key for this selectivity is the

preferred reactivity of the debrominated radical species towards attack at the substituted phenyl position rather than the benzylic site of the nearby internal methyl group [113]. From the formed internal pentadienyl radical 2, the methyl group at the sp^3 -carbon can migrate to the other, external methyl group, yielding the sterically less congested penta-dienyl radical 3 (step 2). Subsequently, both methyl groups are combined and cleaved from the molecule, leaving one hydrogen atom at the initial site of the external methyl substitution (step 3). Since the observed final product is symmetric, this reaction sequence of cyclization, methyl migration and cleavage occurs a second time within the other half of the molecule (steps 4-6), resulting in the final planar structure. The overall reaction appears to be driven by intramolecular strain release and an increase of the planarity of the π -system and hence stabilizing hybridization on the Au(111) surface.

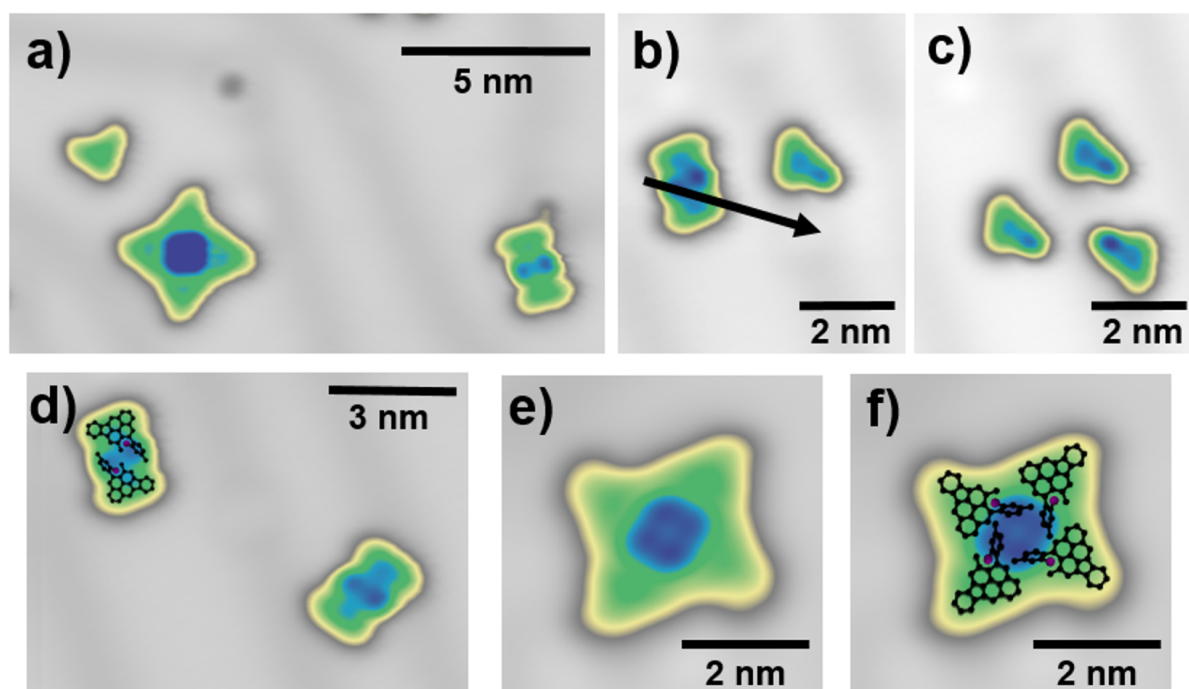


Figure 4.9 – Images after annealing the sample to 160 °C for 5 min. (a) Overview STM image ($V=+0.5$ V; $I=100$ pA). Isolated planar molecules and enlarged dimer and tetramer structures are observed. (b) lateral manipulation of a molecular assembly. By lateral manipulation along the black arrow (Manipulation parameter: $V=+0.01$ V; $I=3$ nA), it could be proven with the following (c) STM image ($V=+1.0$ V; $I=100$ pA) that these enlarged structures are non-covalently coupled, partially planar molecules. (d) Close-up STM image ($V=+1.0$ V; $I=100$ pA) of two dimer structures. One enlarged structure is used to overlay the molecular structure of partially planar molecules on the dimer. (e) Close-up STM image ($V=+0.5$ V; $I=100$ pA) of a tetramer and (f) the same tetramer with the molecular structure of partially planar molecules superimposed. (Colors of superimposed molecules: carbon: black; bromine: purple; for simplicity hydrogen atoms are left out)

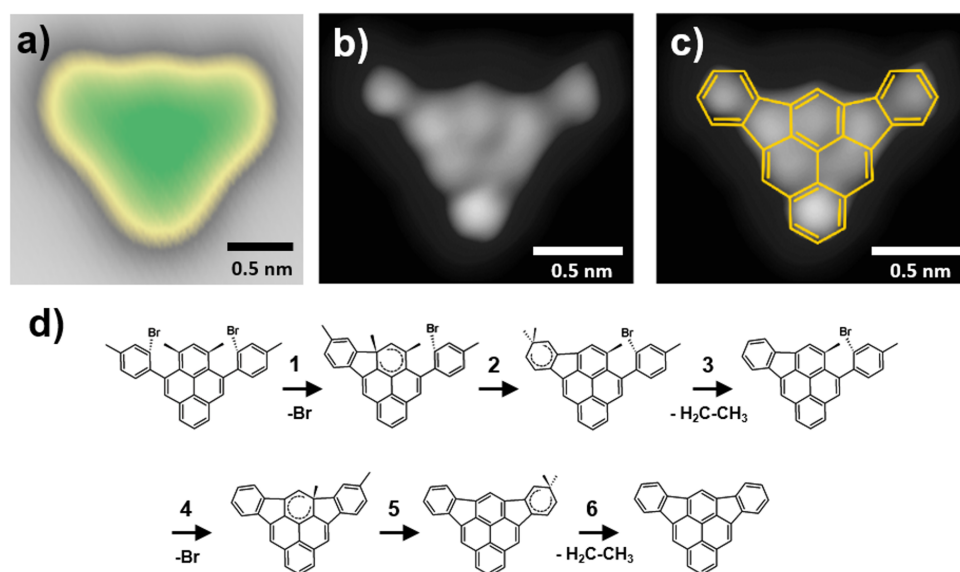


Figure 4.10 – Imaging of single diindeno[1,2,3-cd:1',2',3'-mn]pyrene (DIP) molecules adsorbed on Au(111). (a) Close-up STM image ($V=+0.1$ V; $I=100$ pA) of DIP measured with a metallic tip. (b) DIP imaged with a CO-tip at constant height and $V=+10$ mV. (c) The same molecule superimposed with the relaxed molecular structure of DIP. (d) Reaction mechanism for the on-surface planarization of $\text{Br}_2\text{Me}_4\text{Ph}_2\text{Py}$ to form the planar DIP on Au(111).

To investigate the electronic structure of the obtained DIP molecule, I obtained STS with a metallic tip. Fig. 4.11 b shows the differential conductance spectra on single DIP molecules at the position marked by a red and a blue cross in Fig. 4.11 a. The conductance peaks at +1.5 V and -1.3 V correspond to two tunneling electronic resonances that for simplicity will be referred to as the lowest unoccupied molecular orbital (LUMO) and the highest occupied molecular orbital (HOMO), respectively. Within the bias voltage measurement range allowed by STM, two further well-defined electronic resonances at -1.8 V (HOMO-1) and +2.45 V (LUMO+1) can be measured. On other positions of the DIP molecule, no strong conductance peaks are observed.

For a detailed investigation of the electronic structure, I recorded dI/dV maps at bias voltages corresponding to the resonances attributed to HOMO-1, HOMO, LUMO and LUMO+1 (Fig. 4.11 c). The two five-membered rings are expected to reduce the aromaticity of the DIP molecule [97]. Therefore, in the dI/dV maps, regions of higher differential conductance are located close to the DIP benzene moieties, while regions of lower differential conductance are located on the pentagonal rings (see therefore the overlaid chemical structure in Fig. 4.11 d). This decreased differential conductance is present for all obtained resonances and shows the huge impact of the five-membered ring onto the electronic properties of the molecular structure.

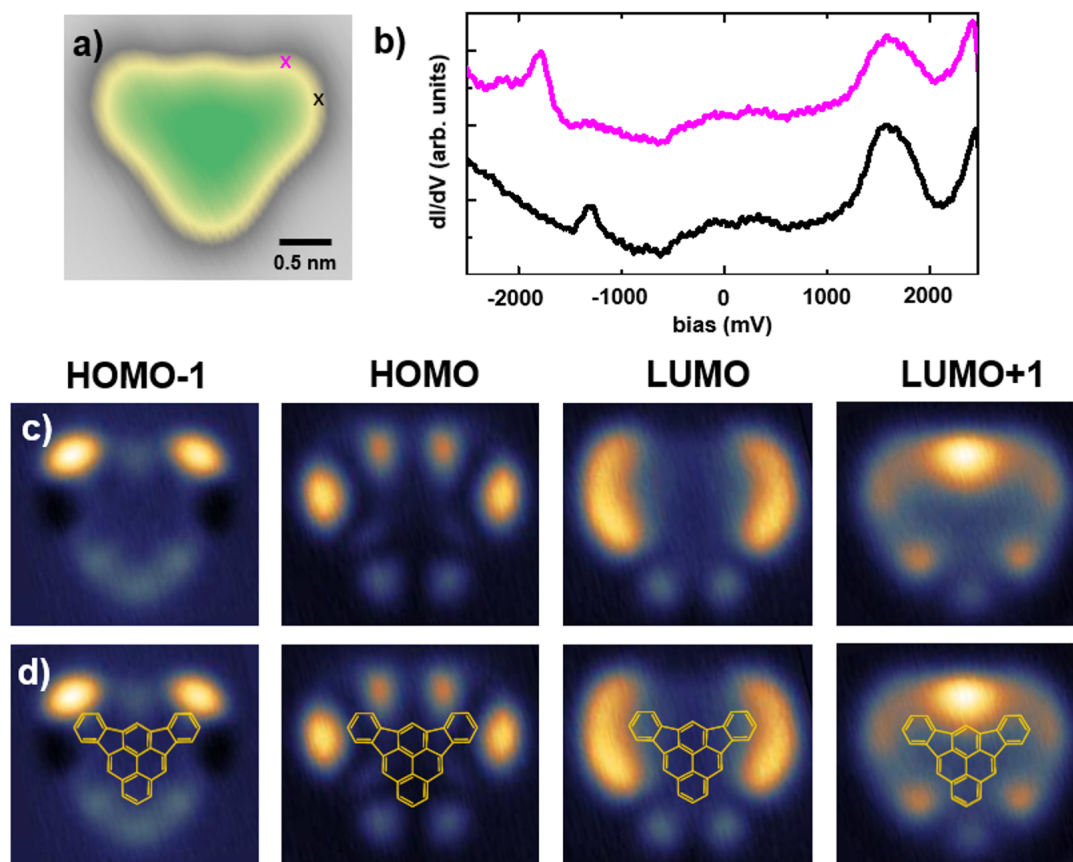


Figure 4.11 – Spectroscopic measurement of single DIP molecules adsorbed on Au(111). (a) Close-up STM image ($V=+0.1$ V; $I=100$ pA) of DIP measured with a metallic tip. (b) Pink and black marks the position of point spectroscopy in (a) and the dI/dV spectra have been taken at constant height; the color of the curves matches with the color with the indicated tip position in (a). Resonances are observed at -1.8 V, -1.3 V, $+1.5$ V and $+2.45$ V. The surface state of Au(111) is observed at -0.5 V. Tip heights were stabilized at $V=+0.5$ V and $I=100$ pA and the spectra range is from -2.5 V to $+2.5$ V. (c) Mapping of the molecular orbital contribution of the DIP tunneling electronic resonances by constant-current differential conductance maps recorded at the identified resonant bias values (HOMO-1: $V=-1.8$ V; HOMO: $V=-1.3$ V; LUMO: $V=+1.5$ V; LUMO+1: $V=+2.45$ V). Image sizes are 3.00 nm \times 2.75 nm. Current for all images was 100 pA. (d) Same maps with the molecular structure of DIP superimposed.

4.4 Conclusion

In this chapter, I have presented two strategies to form non-covalent bonded supramolecular assemblies *via* different attractive interactions. For the case of the first precursor (B_2Me_4Chr) the chemical structure of the molecule suggests that the assemblies are formed by CH- π interaction, while in the second case ($Br_2Me_4Ph_2Py$) the halogen-atoms and the non-planarity of the phenyl-groups are leading to the formation of the supramolecular assemblies *via* X-bonding and π - π interaction, respectively.

Furthermore, I performed the on-surface synthesis of two nanographenes with different properties, resulting from their specific chemical structure. In the first case, I synthesized a molecular structure with a zigzag edge topology using the approach of cyclodehydrogenation that could lead to enlarged nanostructures with this topology. Secondly, I synthesized a non-alternant PAH by exploiting an unusual chemical reactivity after the activation of the molecules *via* dehalogenation. In that case, by the formation of a five membered ring the overall aromaticity is reduced, partially due to the decreased aromaticity at the five-membered rings. I present two further on-surface synthesis experiments in the appendix of the thesis.

5 The passivated silicon surface

Si(001)-(2x1):H is an ideal candidate as a substrate for a planar atomic and molecular technology at the nanoscale. It has a finite gap, and atomic structures can be built by the dehydrogenation of the surface using the STM tip. The resulting surface defects are called dangling bonds (DB's), have electronic states inside the gap and are therefore of great interest. In this chapter, I will describe two preparation methods of passivated silicon, characterize the surface and create DB's and DB-wires on it.

5.1 Introduction

Coinage metal substrates are often used as substrate due to their relatively simple preparation, their ability of building self-assembled layers and molecular nanostructures on their surface and their catalytic effect in chemical reactions to obtain designed molecules [67, 114, 115]. However, for atomic and molecular scale electronics, metals seem not to be appropriate, as they are conducting and have no band gap. Therefore, semiconducting or insulating surfaces are proposed as substrates for molecular scale devices [116, 117]. In this second part of my work, I used as a substrate silicon, as it is generally used in microelectronics. Furthermore, the passivated silicon substrate is a well-known and studied surface [118].

As a substrate for testing atomic scale circuits, I have chosen the hydrogen-passivated silicon surface Si(001)-(2x1):H. The Si(001) surface is characterized by rows of dimers (pairs of atoms bonded to each other). On the Si(001) surface, each Si atom forms only three covalent bonds with its four valence electrons, thus creating a DB. If the surface is exposed to atomic hydrogen (not molecular hydrogen, having a low sticking coefficient) each dangling bond is passivated by a hydrogen atom and the surface becomes inert. A reason behind the interest in the hydrogenated silicon surfaces is the possibility of creating atomically precise DB's by tip-induced desorption of hydrogen atoms [119, 120].

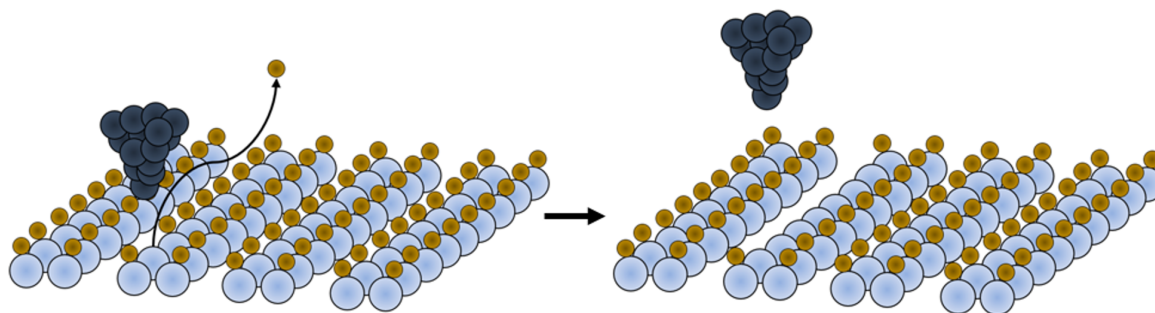


Figure 5.1 – Scheme of the tip-induced production of a DB-wire on Si(001)-(2x1):H.

The surface DB's introduce well-defined electronic states in the surface band gap [121]. In this way, it is possible to create complex DB-structures that can work as atomic scale logic circuits or atomic wires (scheme of Fig. 5.1) [122–125]. In this thesis, I investigated methods for the preparation of this surface and characterized passivated silicon, to later use it as a substrate for achieving DB's and complex DB-structures.

5.2 Preparation of passivated silicon

In this section, I will describe the two different methods I used to prepare a clean Si(001)-(2x1):H surface: the in-situ preparation and the wafer debonding. For the in-situ preparation, I used the method developed by Boland *et al.* [126]. As substrate, I used an highly antimony-doped n-type silicon wafer (0.008-0.020 $\Omega \cdot \text{cm}$). The contact between sample and sample holder needs to be very good, with a resistance below 50 Ω , to be able to heat the wafer to temperatures up to 1200 $^{\circ}\text{C}$ during the preparation. The wafer is heated resistively in the preparation chamber, and the current should never exceed the limits allowed by the cabling of the manipulator (maximum current $I=5.5$ A). After mounting the wafer on the sample-holder (see Fig. 5.2 a), the setup is cleaned in isopropanol and deionized water for 10 minutes in an ultrasonic bath. Then the sample is inserted into the load lock of the UHV system and baked out overnight in the range of 120 $^{\circ}\text{C}$.

As this preparation is very sensitive to residual gases, all steps described below (presented in Fig. 5.2 b) must be performed in a vacuum regime at a base pressure better than 10^{-10} mbar in the preparation chamber. No thermocouple for the read-out of the temperature can be used, as a K-type thermocouple consists of an alloy of chromel and alumel and can contaminate the sample, thus leading to a reduced surface quality. Hence,

I used a pyrometer (LumaSense IMPAC IS 12-Si) for the temperature measurement. As however the pyrometer is only sensitive to temperatures higher than 400 °C, the measurements are not accurate below 600 °C. I degassed the sample for at least six hours at 650 °C and the base pressure must be in the low 10^{-10} mbar regime at the end of this step. During this procedure, the temperature of the manipulator increases significantly. To keep the soldering points of the cabling intact, the manipulator must be cooled down to room temperature by using liquid N₂. Additionally, for different temperatures up to 600 °C the current values are monitored. With these values, it is possible to interpolate the current needed for low sample temperatures and to estimate the temperature starting from room temperature up to 400 °C for the respective current (Fig. 5.2 b). The preparation is illustrated schematically in Fig. 5.2 c. Firstly, I reached the temperature of 950 °C and marked the related current. Afterwards, I stabilized the temperature at 650 °C. The sample needs to be flashed six times at 1150 °C for 15 s, while the current should never exceed 4.5 A. The pressure should be at about $1 \cdot 10^{-9}$ mbar, when flashed the sixth time. A final flash only lasts 5 s at 1150 °C, but this time the pressure should not exceed $3 \cdot 10^{-10}$ mbar. To maintain the reconstructed Si(001)-(2x1) surface, I decreased the temperature fastly to 950 °C and subsequently slowly (1-2 K/s) to about 350 °C.

To obtain a fully passivated silicon surface, all silicon surface atoms must be hydrogenated. Thus, a hydrogen cracker has been installed at the preparation chamber. The proper installation of the system is of huge importance, as the purity of the atomic hydrogen beam affects the surface reconstruction. Before using the cracker, the W-filament must be degassed in several steps. Firstly, the cooling line must be removed from all water and dry nitrogen gas should be purged through the gas line that no water droplets are left. Then the filament is degassed at 400 °C for several hours until the pressure is below 10^{-8} mbar. Afterwards, the water-cooling is connected and a water flow of 90 l/h is supplied. The filament needs to be degassed at 2000 °C until the pressure is again below 10^{-8} mbar, at least for one hour. Before the preparation of the sample, the device is in the stand-by mode (300 °C). The cracker is annealed to 13 A that corresponds to a temperature of about 2000 °C. Then molecular hydrogen is inserted with a pressure of $5 \cdot 10^{-7}$ mbar and is cracked to obtain atomic hydrogen. The sample with a temperature of about 350 °C is driven in front of the cracker for 300 s, after the reconstructed Si(001)-(2x1) surface has been maintained. When the time is over, the heating of the sample is turned off, the sample is driven away from the hydrogen beam, the gas inlet is stopped and the cracker is turned off. Afterwards a passivated silicon sample is obtained. However, the surface quality can locally differ on one prepared silicon wafer. Probably, this is due to a non-uniform heating that has been also detected with the pyrometer on the wafer.

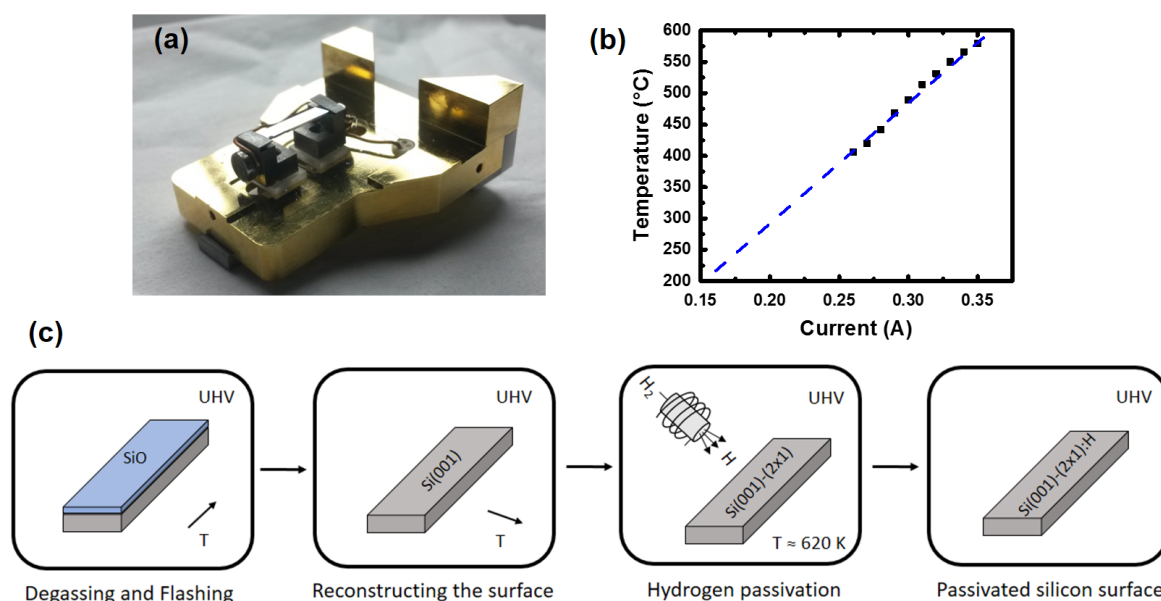


Figure 5.2 – In-situ preparation of Si(001)-(2x1):H in UHV. (a) The silicon sample holder. (b) Current-temperature diagram to interpolate the current needed for temperatures below 400 °C. (c) The route towards getting a reconstructed passivated silicon surface including the main steps degassing and flashing, the reconstruction of the surface and the hydrogen passivation of the reconstructed surface to obtain Si(001)-(2x1):H.

For the wafer debonding method, I used hydrogenated silicon samples prepared at the lab of CEA-LETI in Grenoble. Hydrogen passivated silicon samples can be conserved in UHV conditions only. In ambient conditions, silicon samples, even if passivated, form an oxide layer at the surface after several hours [127]. A strategy to prevent the surface from all kind of contaminants is to hermetically encapsulate it with a second passivated silicon surface [120,128,129]. In this case, van-der-Waals forces held the layers together, so that no impurities can contaminate the surface even at ambient conditions. During the preparation performed at CEA-LETI, a p-type Si(001) crystal with a resistivity of 8-10 $\Omega \cdot \text{cm}$ was etched with hydrofluoric acid and subsequently cleaned with deionized water (Fig. 5.3 a). By this chemical reaction, the native oxide of the silicon oxide layer was removed. Due to the etching process, most of the free DB's were hydrogenated, while the rest was fluorinated, oxygenated or contaminated with carbon. To maintain this situation, the sample was transferred into an environment with a pure N₂-atmosphere. To remove all contaminations, a purified hydrogen atmosphere was generated. A clean Si(001)-(2x1):H surface was obtained by heating the sample in-situ to about 800 °C (Fig.

5.3 b). Subsequently, the surface is encapsulated with a second passivated silicon wafer. The 200 mm wafers are cutted into pieces of 10 mm x 10 mm (Fig. 5.3 c).

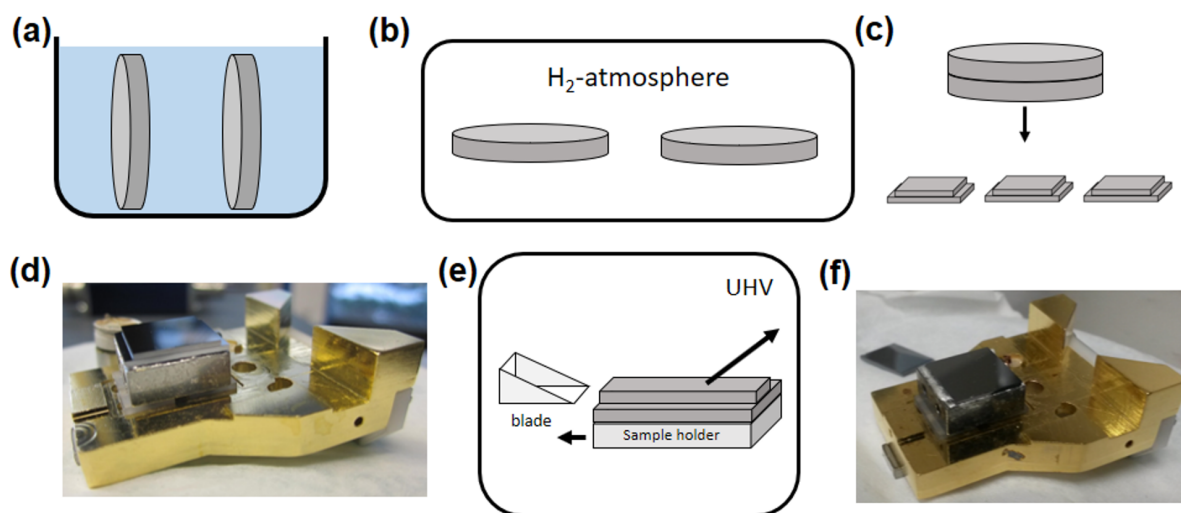


Figure 5.3 – Packaged passivated silicon surfaces. Process flow description of (a) chemical cleaning, (b) surface reconstruction, (c) bonding of a silicon cap and dicing. (d) Silicon sample holder before debonding, (e) a scheme of debonding the surface within UHV and (f) the silicon sample holder after debonding of the cap.

To open the encapsulated samples in the preparation chamber, I used a specially designed sample holder. I glued the wafer with iridium on a molybdenum block, as shown in Fig. 5.3 d. Drawback of this method is that no annealing of the sample is possible. I installed a blade in the preparation chamber of the UHV system on the storage to debond the packaged wafers (Fig. 5.3 e). To make the debonding of the wafers possible, bevels are etched in between them. Thus, it is possible to insert the blade inside the bevel. By slowly driving with the sample against the blade, the silicon cap can be detached (Fig. 5.3 f).

In Fig. 5.4, two overview STM images of the prepared passivated silicon surfaces with the two different methods are shown. In both Figures one can recognize the clear appearance of the Si(001)-(2x1):H. In Fig. 5.4 a the in-situ prepared surface is shown. Clearly one can observe defects, like DB- and some dihydride-defects on the surface that will be described in the next section. Further adjusting of the parameters can possibly reduce the amount of defects. However, the defect density is not too high for the planned experiments, as only a few defects are detected on the overview image. Less defects are

found on the packaged surface (Fig. 5.4 b) and only a few missing dimer rows can be detected, two dihydride-defects and one DB can be found on this overview image. This very low defect density clearly shows the capability of packaging silicon surfaces and re-opening after months at ambient conditions.

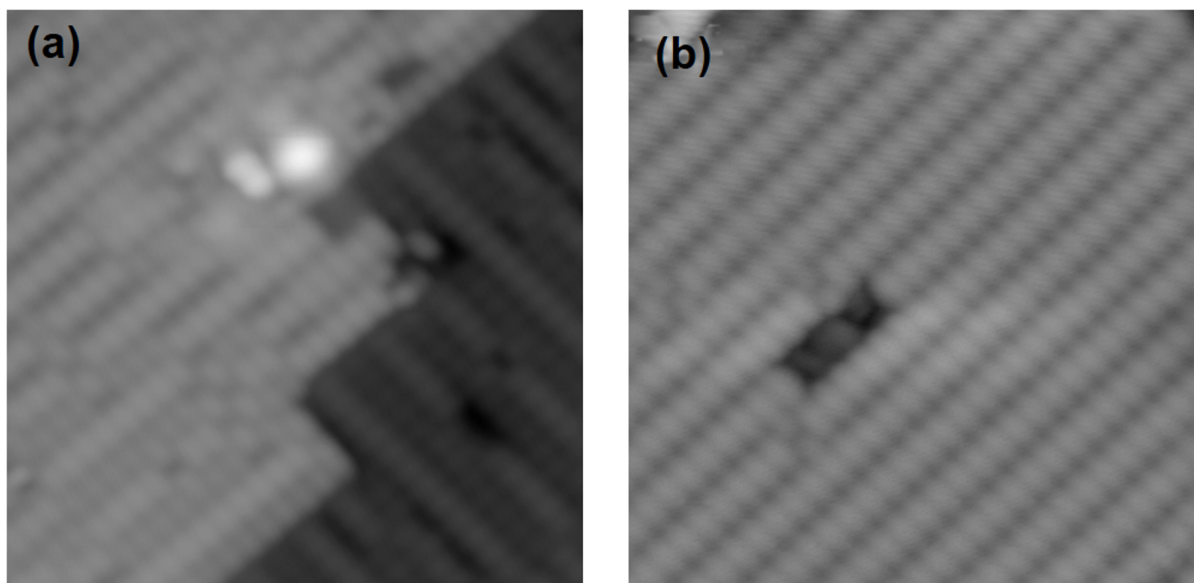


Figure 5.4 – Overview STM images of passivated silicon Si(001)-(2x1):H (a) obtained by in-situ preparation (Image size: 10 nm x 10 nm, V=-2.0 V, I=50 pA) and (b) packaged Si(001)-(2x1):H and opened in UHV. (Image size: 9.1 nm x 9.1 nm, V=-2.0 V, I=21 pA)

5.3 Characterization of Si(001)-(2x1):H

After having addressed two different methods to produce the passivated silicon surface, I will describe in this section the surface texture of the Si(001)-(2x1):H. Fig. 5.5 shows scheme and STM images of the defect-free passivated silicon surface. One can observe the 2x1-reconstruction and the scheme shows that the surface is completely hydrogenated, and so the surface silicon atoms have no open p_z -bonds. Hence, this passivation is also changing the configuration of the silicon-dimers in comparison to the unpassivated surface with the same reconstruction. The dimers are not buckled, so that after hydrogenation a 2x1-reconstruction is notated, instead of a possible 4x2- or 2x2-reconstruction for the unpassivated silicon surface (Fig. 5.5 b) [130].

Figs. 5.5 c and d presents two STM images of the same area of a defect-free silicon surface at different imaging conditions. At negative bias voltage one can observe the filled state, while at positive bias the empty state of the sample is probed. The filled-state image has the highest intensity of the current at the center of the dimer rows of the 2x1-reconstruction, while a minimum is observed in between these dimer rows. For clarity, I superimposed the lattice to the STM image. For an empty state image, the observed pattern seems to be similar. However, the maximum becomes a minimum and vice versa, as compared to the filled state image. Hence, the new maximum is located at the inter-valleys of the dimer row and the minimum at the center of the dimer rows. This behavior is known as contrast inversion of the passivated silicon surface at the different bias voltages [131], and is typical for semiconducting surfaces.

The STM images show that there is a competition between states localized at the dimers and states localized in between the dimers. Yap *et al.* demonstrated that the maximum in the empty state image are Si-Si antibonding states that couple to bulk silicon channels and are located in the dimer valley [132]. For the maximum in the filled state image, Si-Si bonding states are located at the dimer rows. The understanding of these images is of huge importance for the correct interpretation of silicon dimer rows, for the determination of hydrogen atoms and for the precise construction of DB's.

I will consider now the two predominant defects. A DB is an unsatisfied valence on an immobilized atom. On this surface, a DB is a silicon surface atom that is not hydrogenated [133]. This results in new electronic states within the band gap of the surface. By imaging at different conditions, I could observe single DB's by different features on the surface. While in a filled state image the DB's appear as bright spot with an increased height at the dangling bond position, in an empty state image the DB is surrounded by a dark halo. To understand this behavior, one should consider the different charge states of the defects. In fact, there are three possible different charge states, a negative charge state (DB with two localized electrons as in Fig. 5.6 a), a neutral state (DB with one localized electron) and a positively charged state (DB with a localized hole as in Fig. 5.6 b). The halo is attributed to a charging of the DB-state at this imaging condition, while the halo emerges due to a screening of the surrounded area for this positively charged DB-defect [125, 133–135].

Another common defect is the so-called dihydride-defect that is visualized twice in the images in Figs. 5.6 d (filled state image) and e (empty state image). While for the DB one hydrogen-atom is missing on a silicon-surface atom, for a dihydride-defect one silicon-surface atom covalently binds to two hydrogen atoms. Therefore, the bonding between the silicon surface atoms is missing (scheme in Fig. 5.6 f) [136].

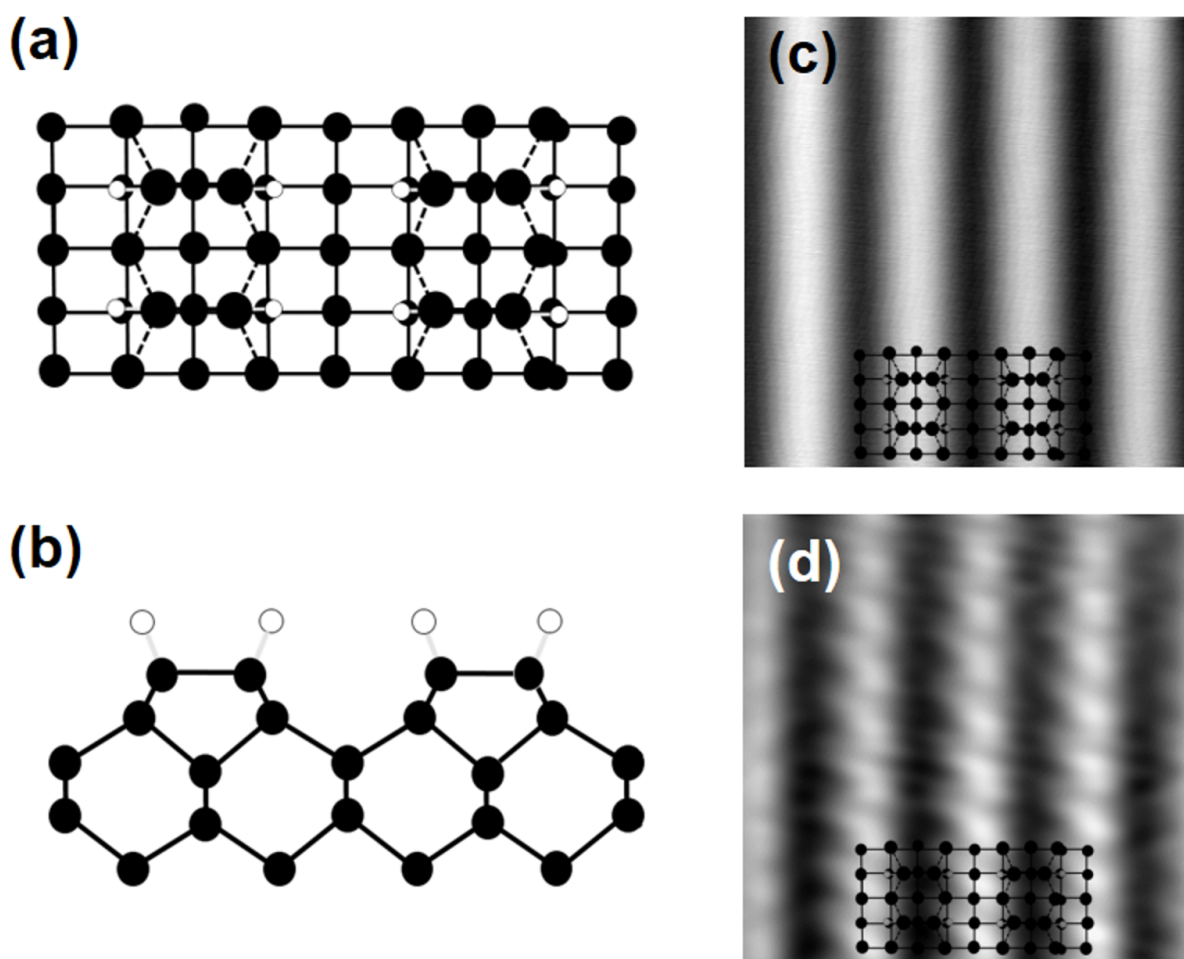


Figure 5.5 – Defect-free Si(001)-(2x1):H. Scheme of the passivated silicon surface as a top view (a) and side view (b). (c) Filled state STM image and (d) empty state STM image of the same area. The scheme of the silicon surface is superimposed in both images. (Image sizes: 3.2 nm x 3.2 nm, $I=100$ pA, (c) $V=-2.0$ V and (d) $V=2.0$ V)

To prepare transport experiments on the passivated silicon surface, it is necessary to understand the behavior of contacting the STM tip with the surface. To this aim, I performed I-z measurements, for that the tip is stabilized with a predefined voltage above a certain position on the surface and the tip-height is varied, while the current is recorded. These measurements have been performed for different surfaces or atop molecules and show most likely three different regimes (tunneling and van-der-Waals interaction, mechanical deformation, chemical contact) [137, 138]. A typical example of an I-z curve above a hydrogen atom of the reconstructed surface is shown in Fig. 5.7 a. In the inset the position of the curve is marked with a cross. For different applied bias voltages

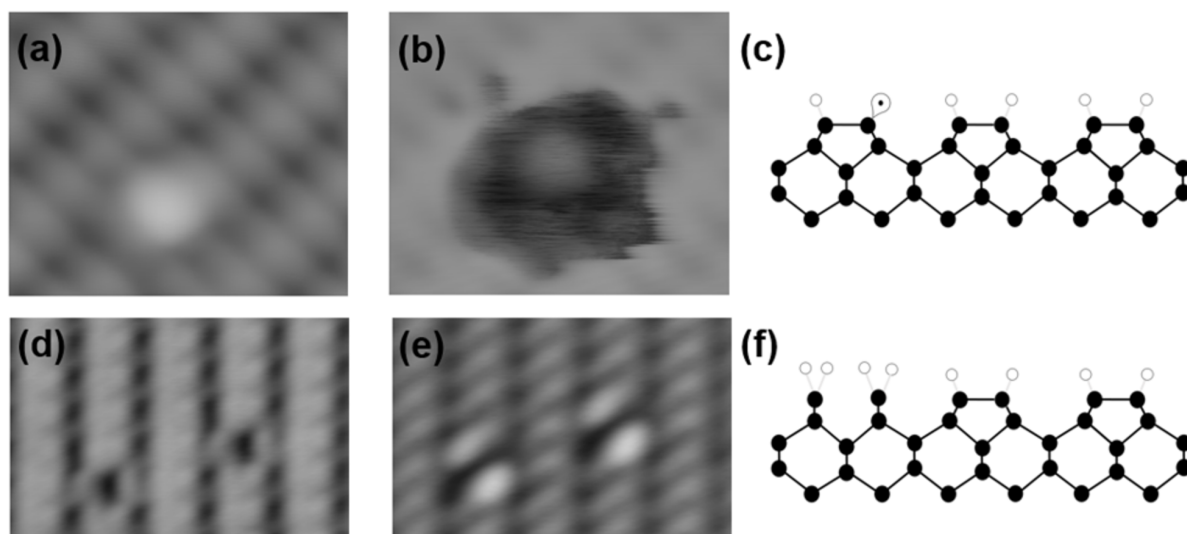


Figure 5.6 – Predominant defects on the prepared passivated silicon surface. (a) Filled state STM image of a single DB-defect and (b) empty state image of the same area. (Image sizes: 3.0 nm x 2.5 nm, $I=50$ pA, (a) $V=-1.5$ V and (b) $V=2.0$ V) (c) Scheme of the side view of the defect. (d) Filled state STM image of a dihydride-defect and (e) empty state image of the same area. (Image sizes: 3.85 nm x 2.5 nm, $I=50$ pA, (d) $V=-2.2$ V and (e) $V=2.2$ V) (f) Scheme of the side view of the defect.

that are not in the band gap, the same behavior is reproduced. In the first regime I an almost linear behavior on this logarithmic scale can be observed. This behavior nicely reproduces the tunneling regime, for that the tunneling current decreases by one order of magnitude when the tip is retracted by 1 Å. By further approaching with the tip towards the surface, the current saturates and reaches a maximum followed by a decrease of the current, what seems to be unlikely (regime II). To understand this behavior, one needs to consider the exact geometry of the dimer rows. A buckling of the dimer row leads to a decrease of the tunneling current. This behavior is also observed on the unpassivated substrate, where dimer rows buckle and are slightly tilted with respect to the surface plane. The observed decrease of the current is probably due to a buckling and driven by the mechanical deformation induced by the tip. I would exclude that tip induced band bending and metal-semiconductor Schottky-barrier can cause this effect. The tip induced band bending can be excluded, as one would expect a further increase of the tunneling current, when the tip is approaching [139]. The metal-semiconductor Schottky-barrier can be excluded, as the effect has been demonstrated for several tips, while the apex of the tips are most likely covered by silicon atoms and do not consist of metal atoms for all of those tips [140]. Further approaching leads to a further increase of the current due to a reached maximum angle of the dimer row with a subsequent contact of surface and tip. This means that by approaching the tip towards the silicon sample,

we are firstly in the tunneling regime involving van-der-Waals forces. Further approach leads to a mechanical deformation of the dimer row that buckles underneath the tip and finally resulting in a contact between tip and surface.

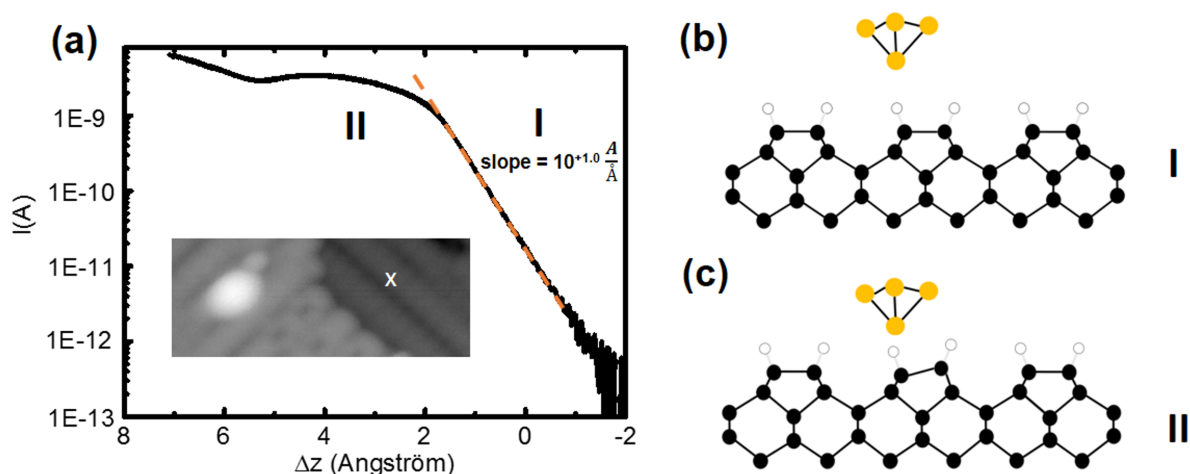


Figure 5.7 – I-z spectroscopy on top of a hydrogen atom on Si(001)-(2x1):H. (a) I-z curve taken at the position marked with the cross in the inserted filled state STM image. (Image size: 5.5 nm x 3.0 nm, $V=-2.5$ V, $I=15$ pA, parameters of the I-z curve: $V=-2.5$ V and stabilized at 10 pA) (b) Proposed scheme of the approach of the tip as shown in the I-z curve in part I and (c) proposed scheme of the bending of the dimer resulting in a decrease of the current (part II), while the tip is further approached towards the surface.

5.4 Tip-induced formation of dangling bonds

After having characterized the passivated silicon surface, I investigated the formation of atomic structures on this surface. The main goal was here the construction and characterization of DB atomic structures. In the literature, several groups propose to use these atomic structures as building blocks for single atom transistors, quantum dots, quantum wells, logic gates, or as atomic wires [121, 123–125, 141–147]. The ability to produce DB's with atomic precision has a long-standing history and began already in the 1990's [148, 149]. The energy of the tunneling electrons can be used to locally dehydrogenate molecules or to detach hydrogen from the silicon surface atoms. A voltage pulse of more than +3.1 V needs to be applied. In the case of Fig. 5.8 a, a voltage pulse of +3.5 V has been applied at the position marked with the black cross. The knowledge

of the position of the hydrogen atom, combined with the ability to precisely position the tip on a surface atom enables us to build nanostructures at the atomic scale. During the voltage pulses, changes in the current traces are observed, when a modification on the surface takes place (see Fig. 5.8 b). In Fig. 5.8 c, a further STM image after the pulse is reported. On this image, one can identify a new DB at the exact atomic position of the voltage pulse. The process is sketched in Fig. 5.8 d and the atomic precision could be achieved in more than 80 % in dozens of cases, while in the other cases DB-dimers, close-spaced DB's, or DB's on the wrong dimer rows are produced.

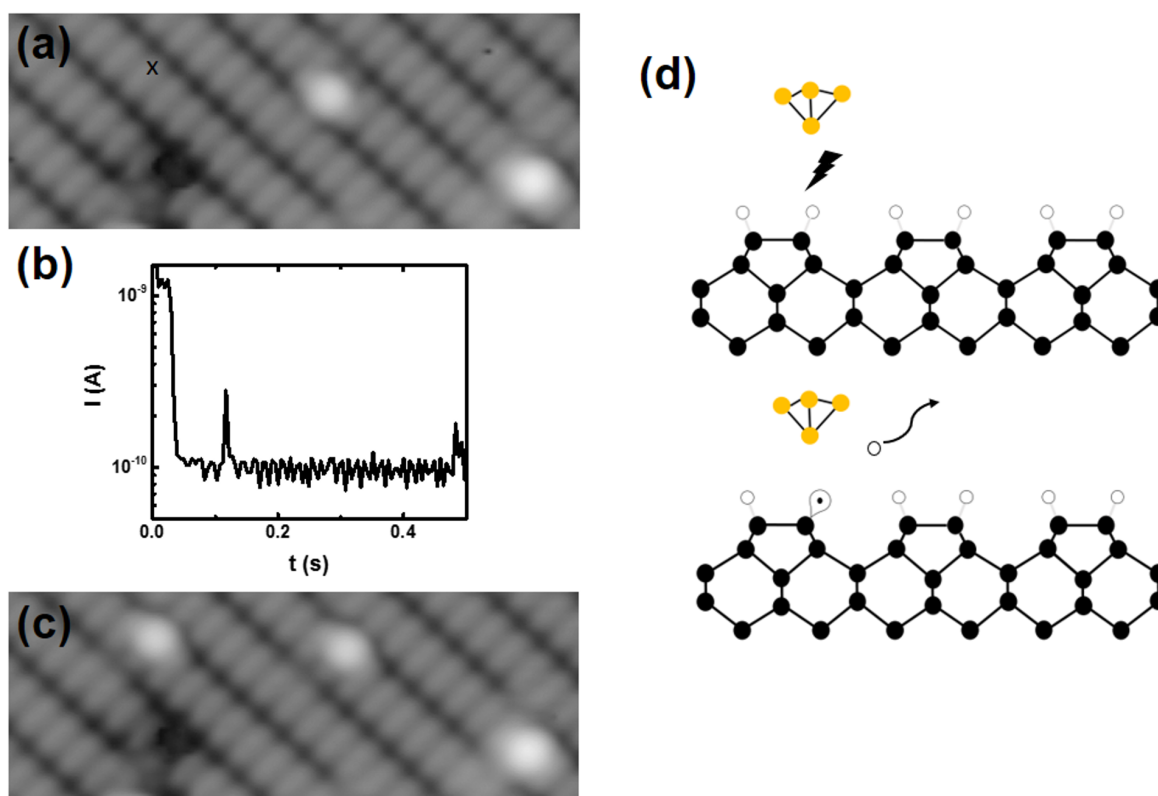


Figure 5.8 – Tip-induced dangling bond production. (a) Filled state STM image of Si(001)-(2x1):H . (b) Current signal of the voltage pulse obtained at the position marked with the cross in (a) and (c) the same area of the surface as imaged in (a). (Image sizes: 7.5 nm x 2.8 nm, $I=50$ pA, (a) $V=-2.2$ V, voltage pulse: $V=3.5$ V, $t=5$ s) (d) Scheme of the tip-induced dangling bond production using voltage pulses.

In the last years, several groups developed different methods to passivate DB's on the surface [150–152]. One strategy is to passivate the surface using molecules. In this means, a molecule named TEMPO that has one radical-site, has been used to re-passivate the surface after the adsorption with the radical site on the DB-position [150]. However, this passivation can be only applied globally by a sublimation of the molecules and thus all DB's are re-passivated. To erase locally a DB, I used the STM tip as already shown by Wolkow *et al.* [151]. I obtained the functionalized tip by creating a DB at another position, resulting most probable in the hydrogen adsorption on the tip. After scanning above a DB-defect (Fig. 5.9 a), one can precisely approach with the tip towards the surface above the DB-position (marked with a black cross). A typical I-z curve can be seen in Fig. 5.9 b. During approaching, a switching behavior between two states is clearly observed. While this is probably due to a back and forth switching of the single DB on the dimer-row, a sudden jump in the current trace could be observed after the approach to about 4.7 Å. In the subsequent STM image, no DB-defect can be detected and a fully hydrogenated surface is imaged, proving the successful erasing of a DB-defect. This bond-formation is purely mechanical and can be achieved without any applied bias [151, 152]. A scheme of the erasing is visualized in the Fig. 5.9 d.

I produced DB's at the positions marked with the white crosses in Fig. 5.10 a. In addition, I could change the position of a single DB on a dimer row. The tip was positioned closely to the position to that the DB on the Si-dimer shall be switched and a voltage pulse with a positive bias was applied in a voltage range for that not yet a DB will be produced. This position was marked with a gray cross in Fig. 5.10 a. The changes achieved by those three voltage pulses are shown in Fig. 5.10 b. I observe that one voltage pulse leads to the creation of a single DB, while with the other voltage pulse a close-spaced DB-pair was constructed. This is proving that not all voltage pulses led to the creation of a single DB. The voltage pulse marked in gray resulted in the switching of the single DB from one site of the dimer to the other site. Fig. 5.10 b shows different produced structures of DB's, the single DB, as well as two different kinds of closed-space DB-dimers that are DB's located at the nearest-neighbor Si-dimer. These can be either dimers that are in the “cross”-conformation (top part of the Figure) or it is a dimer in the “line”-conformation (down part of the Figure) [153].

I used scanning tunneling spectroscopy to validate the electronic structure of Si(001)-(2x1):H and of the created atomic structures, observe a band gap of about 1.9 eV on the bare surface, which is in good agreement with the DFT-calculated band gap of the substrate [154]. Furthermore, I recorded STS spectra on the single DB (as marked with the red cross in Fig. 5.10 b) and on one DB of the two closed-space DB dimer. In

these spectra, three distinct peaks can be observed that can be assigned to states of the DB's. Both DB-structures show the same signature in the dI/dV -signal. However, for the closed-space DB-dimer, the distinct peaks are shifted closer to the Fermi-level. This can be explained, as each DB is introducing a new π - and π^* -state. The shift can be understood to result from the overlap and thus from the electronic coupling between nearest-neighbor DB states. In the literature, it has been already discussed that the states shift closer to the Fermi-level for longer DB-wires and thus the gap between the states is reduced [122].

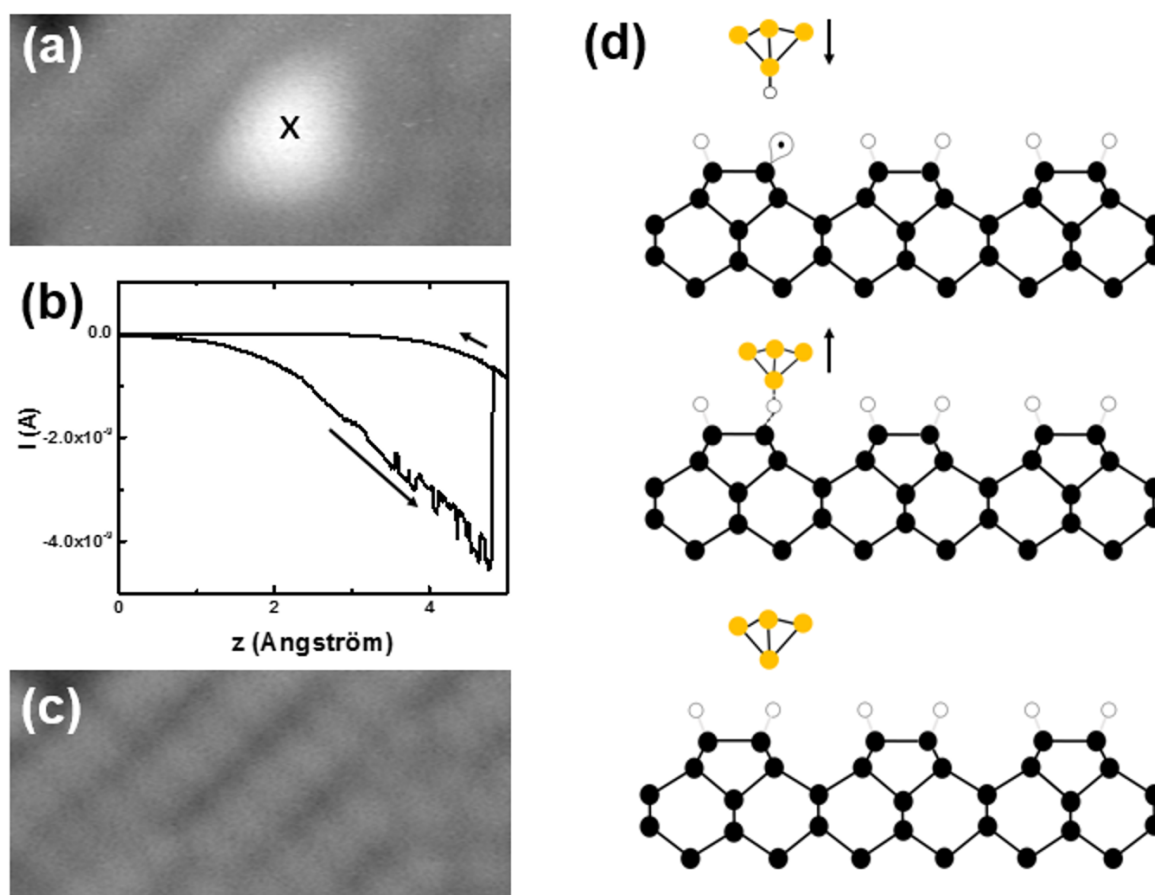


Figure 5.9 – Erasing of dangling bonds using a hydrogenated tip. (a) Filled state STM image of a DB defect. (b) The current signal taken during approaching a hydrogen terminated tip atop a DB-defect as marked by the cross in (a) and (c) the same area as in (a) after the approach without visualized DB-defect. (Image sizes: 5.0 nm x 2.3 nm, $I=15$ pA, $V=-2.5$ V, approach parameters: $V=-2.5$ V, $\Delta z=5$ Å) (d) Scheme of the erasing of a DB-defect using a hydrogenated tip.

Moreover, I created a DB-wire on the passivated silicon surface by removing hydrogen atoms in a line, creating in every second dimer row a single DB. The main contribution of the transport is expected to be through the DB p_z -orbital. However, it has been shown that the transport takes place mainly through subsurface atoms, when closed spaced DB's are produced. This subsurface transport can be reduced by inserting hydrogen atoms as defects within the wire on every second dimer row [131]. The subsurface states are therefore decoupled from the DB's and thus the subsurface transport is interrupted [122]. In the image sequence of Fig. 5.11 b the ability to prepare DB-wires is presented. In the case shown in Fig 5.11 c, I used the tip of the STM to generate a wire with the length of seven single DB's. This is a possible route to obtain long atomic wires on the silicon surface, that can be used as a model-system to perform transport measurements. The single DB appears similar as presented in the previous sections. By adding a second DB, which can be concerned as shortest wire consisting only of two DB's a slight asymmetry between the two DB's can be observed. One DB appears brighter, while the second DB has a slightly lower apparent height. This difference might be due to a slight change in the buckling between those two DB's. For longer chains, starting with three DB's, the DB-wire appears symmetric. It is clearly visible that the edge DB's on the wire with 7 DB's are slightly shifted to the other side of the dimer row.

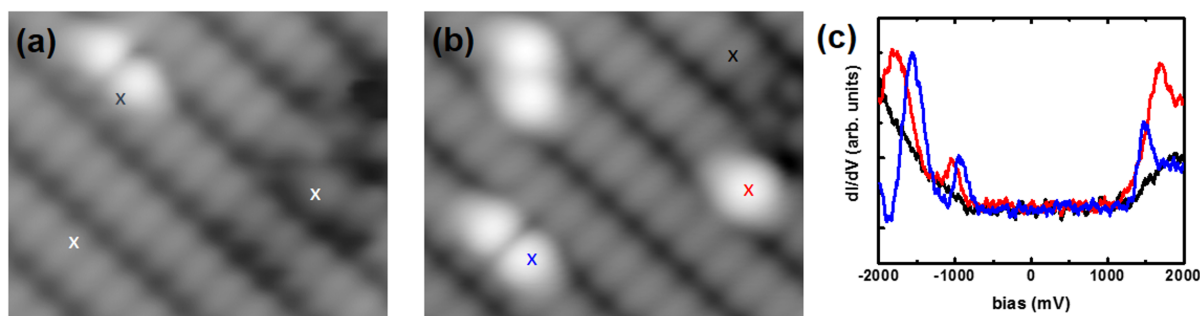


Figure 5.10 – Electronic structure of DB's on passivated silicon. (a) Filled state STM image of a Si(001)-(2x1):H. DB's are produced with voltage pulses at positions marked with the white cross (parameters: voltage pulses: $V=3.5$ V, $t=5$ s), while a DB-position is switched at the position marked with the black cross (voltage pulse: $V=2.5$ V, $t=5$ s). (b) The same area as imaged in (a). (Image sizes: 4.0 nm x 3.25 nm, $I=50$ pA, $V=-2.2$ V) (c) Spectra taken atop the surface (black), a single DB (red) and atop a close-spaced DB pair (blue).

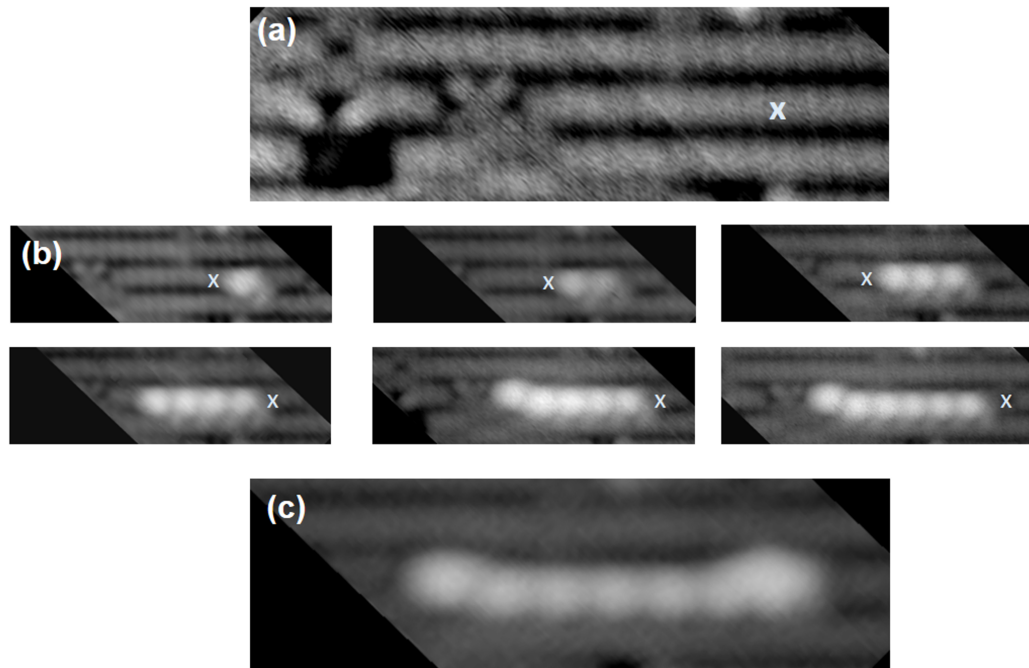


Figure 5.11 – Creation of long dangling bond wires on Si(001)-(2x1):H. (a) STM image of the silicon surface before the production of the dangling bond wire. (b) STM images for the step-by-step DB-production of the wire. Crosses are marking the position of the voltage pulses. (c) Filled state STM image of a DB-wire with a length of 7 DB's. (Image sizes: 10 nm x 3 nm, $V=-2.2$ V, $I=15$ pA, voltage pulse parameters: $V=3.5$ V, $I=100$ pA, $t=5$ s)

5.5 Conclusion

In this chapter, I presented two different preparation methods to obtain in UHV passivated silicon Si(001)-(2x1):H. In particular, I performed the in-situ preparation of the passivated silicon surface and debonded surfaces prepared elsewhere. With both techniques, I obtained clean surfaces with only a few atomic defects after UHV-treatment. To understand the complex structure of Si(001)-(2x1):H, I characterized in detail surface, defects and a contact between surface and tip. This passivated silicon surface can be used as substrate to construct atomic defects, so called DB's that can be considered as possible building blocks for electronic elements at the atomic level. I could reproduce the known methods to create DB's with the tip of the STM and to erase them, if created at a wrong position. Furthermore, I described the electronic structure of the DB's and produced a DB-wire, which is an important step towards possible transport measurements along these wires by using a new generation of multiprobe-systems (see Chapter 7).

6 Organic molecules on passivated silicon

As described in chapter 5, a possible strategy towards an atomic scale electronics is to use DB-wires on the Si(001)-(2x1):H surface for connections between active elements formed by organic molecules. Using this approach, the active device size can be reduced down to the single molecule level. Therefore, molecules with specific electronic properties like molecular switches or logic gates working on the Si(001)-(2x1):H surface are required. In this chapter, I will discuss the on-surface generation of PAH's after deoxygenation that can be useful to design functional molecules on the Si(001)-(2x1):H substrate. Furthermore, I will present the formation of molecular chains on the surface by molecular assembly. Additionally, I will show how to use a molecule of these chains as a molecular switch. This chapter has been partially published as article in *Nanoscale*. Parts of the text and figures are reproduced from reference [155] with permission from the Royal Society of Chemistry.

6.1 Introduction

On-surface chemical reactions make possible the synthesis of molecules and nanostructures that are not accessible by solution chemistry [15, 28, 66]. Noble metal surfaces are normally used as substrates for on-surface synthesis, as for example presented in chapter 4, mainly because of their catalytic behavior [111]. However, the electronic interaction of the molecules with the metal surface makes technological applications difficult, where the electronic decoupling of the molecules from the substrate would be desirable. This decoupling can be, for example, achieved using passivated semiconducting or insulating surfaces. However, successful reactions on these surfaces are rarely observed and must be further exploited [156–158].

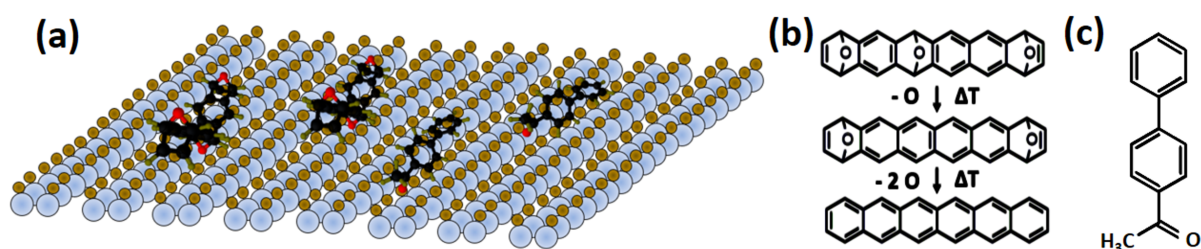


Figure 6.1 – Organic molecules on passivated silicon. (a) Scheme of the passivated silicon surface with the molecules that are investigated within this chapter. (b) Scheme of the induced reduction of the epoxy-groups from HnO_3 , with one selected intermediate diepoxyhexacene (HnO_2) to achieve hexacene is investigated in the second section of this chapter. (c) Chemical structure of acetylbiphenyl that is investigated in the third section of this chapter.

An ideal candidate as a substrate for technology applications is $Si(001)-(2 \times 1):H$, as described in chapter 5. In the past years, several different organic molecules on passivated semiconductors have been studied [159–163]. The molecules are electronically decoupled from the silicon substrate by the hydrogen layer [164, 165], and the unaltered electronic structure of molecules can be therefore observed [166]. The purpose of this chapter, is to prove that the deoxygenation reaction to form PAH's from precursors with epoxy-groups (see Fig. 6.1 b) is possible on $Si(001)-(2 \times 1):H$. Furthermore, I investigated the molecular assembly, as well as the possible switching of ABP (chemical structure in Fig. 6.1 c).

6.2 Hexacene generated on passivated silicon

Acenes are widely studied molecular systems with scanning probe techniques [26, 167–169] and those PAH's are of interest for applications in molecular electronics and spintronics [11, 170–173]. Acenes larger than pentacene, however, have a very limited stability, are not soluble and are difficult to synthesize by solution chemistry [174]. Recently, different approaches have been achieved that allow the on-surface synthesis of long acenes [29, 83, 84, 175, 176] up to a length of undecacene [177]. These long acenes are of high interest, as they are expected to have promising electronic properties, like a reduced energy gap or a diradical character [178, 179]. Our group has demonstrated that the deoxygenation of epoxyacenes is a powerful tool to synthesize acenes of increasing length on the $Au(111)$ surface [29, 78, 84]. However, the on-surface generation of long

acenes on passivated semiconductors or insulating surfaces was, to my knowledge, not achieved yet. In this section, I want to show that the deoxygenation reaction to form acenes from epoxyacene precursors (see Fig. 6.1 b) is possible also on Si(001)-(2x1):H.

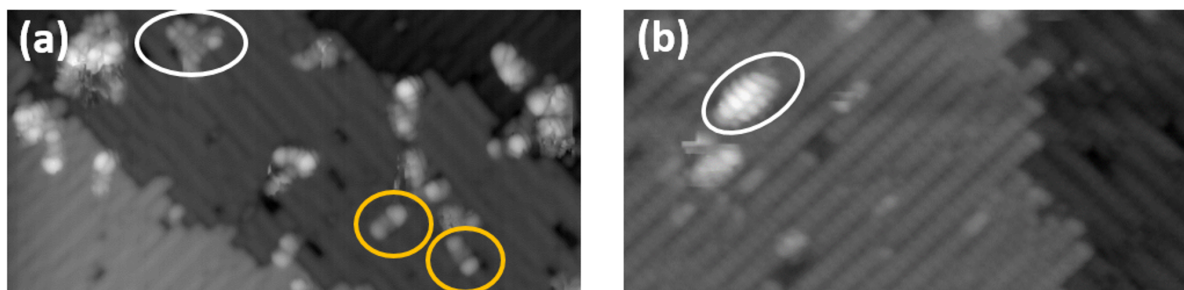


Figure 6.2 – Overview image of the surface after the different preparation steps. (a) A typical overview STM image after the deposition of HnO_3 and subsequently heating of the surface to 250 °C for 5 min. The yellow circles show precursor or partially deoxygenated molecules. The white circle presents a completely reacted molecule. In addition, larger adsorbates are present on the surface ($V=-3.0$ V, $I=15$ pA, image size: 30 nm x 15 nm). (b) Overview image after further annealing to 300 °C for 5 min. The red circle presents a completely reacted molecule ($V=-2.5$ V, $I=15$ pA, image size: 20 nm x 10 nm).

To explore the on-surface reaction, I sublimated the precursor molecules HnO_3 on the Si(001)-(2x1):H surface at room temperature and annealed the sample directly to 250 °C for five minutes. A certain amount of larger agglomerates is present on the surface, as shown in the overview STM image in Fig. 6.2 a. Additionally, precursor and partially reacted molecules are visible (these molecules are encircled in yellow). One can see in this image one molecule with the appearance of hexacene attached to several defects (surrounded by a white circle).

After a further annealing step to 300 °C (Fig. 6.2 b), I could observe a reduced molecular coverage and no enlarged agglomerates, but a higher concentration of DB-defects on the surface. Only molecules that have the appearance of hexacene and that are attached to dangling bond defects could be observed on the surface.

Firstly, I focused on the precursor molecules HnO_3 and partially reacted molecules on the Si(001)-(2x1):H after annealing the sample to 250 °C. Due to the synthetic procedure described in ref. [84], HnO_3 is obtained as a mixture of the four possible diastereomers, which are used as hexacene precursors for the on-surface experiments. As one can see in the STM image of Fig. 6.3 a and in the corresponding linescan of Fig. 6.3 b, after this first annealing I still observe unreacted molecules on the surface, characterized by three

maxima in the STM images. It is known from the literature that molecules on Si(001)-(2x1):H preferentially adsorb at dangling bond defects [162]. The shoulder visible in the linescan of Fig. 6.3 b can therefore indicate a dangling bond defect.

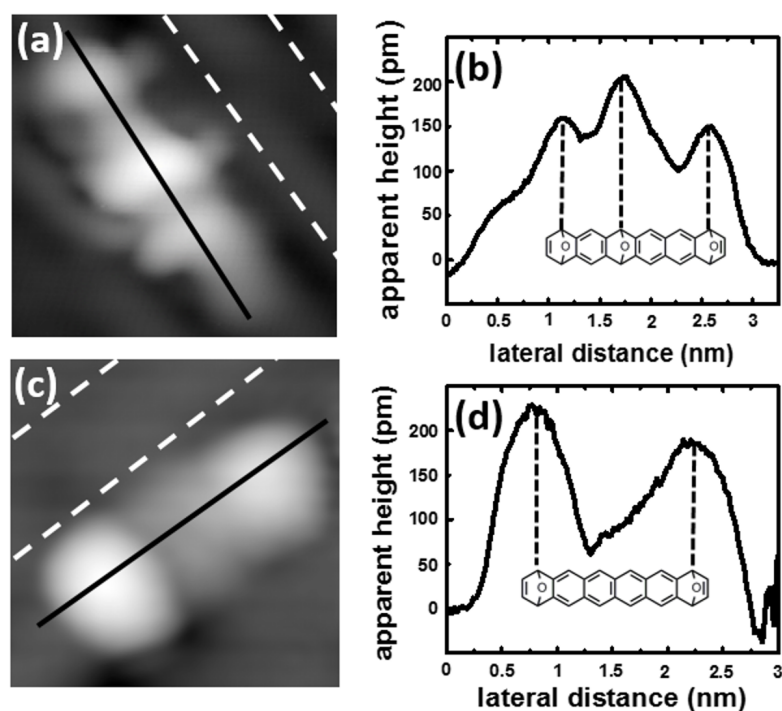


Figure 6.3 – STM images of the precursor HnO_3 and the intermediate HnO_2 on Si(001)-(2x1):H. (a) Precursor molecule HnO_3 on passivated silicon ($V=-2.0$ V, $I=50$ pA). The white dashed lines show the dimer row direction. A linescan recorded along the black line is shown in (b). (c) Partially reacted molecule without the central epoxy group ($V=-3.0$ V, $I=15$ pA). The white dashed lines are parallel to the dimer row direction and the black line indicates the position of the linescan presented in (d). Images sizes: 2.5 nm x 2.5 nm.

As one can see in Fig. 6.3 b, the apparent height of the molecule at the oxygen positions differs from case to case by around 50 pm. As the sublimated molecules consist of the mixture of the four different diastereomers, the oxygen atoms of the molecule are oriented in different directions when adsorbed on the surface. The epoxy group can point either towards or away from the surface, thus explaining the significant apparent height difference. More often, I observed partially reacted molecules, as shown in the example of Fig. 6.3 c. In those cases, the reduction of the central epoxy group has occurred, so that the molecule is flat at this position. The linescan in Fig. 6.3 d clearly shows that only the two outer maxima are visible in this case.

After this first annealing step to 250 °C, not all molecules have been completely deoxygenated. Notably, and contrary to the case of Au(111), on Si(001)-(2x1):H voltage pulses never lead to the generation of hexacene. To increase the reaction rate, I therefore heated the substrate further to 300 °C. A slightly increased amount of DB defects and no change in the reconstruction are observed [180,181]. Most molecules desorb, so that the coverage decreases significantly (see Figure 6.2 b), but completely flat molecules can be now observed on the surface.

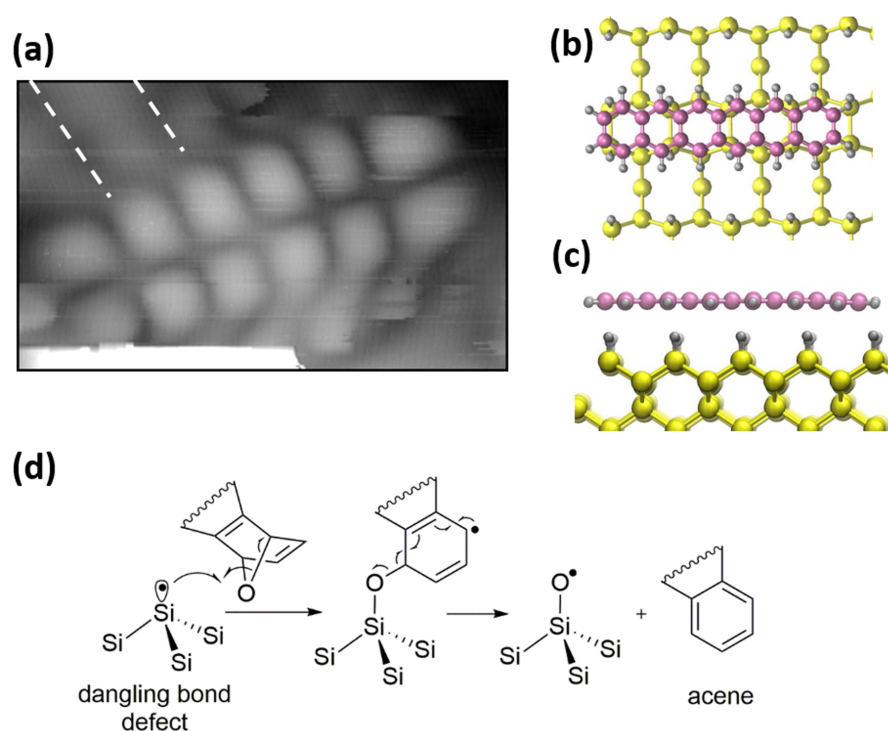


Figure 6.4 – Hexacene on passivated silicon. (a) STM image of a single hexacene molecule on Si(001)-(2x1):H (Image size: 2.5 nm x 1.5 nm, $I=30$ pA, $V=-2.0$ V). The white dashed lines show the dimer row direction. (b) DFT-calculated optimized hexacene on Si(001)-(2x1):H (top view); (c) side view. (d) Proposed mechanism for the acene generation on passivated silicon *via* the reaction of the epoxyacene precursor with a dangling bond defect.

In Fig. 6.4 a, a STM image of a fully reacted molecule is presented. By tunneling at negative bias voltage, $V_{\text{bias}} < -2.0$ V, the molecule shows two rows of six lobes, in good agreement with the case of pentacene on the same Si(001)-(2x1):H surface, showing two similar rows of five lobes [164]. By comparing hexacene with pentacene, I can conclude that the deoxygenation reaction is completed and I can assign the molecule in Fig.

6.4 to hexacene and the lobes at negative voltage to the signature of the HOMO of the molecule.

As discussed in ref. [164] for the case of pentacene, the molecule and the silicon surface atoms are spatially separated by about 5 Å due to the hydrogen layer. Consequently, the adsorption energy and the diffusion barrier for acenes on passivated silicon are rather small [163, 164]. This separation leads to an electronic decoupling and almost no hybridization of the molecule with the surface silicon atoms. This conclusion is supported by DFT calculations done by Dr. D. A. Ryndyk: Figs. 6.4 b and 6.4 c show the top-view and side-view of the relaxed structure of hexacene on the fully passivated silicon surface, demonstrating the weak interaction between the molecule and the substrate. Moreover, the low interaction with the substrate increases the mobility of the molecule on the surface. After the reaction, the molecules therefore diffuse until step edges, defects or silicon dangling bonds block them. As a consequence, I mainly observed hexacene anchored to dangling bond defects or other adsorbates, as shown in the lower left part of Fig. 6.4 a by a bright spot (for another example see also Fig. 6.2 a).

The observed reaction can be understood considering the role of the Si-H bond as reducing agent of oxygen-containing functional groups. In fact, hydrosilanes are excellent reducing agents in solution chemistry [182]. Similarly, hydrogen terminated silicon surfaces can reduce carbonyl functional groups, and the dangling bond defects may be involved in the reaction mechanism [183]. In the case of epoxyacenes interacting with the silicon surface, a similar reaction can occur. As the formation of a Si-O bond take place probably on DB-defects [184, 185], I suggest that the adsorption of the precursor molecule on a DB can lead to a first C-O bond cleavage of the epoxy group facing towards the surface (Fig. 6.4 d). Subsequently, a second C-O bond cleavage would form the acene molecule.

In several cases, I observed hexacene molecules anchored to a defect. A typical example is shown in Fig. 6.5 a. Similar to the case of the free molecule of Fig. 6.4, at negative bias voltages I could clearly recognize the HOMO-like signature with the double row of six lobes. However, there is in this case an asymmetry in the apparent height of the lobes of the molecule. As clearly visible in the linescans of Fig. 6.5 b, one of the lobes is significantly lower by 100 pm in comparison to the neighbor one.

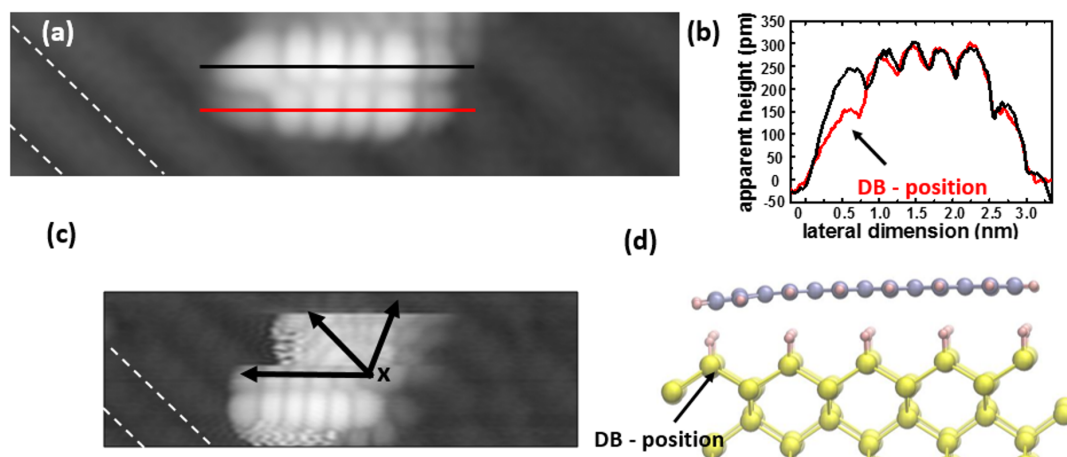


Figure 6.5 – Hexacene interacting with a single DB on Si(001)-(2x1):H. (a) STM image of hexacene with a slightly asymmetric appearance (Image size: 8 nm x 2 nm, $I=15$ pA, $V=-3.5$ V). (b) Linescans over the two rows of six lobes. The position of red and black curves is marked with lines in the image (a). (c) Rotation of a single hexacene molecule. Scanning along the fast scan axis leads to the rotation of the molecule. We indicate the different directions of the molecule by blue arrows on the molecule. The anchoring point is marked with an x (image size: 8.00 nm x 2.75 nm, $I=15$ pA, $V=-3.5$ V). (d) Side view of the optimized structure of hexacene on a single DB.

Moreover, quite commonly the hexacene molecules rotate around a fixed point during scanning under the effect of the STM tip (Fig. 6.5 c). As one can see, the long axis of the molecule points in three different directions, marked with arrows. The center of rotation, indicated by a cross, corresponds to the lobe showing a lower apparent height. I can therefore conclude that the molecule is anchored to the surface at that point, and that the anchoring point influences the apparent height of the corresponding lobe. Always one of the outer lobes shows lower apparent height. Thus, I conclude that the preferred adsorption site of the molecule is on the last benzene ring above the defect.

DFT calculations indicate that the decreased conduction, *i.e.* the lower apparent height of one of the lobe, is due to a bending of the molecular skeleton towards the silicon surface (see Fig. 6.5 d). In particular, the calculations suggest that the molecule is adsorbed above a single DB and is lower in height by around 50 pm.

To determine the origin of the anchoring, I detached the molecule by scanning over its area at a positive bias of +2.0 V (see Fig. 6.6 b). The molecule is inelastically excited and detached from the defect [166]. Afterwards, I observed a single DB at the exact position where the molecule was anchored (*i.e.* where the apparent height of hexacene was lower). As at these scanning parameters no single DB can be produced, I have experimentally proven that the hexacene molecule anchors preferentially at single

DB. This influences the apparent height in the STM images at the position of the DB-molecule complex and anchors the molecule on the surface.

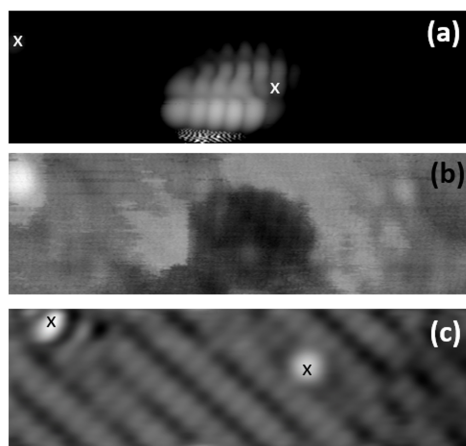


Figure 6.6 – Hexacene detached from a DB-defect. (a) Hexacene molecule above a single DB. The white cross marks the position of a defect on the surface and the other cross marks the position where the DB has been found in (c) below the molecule. The color code is chosen to be black and white to focus just on the molecule, as we had a slight double tip (image size: 10 nm x 3 nm, $I=80$ pA, $V=-3.0$ V). In (b) we show the image during a measurement at positive bias. Clearly the molecule was removed from the DB (image size: 10 nm x 3 nm, $I=20$ pA, $V=+2.0$ V). In Figure (c) we clearly visualize the DB (image size: 10 nm x 3 nm, $I=20$ pA, $V=-2.5$ V). With the help of the defect, the position of the DB underneath the molecule can be marked in (a).

To further characterize the electronic properties of hexacene adsorbed on Si(001):H, I recorded the differential conductance spectra on hexacene molecules interacting with single dangling bonds. This was not possible for purely physisorbed molecules because of their high mobility. Two distinct resonances at -2.0 V and -3.1 V are observed that are called for simplicity HOMO- and HOMO-1-resonances (black curve of Fig. 6.7 b). At positive bias I could not observe resonances because their typical energy values lies in the surface electronic band gap, as already observed for pentacene on the same substrate [164].

By comparing the observed resonance of hexacene on Si(001):H with the literature values for pentacene, I observed a shift of the HOMO-resonance from -2.5 V to -2.0 V [164]. This confirms that by increasing the number of fused benzene rings, the resonance shifts towards the Fermi-level. The differential conductance of the molecule locally measured at the position of the DB-site (red curve) is not significantly different from other positions. This suggests that the molecule weakly couples to the DB-site

and that hexacene is not covalently bonded to the silicon surface atom, as the electronic structure is not changing strongly above this position. In conclusion, I have proven the conversion of triepoxyhexacene into hexacene on the Si(001)-(2x1):H surface and characterized the reaction product, when physisorbed on the surface or when adsorbed on a single DB.

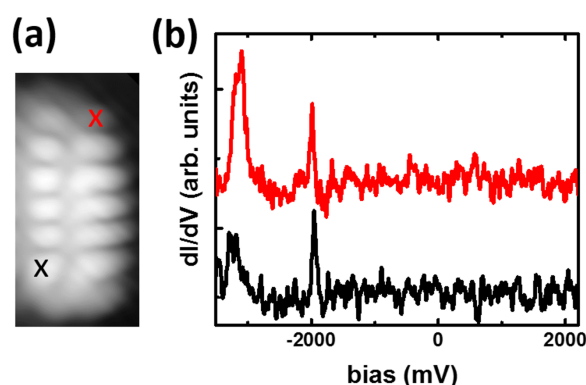


Figure 6.7 – Scanning tunneling spectroscopy of hexacene interacting with a single DB. (a) STM image of hexacene (image size: 1.7 nm x 3.3 nm, $I=60$ pA, $V=-3.1$ V). The blue cross corresponds to the position above the DB. (b) Differential conductance measured on the molecule above the DB and above a position on the molecule that is not close to the DB defect. The colours of the curves correspond to the colours of the crosses as marked in Figure (a).

6.3 Acetylbiphenyl on passivated silicon

The molecule acetylbiphenyl (ABP, molecular structure in Fig. 6.8 a) has been extensively investigated in recent years. On the Au(111) surface, our group demonstrated that the molecule forms assemblies and can be controllably directional manipulated *via* voltage pulses [34, 186, 187]. This will be discussed in chapter 7 in detail. On the unpassivated Si(001) surface, the adsorption and STM tip-induced manipulation of acetophenone molecules was studied by Schofield *et al.* [188]. This molecule has the same chemical structure as ABP with one phenyl ring less. They show that these molecules strongly couple to the silicon-substrate, and that they can manipulate the molecule through its phenyl ring assuming an up-right surface conformation. However, these switching is not reversible [189]. A better candidate for a possible switch is ABP. Our group recently

showed that the molecule can be switched between two stable conformations using the tunneling current of the STM-tip and demonstrated that the molecule can selectively passivate and depassivate a DB-pair on the silicon surface. Thus, this molecular switch can possibly provide a logical input in a DB quantum circuit [170].

Furthermore, molecules that contains a C-O double-bond as functional group are known to grow on this substrate in chains, after chemisorption on the surface [184]. These assemblies of organic molecules on the passivated silicon surface are of interest, as they are considered as materials for future semiconductor nanoscale devices [190–197]. The substrate is a perfect template, as the parallel dimer rows are separated by 3.8 Å. Thus, the phenyl-rings of the organic molecules are π -stacked and can act as conducting channel and are thus considered as components for electronic devices [190, 198–201]. Starting from the adsorption of ABP that resulted in the growth of nanostructures on passivated silicon, I will furthermore investigate the switching behavior of ABP on Si(001)-(2x1):H.

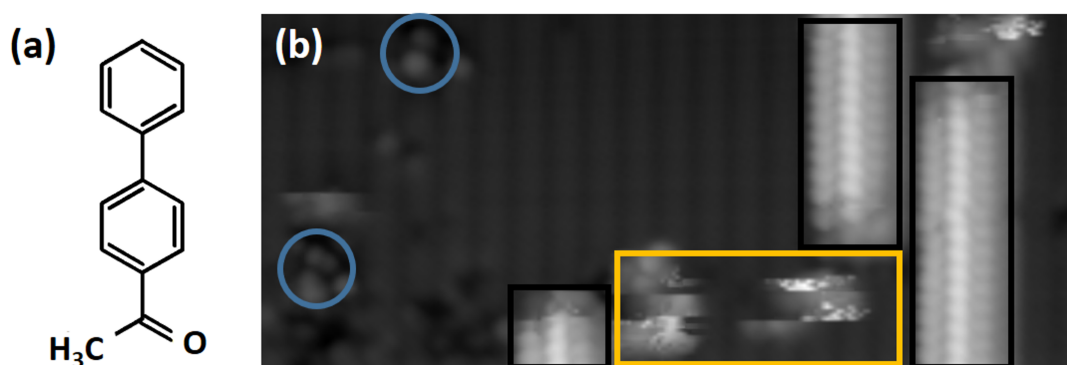


Figure 6.8 – Acetylbiphenyl on passivated silicon. (a) Molecular structure of acetylbiphenyl. (b) Overview STM image of a submonolayer of acetylbiphenyl on passivated silicon. Blue surrounded are single isolated molecules, while molecular wires are marked by black rectangular. The yellow rectangular marks instable imaged molecular nanostructures. (image size: 17.0 nm x 7.5 nm, I=20 pA, V=-2.5 V)

In Fig. 6.8 b a typical overview STM image of the silicon sample after the adsorption of a submonolayer of ABP molecules is presented. Different molecular structures can be identified on the surface and are marked in the image. Unambiguously, I observed molecular nanostructures (molecular lines) that are marked by the black rectangular. ABP molecules in those lines are covalently attached to the surface and grow in lines as

nanostructures. The mechanism of the growth process will be described later within this section. Furthermore, the structures highlighted with the blue circles are probably single ABP molecules on the surface.

Additionally, disorderly grown nanostructures (marked with the yellow rectangular) are present on Si(001)-(2x1):H surface. This growth can be ascribed to the different resonance structures of the C-radical of the ABP molecule after the covalent attachment of the oxygen to a silicon surface atom. This radical enables to extract a hydrogen atom at a certain position on the surface without any control [202]. However, as these structures are only rarely observed and are not of importance for nanoscale devices, I will not discuss the disorderly assemblies in detail.

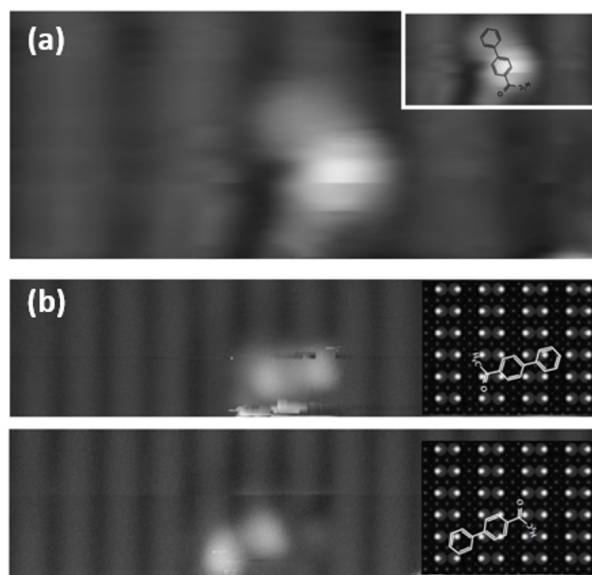


Figure 6.9 – Isolated ABP on passivated silicon. (a) STM image of ABP laying on passivated silicon. As inlay, the chemical structure of ABP is overlaid atop the molecule. (image size: 3.5 nm x 1.5 nm, I=50 pA, V=-2.0 V) (b) ABP laying on passivated silicon. Between the upper and lower image the molecule rotated during imaging. As inlay a schematic of the adsorption of ABP is presented. (image sizes: 10.0 nm x 2.3 nm and 10.0 nm x 2.5 nm, I=11 pA, V=-2.0 V)

Fig. 6.9 a presents a single isolated ABP molecule on the Si(001)-(2x1):H. Due to their lateral size on the surface, it is evident that the molecule lays planar on the surface (see inlay in Fig. 6.9 a). As the molecule can be imaged stable on the surface without motion in comparison to the biphenyl molecule that has no aceto-group on one side, I conclude that the molecule strongly binds to the surface [203]. To stabilize the biphenyl molecule, Dujardin *et al.* constructed a molecular mold by de-passivating a part of the Si(001)-(2x1):H [203]. In the here presented case of ABP, the molecule can be not only imaged stable, but can be also rotated around the anchoring point as shown in Fig. 6.9 b. The aceto-group is known to favor a chemical anchoring on the silicon surface and hence I expect that the molecule anchors to the surface atop a single DB with the oxygen of the molecule. Thus, a surface connection *via* the aceto-group has been achieved on the Si(001)-(2x1):H surface, showing the ability to form a strong molecule-surface connection by using a well-chosen functional group.

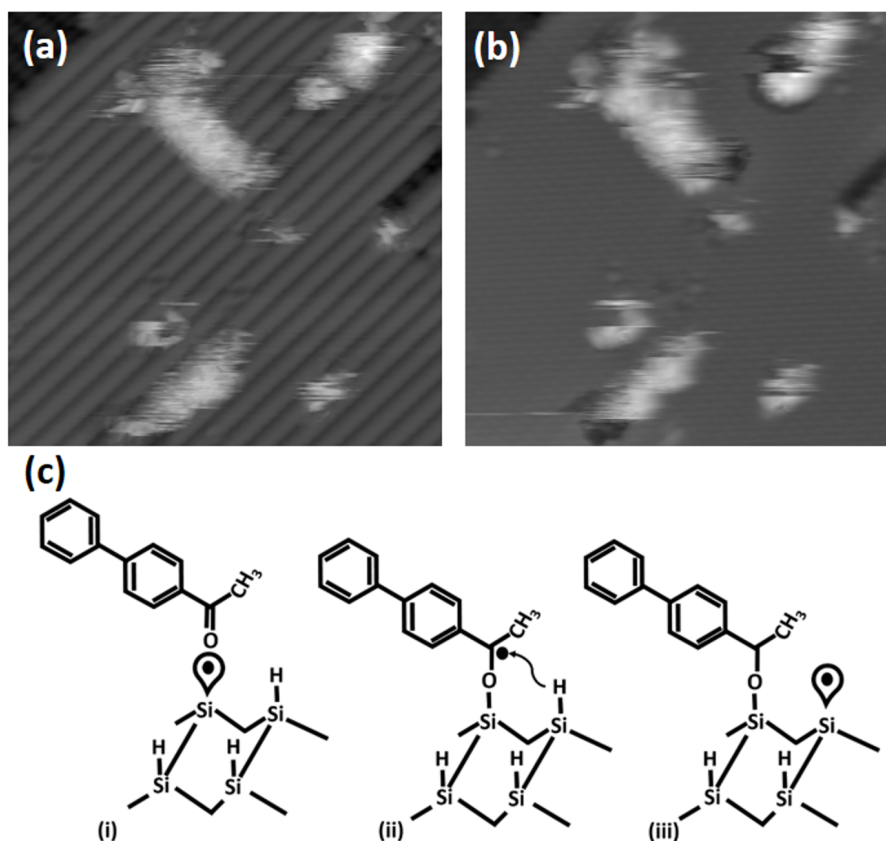


Figure 6.10 – ABP chains grown on Si(001)-(2x1):H along the dimer rows and perpendicular to the dimer rows (image sizes: 15 nm x 15 nm) for (a) a filled state image (I=20 pA, V=-2.0 V) and (b) for an empty state image (I=20 pA, V=+2.0 V). (c) Schematic of the chain reaction mechanism parallel to the dimer row direction of ABP with a DB on the Si(001)-(2x1):H.)

Fig. 6.10 a shows a filled state STM image of two grown one-dimensional ABP chains on passivated silicon. Two growth-directions of the adsorbed molecules can be observed on the passivated silicon. The directions are one along and the other one perpendicular to the dimer row direction. Furthermore, the molecular chains are imaged blurred by STM, possibly due to a strong molecule-tip interaction. An empty state STM image is shown in Fig. 6.10 b and the mechanism of the self-directed growth process is presented in Fig. 6.10 c. This process involves a radical addition reaction between the aceto-group of the ABP molecule and one Si-radical of the surface (DB-position) on the otherwise hydrogenated silicon surface. An oxygen-silicon bond forms, so that the C-O double bond breaks and a single bond is formed. Thus, a carbon-centered radical is created. To ensue a chain reaction, the radical species must succeed in abstracting a hydrogen atom from an adjacent Si-H surface site. This results in the formation of a chemisorbed ABP-molecule and a created new DB (Si-radical site). Thus, a new molecule can be added to the created Si-radical site, resulting in the self-directed chain growth.

Interestingly, similar to the case of acetophenone [184], both growth directions can be observed on-surface, proving that the aceto-group and the resulting carbon-oxygen distance is the driving force for both growth directions. Thus, I can expect that a molecule with a higher complexity and attaches with the aceto-group to the surface would probably also grow parallel and perpendicular to the dimer row directions. After a closer look to the empty state image of Fig. 6.10 b, I could clearly observe protrusions at one of the ends of the molecular chains. Keeping in mind the chain reaction mechanism, resulting in the abstraction of hydrogen atoms and knowing that single DB's are imaged as dark protrusions in empty state images [133], I could determine the growth direction. In this case, the growth starts from the position at that no dark protrusion is imaged and the last ABP molecule of the chain has created a DB-site. It seems to be likely that the molecular chain growth stopped, as no new molecule diffused towards the new created DB, due to the low molecular coverage.

To investigate the possible switching of a molecule, I recorded close-up images of the end-molecules of grown molecular chains (Fig. 6.11 a). To understand the adsorption of the molecule on the surface, Dr. X. Bouju has performed molecular dynamics calculations (Fig. 6.11 b). These calculations show that the molecules have an up-right standing conformation. Thus, for a close tip-sample distance the molecules are imaged blurred due to the strong interaction between tip and molecule, resulting in the continuous motion of the molecule during scanning. This interaction can be reduced by increasing the tip-sample distance. Consequently, the molecular chains can be clearly imaged as shown in Fig. 6.11 a.

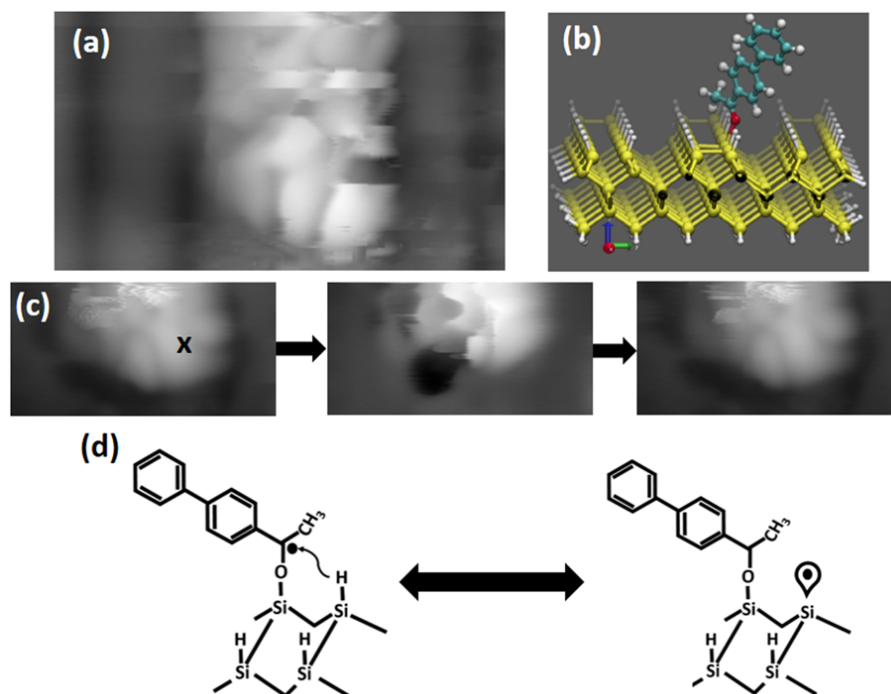


Figure 6.11 – Adsorption and switching of molecules of ABP nanostructures grown on Si(001)-(2x1):H along the dimer rows . (a) Filled state-STM image of the end of a grown ABP line. (image size: 3.5 nm x 2.0 nm, $I=20$ pA, $V=-2.0$ V) (b) Molecular dynamics calculation of ABP adsorbed on passivated silicon. (c) Empty state STM image of the same ABP line. The cross marks a position of a voltage pulse (parameters: $I=18$ pA, $V=2.9$ V, $t=5$ s) leading to a DB formation. This DB can be passivated again by scanning over the area. (image size: 3.0 nm x 1.5 nm, $I=20$ pA, $V=+2.2$ V) (d) Scheme of the passivation and de-passivation of the single DB.

I applied voltage pulses on top of one molecule at the end of a chain, as marked by the cross in Figure 6.11 c. After further imaging the same area, a single DB appears now as a dark protrusion. This shows a hydrogen atom transfer from the surface to the molecule. Similarly, hydrogen transfers within single molecules have been studied extensively using the tunneling current of an STM tip on metal substrates [204, 205]. Furthermore, I could achieve the back-transfer of hydrogen to the surface by scanning over the area. I never observed any back switching during the voltage pulse, but the back transfer is achieved by scanning over the molecule with a decreased tip-sample distance. A scheme of the hydrogen transfer is shown in Fig. 6.11 d.

6.4 Conclusion

In this chapter, I have shown the conversion of triepoxyhexacene into hexacene on the Si(001)-(2x1):H surface. A possible mechanism for this reaction is the deoxygenation favored by the adsorption on a dangling bond defect. Due to the passivation layer, the molecule is decoupled from the silicon substrate. Furthermore, I observed the anchoring of hexacene to a single silicon dangling bond and investigated the electronic interaction. The presented experiment shows a possible route for the on-surface synthesis of large acenes and complex polyaromatic molecules on passivated silicon.

In the second section, I presented the adsorption of the molecule ABP on the same substrate. The single molecules that are probably anchored at a DB lay with their phenyl rings flat on the surface, but the molecule forms mainly assemblies on the surface. I found disorderly assemblies of ABP on Si(001)-(2x1):H, but mostly one-dimensional chains of molecules covalently anchored to the surface. As these molecules are π - π interacting with each other, the π -stacked phenyl rings can be considered as a conducting channel. Beside molecular chains growing parallel to the dimer row direction, ABP is also growing perpendicular to the dimer row direction. Furthermore, a molecule at the end of the grown molecular chain can reversibly passivate and depassivate a single DB by a hydrogen transfer between molecule and silicon surface atom induced by the tip of the STM.

7 Testing a low temperature four-probe STM

For the development of electronics at the atomic scale, new interconnection machines are needed, able to address atomic scale contacts to single molecules. To this aim, CEMES-CNRS in Toulouse installed a new LT-UHV four-probe STM and SEM device. This machine is particularly optimized to perform transport experiments on the atomic scale. During my PhD thesis, I had the chance to work for eight weeks at CNRS participating to the test phase of the experiment. The scientific exchange took place in the frame of the European Project PAMS. In this chapter, I will firstly describe the setup of this machine and present a performance test of the SEM, as well as of the four scanner units of the STM. I will show that each scanner of this machine has the capability to perform experiments with atomic precision, by means of a manipulation experiment of single molecules. This chapter has been partially published as article in the European Physical Journal Applied Physics. Parts of the text and figures are reproduced from reference [187] with permission of the journal.

7.1 Introduction

Understanding the electronic and transport properties of atomic and molecular nanostructures is of fundamental importance [11, 206]. For this purpose, different measurement techniques have been developed in the last 20 years [75, 207–219]. Vertical probe techniques based either on break junction experiments or a pulling of nanostructures from the surface by using a single-probe STM have been presented [220–222]. Thereby a precise junction between the tip and the nanostructure, in this case an atom or a molecule, can be formed [75, 212, 214, 223–226]. However, for the realization of electronic devices, planar surface transport properties need to be investigated and multi-probe experiments need to be performed [227, 228]. These experiments should have an atomic scale precision, while the distance between the probes must be in the small nm-

regime [229–231].

Multiprobe state-of-the-art measurements have been recently used to measure the conductance of self-assembled molecular structures or transport properties of graphene nano-constrains and planar atomic-scale structures [211, 216, 218, 232]. Scanning tunneling potentiometry with two tips that serve as current suppliers, while the third probe operating in the STM mode measures the local potential and provides information about the conductance of nanoscale systems [210, 233, 234]. To characterize the atomic or molecular scale systems on a surface, however, the distance between the probes must be still reduced and the planar transport measurements at the atomic level need a high stability.

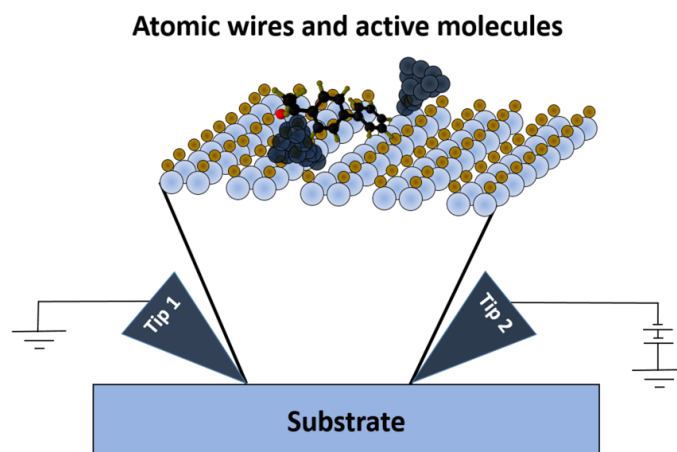


Figure 7.1 – Scheme of a proposed setup of an interconnection machine. The tips that measure the transmission of an atomic wire are positioned with the help of a scanning electron microscope. The active elements that are molecules are placed on this atomic wire on the semiconducting surface.

One possible setup for transport measurements in a planar configuration can be seen in Fig. 7.1. In this experiment, transport measurements along a DB wire constructed on a passivated silicon surface are planned [119, 120, 146, 235]. Thereby two tips would measure the transport through the atomic wire, while a third one would actuate a molecular switch that would change the conductance through the wire significantly. To do that, all tips of the four-probe STM independently need to have a high stability as well as atomic precision. During my stay in Toulouse, I tested the capability of the low temperature UHV four-probe STM developed in collaboration with the company ScientaOmicron and installed in CEMES-CNRS.

7.2 The four-probe STM

In this section, I will describe the four-probe STM and SEM, explaining in detail the different chambers and the composition of the scanner. Fig. 7.2 a shows the vacuum system with its high complexity. On the left-hand side one can see the core of this system composed by the four-probe STM, the cryostat and the SEM located above the STM. Around the STM, a carousel with 28 pockets is placed, that can be used as a storage for tips and samples.

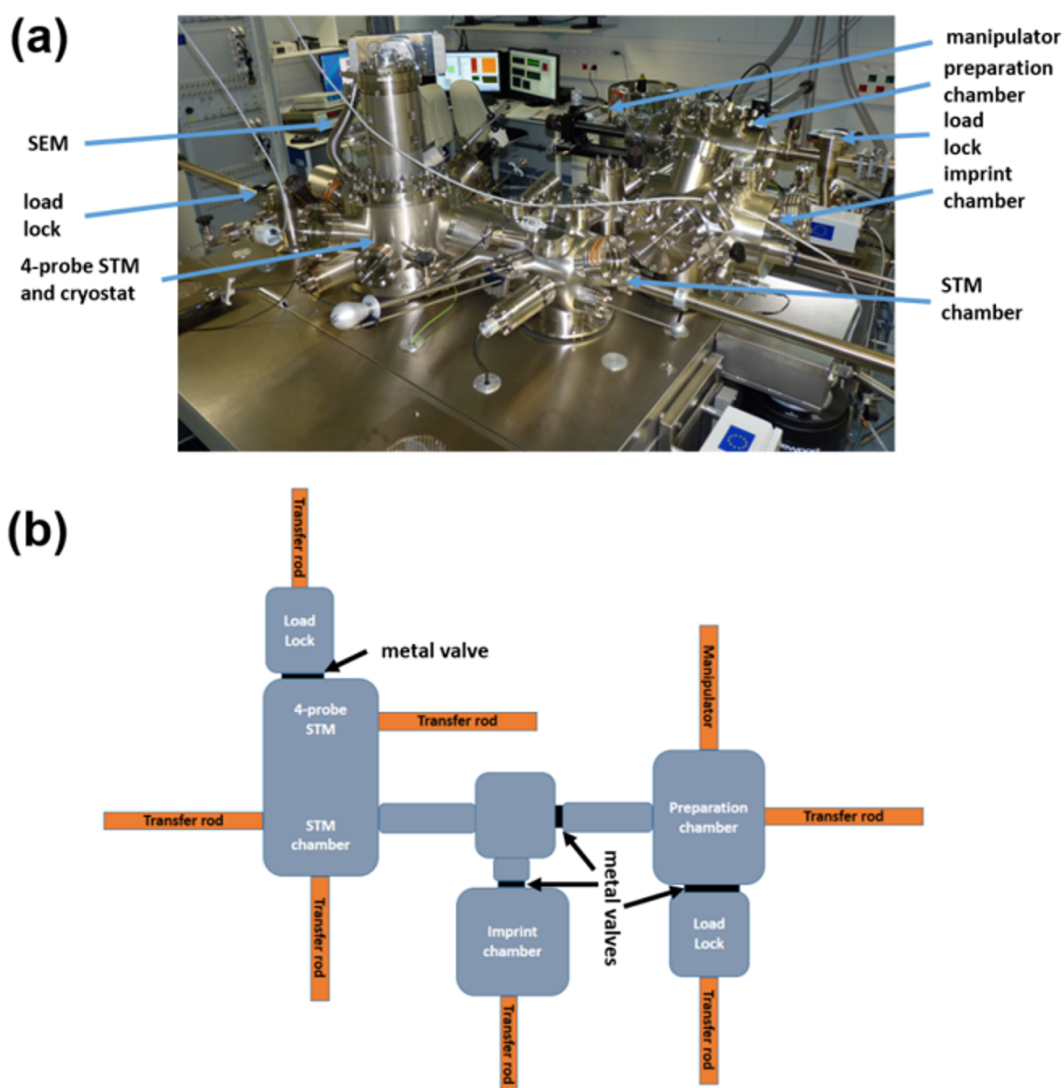


Figure 7.2 – Setup of the vacuum system of the LT-UHV four-probe STM and SEM. (a) Picture of the UHV system used during the work at the Picolab in Toulouse. (b) Corresponding scheme of the UHV system showing the different five chambers: Two load lock, preparation chamber, imprint chamber and STM chamber.

Furthermore, the system contains one chamber that can be used for the sample preparation (right-hand side on Fig. 7.2 a). This chamber is equipped with a manipulator to prepare samples by a pyrolytic boron nitride heater, a sputter gun and several flanges for the connection of evaporators for molecules or metal atoms. At one of these flanges, I connected my home-built evaporator with incorporated crucible for organic molecules. The third chamber of this system is designed for printing in UHV conditions. Printing metal structures on non-conducting surfaces can allow to obtain metallic nanopads contacting atomic and molecular structures on the surface. The nanopads can be formed for example on MoS_2 after self-assembly of the gold atoms to form triangular nanopads. They can be printed onto the substrate of choice and manipulated by the STM to the desired position [236].

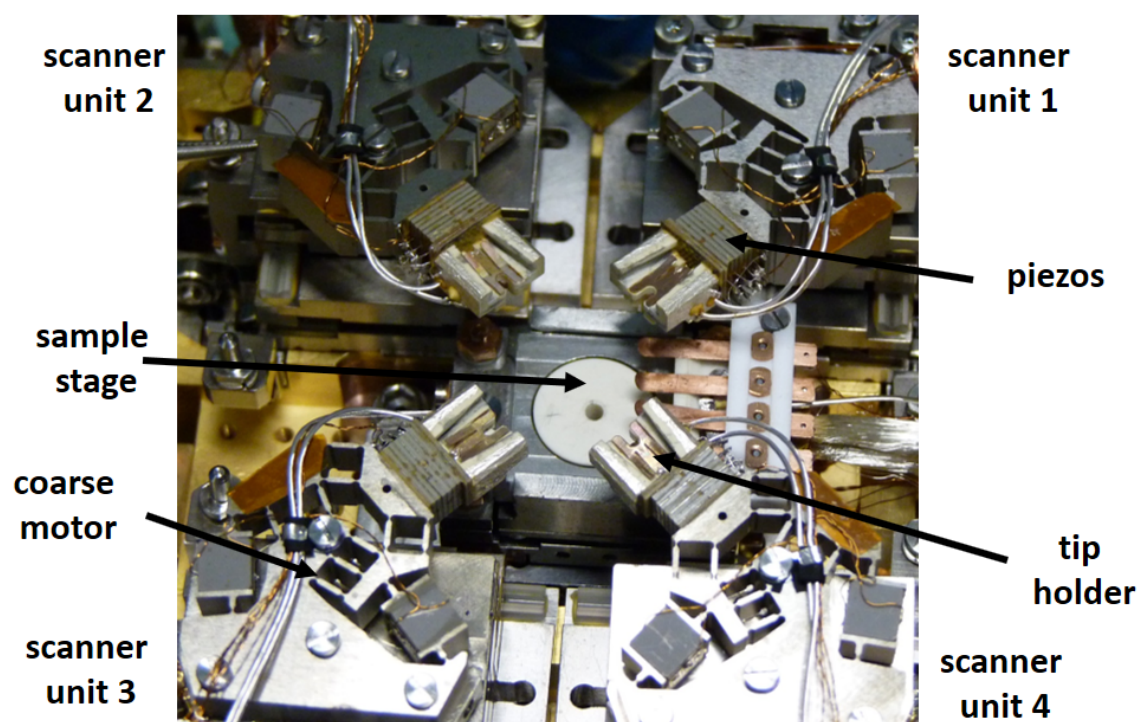


Figure 7.3 – The head of the four-probe STM with its sample stage and its four scanner units.

The nanoprobe has two load locks, one directly positioned at the four-probe STM, mostly used for the insertion of tips in the vacuum system, and one located at the preparation chamber that can be used for the transfer of samples into the UHV. The transfer of sample and tips is performed by a variety of transfer rods within the vacuum chamber. A scheme of the UHV-system is presented in Fig. 7.2 b. It is pumped by a system of three turbopumps and two ion getter pumps that are combined with titanium sublimation pumps. Hence, a pressure in the range of 10^{-10} mbar is obtained.

Figure 7.3 shows the core of the nanoprobe, revealing its complex construction. The sample stage is situated in the center of the photograph. The sample holder can be introduced and locked for a proper vibration isolation. For further isolation, the complete setup can hang freely on a spring system. The four different scanner units can be seen in the Figure and are numbered. The design of the scanners is completely different, as compared to the machine at TU Dresden. While the scanner in Dresden is a Besocke-Beetle type design, the scanner of the four-probe STM consists of sandwiches of piezoelectric actuators. These piezoactuators have a scanning range of $2\ \mu\text{m}$ at low temperatures for each scanner. For the coarse movement of the tips above the sample, each scanner has a motor embedded and has a $4\ \text{mm} \times 4\ \text{mm}$ range. Due to the large size of the nanoprobe, the cryogenic temperature of 5 K can be held only for 38 hours.

7.3 Performance test of the four-probe STM on Au(111)

The main difference between the nanoprobe and standard scanning tunneling microscopes is that this machine is designed to perform electrical four-point measurements, keeping a sub-nanometer stability for the different probes independently. The precise control of the tip positions can be obtained by the navigation using a SEM. The Gemini SEM from the company Zeiss is for that purpose installed on the sample stage. To allow the positioning of two tips in close proximity, the tips cannot be vertical. New tip holders have been designed that can be seen in Fig. 7.4 a. In one of the holders the tip (I) has an angle of 45° with respect to the sample stage. This design enables to visualize the tip apex with the SEM. However, the vertical tips are easier to handle for STM purposes, because quite often during measurements with the 45° tip, some filth drops on the surface. This is probably due to the larger surface area of the tip apex that is in close proximity to the surface. If a part of this apex is contaminated, it can easily happen that

the tip drops some of the contaminants onto the surface. Accordingly, to test the stability of the four-probe STM, mostly vertical tip holders (II) have been used. To combine the two advantages of the ability of imaging the apex with the SEM and to approach this tip with a second tip, while being a good tip for STM purposes, tip holder (III) has been designed. This tip holder has a notch and thus the apex can be visualized when the tip apex is only slightly bended.

The three different tips have been imaged by the SEM of the nanoprobe (Fig. 7.4 b). The SEM overview-image directly show that the tip apex of the 45° tip can be nicely observed, while the vertical tip (II) and (III) are not visible or hardly to identify. Furthermore, when several vertical tips are approached to each other, the approach is limited due to the tip holder itself. As one can see, tip holder (II) and (III) are touching each other in this image, causing perturbations to the STM measurements. Hence, only 45° tips should be used for transport measurements, and not more than one tip with a vertical tip holder (III) can be used at a time.

One 45° tip imaged with the SEM can be seen in Fig. 7.4 c. Here the tip end is very nicely resolved. However, it is not possible to estimate the exact position of the end atoms of the tip apex that are responsible for the tunneling from surface to tip. In the specific case of Fig. 7.4 c, the tip apex is relatively blunt with a large tip apex radius of about 100 nm.

Another critical experimental aspect for the transport measurements is the approach of several tips to each other. Images of the STM tips with the SEM need to be taken before the tips are moved by the coarse motors and thus this approach can be very time-consuming. However, the approach must be fulfilled carefully, as tip crashes of tips need to be prevented. The duration of this approach is of importance, as the cooling down time of the machine is limited to 38 hours. In 7.4 d, close-up SEM images of tips (I) and (III) of Fig. 7.4 b are shown. To approach the two tips to each other, I needed approximately two hours to reach a distance of less than 600 nm. As the scan range of each scanner unit is about 2 μm , the distance is distinctly below the necessary one to finally approach the tips by using the STM scanner units to be able to perform transport measurements in the low nanometer-regime (tenth of nanometer). One problem is that the exact position of the tip apexes is difficult to localize. As the end atom of the tip can be considered at different positions, it can occur that the interaction between the tips become too large. This increases the minimal tip-to-tip distance needed without influencing each other. The exact position of tip apexes with respect to each other can be estimated by comparing STM images.

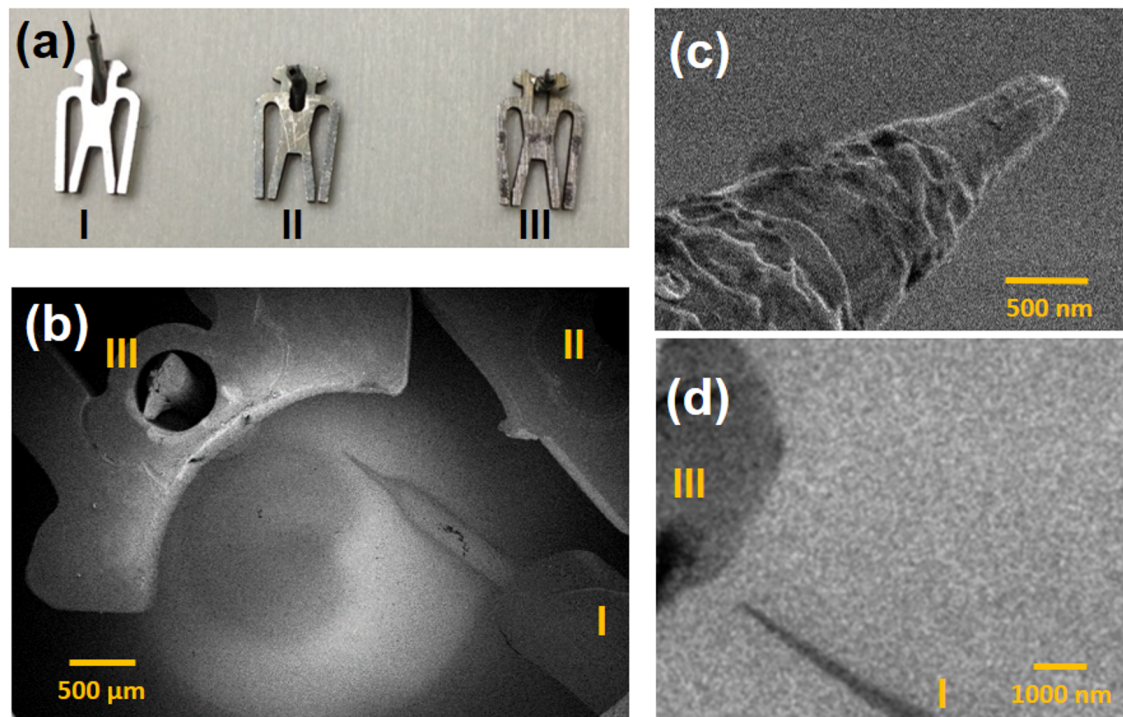


Figure 7.4 – The tips of the four-probe STM. (a) An optical photo of the three different tip holders. I is a 45° tip holder, while II is a vertical tip holder and III is a vertical tip holder with notch. (b) Overview SEM image of the three different W-tips after electron bombardment in UHV, as presented in the photograph in (a). (c) Close-up SEM image of a 45° W-tip. (d) SEM image after approaching tip I and III of (b) up to a tip-to-tip distance of 600 nm.

After having tested the SEM, the next step was to investigate the performance of each STM scanner of the four-probe STM. To do that, I used the Au(111) surface fixed on a standard Omicron sample holder (Fig. 7.5 a). This sample has been introduced into the UHV system of the nanoprobe and has been prepared by sputtering with Ar⁺ at a pressure of 1×10^{-5} mbar and an energy of 1 keV leading to a current of 5 μ A for 30 min. Afterwards, the Au(111) sample was annealed to 500 °C for 20 min. After four cycles of sputtering and annealing, an atomically clean Au(111) surface is obtained.

By each tip of the four-probe STM, I imaged the surface terraces, the mono atomic steps, and the herringbone reconstruction, as shown in Figs. 7.5 b-e. Those images were recorded using all of the four tips alternatively or in parallel. Fig. 7.5 b has been recorded with scanner 1, Fig. 7.5 d with scanner 2, Fig. 7.5 e with scanner 3 and Fig. 7.5 c with scanner 4. Also the ability to scan the surface with atomic resolution could be proven, as shown in Fig. 7.5 f. In this case, tip 4 has been initially used, but also all other scanners could achieve atomic resolution, *i.e.* have a stability of about 6 pm.

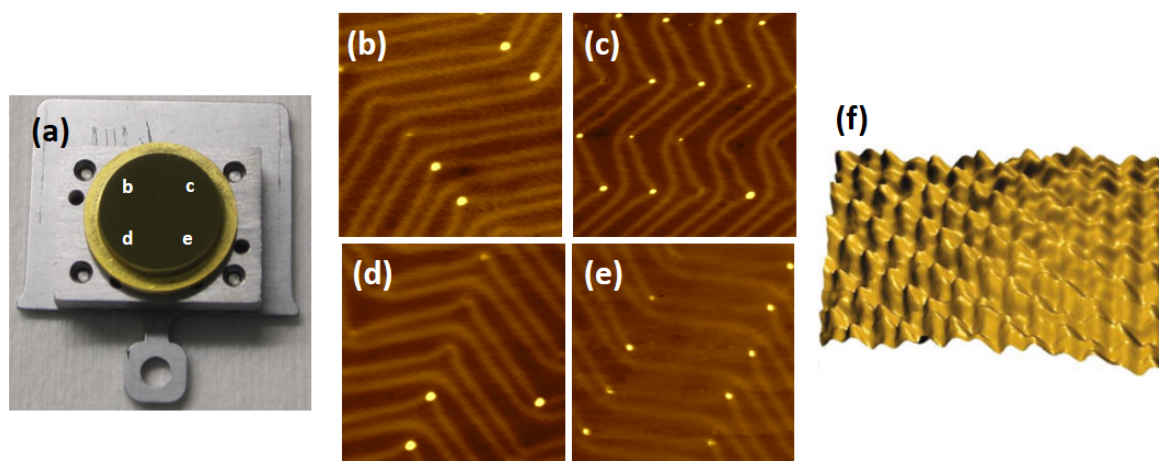


Figure 7.5 – The Au(111) surface measured on the four-probe STM. (a) An optical photo of the Au(111) crystal that is 8 mm in diameter mounted on its UHV sample holder with the STM image locations indicated for (b) to (e). STM images of the prepared Au(111) surface recorded with (b) scanner 1, (c) scanner 4, (d) scanner 2 and (e) scanner 3 on the four-probe STM (image size: 40 nm \times 40 nm, $I=1.0$ nA, $V=1.0$ V). (f) A pseudo 3D STM image with atomic resolution with a corrugation of about 6 pm (Image size: 1.63 nm \times 2.48 nm, $I=300$ pA, $V=200$ mV recorded on scanner 4 on the four-probe STM).

7.4 Manipulation of ABP assemblies

To prove the full capability of the four-probe STM, I tested imaging and manipulation of molecules and supramolecular assemblies with the different tips. To this aim and furthermore to participate at the first Nanocar race [237], I decided to use a known molecular system, the windmill, which is a supramolecular assembly formed by four ABP molecules interacting by hydrogen bonds on the Au(111) surface [34]. A few milligram of ABP powder was introduced in a small crucible of the home-built evaporator, which was mounted on a port of the preparation chamber with a controlling valve at its nozzle. As compared to the preparation in Dresden, it was necessary on the Toulouse instrument to adjust the evaporation time and the crucible temperature because of the different distance between the port nozzle and the Au(111) surface in the two vacuum chambers. To form windmills on the surface, one needs a minimum molecular flux onto the surface. Therefore, the crucible in Toulouse was heated up to 40 °C during the sublimation. The on-surface formation of even more windmill structures was achieved by heating up the Au(111) surface up to 55 °C during 300 s of sublimation.

After the evaporation and heating steps, the Au(111) surface was transferred to the four-probe STM. Low voltage and low feedback-loop currents down to 50 mV and 10 pA were used to image the molecular assemblies on Au(111) using any of the four STM tips. The different observed ABP dimers, trimers and tetramers are presented in Fig. 7.6. After fine tuning of the evaporation, the heating times and the Au(111) surface temperature, it was possible to get 30 % of windmills on the Au(111) surface with a low submonolayer coverage (Fig. 7.6 a). Another tetramer was rarely observed (Fig. 7.6 b), seemed to be very stable and it was not possible to manipulate these tetramers by voltage pulses. The trimers of Fig. 7.6 c and d were found to be very stable, while trimers of Fig. 7.6 e can be converted into trimer d after a voltage pulse. Among all those on-surface assembled molecular structures formed by ABP monomers, the windmill tetramers has shown to have the capability to a stable non-mechanical manipulation in a controlled way by inelastic tunneling electrons.

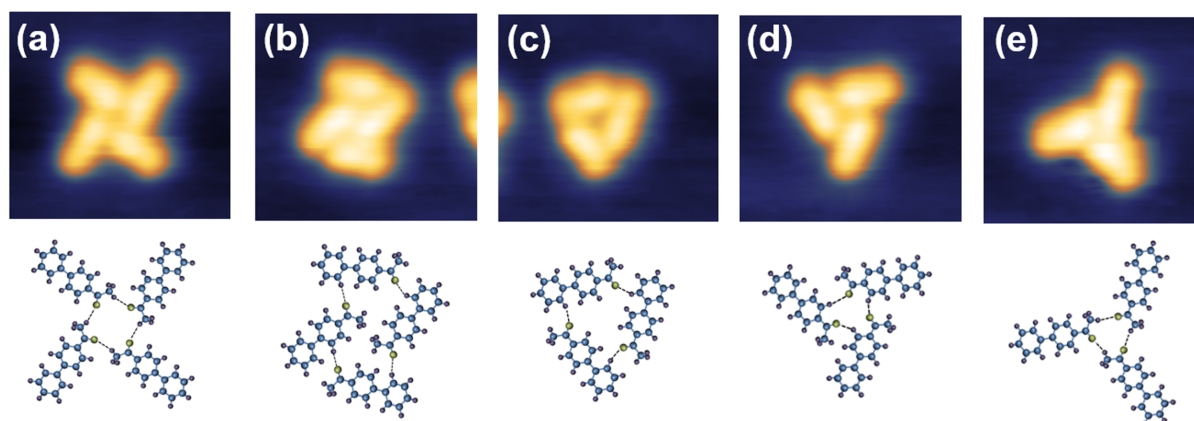


Figure 7.6 – Supramolecular assemblies of ABP observed after sublimation of molecules with a submonolayer coverage. The supramolecular assemblies of (a) and (b) are ABP tetramers with (a) the windmill, while (b) is another stable tetramer of ABP. (c)–(e) are the often observed ABP trimers (image size: 5 nm × 4 nm, I=50 pA, V=500 mV). Underneath the STM images the atomic structure of the respective supramolecular assemblies on Au(111) are presented. With blue: carbon atoms, green: oxygen atoms and purple: hydrogen atoms (dashed lines, the on-surface formed hydrogen bonds).

After the evaporation of ABP and the successful on-surface generation of windmills, the nanostructures are distributed randomly all over the herringbone reconstruction. To controllably manipulate windmills, I was cleaning parts of the herringbone reconstruction to create space. This made also possible to test the lateral manipulation tool of the nanoprobe. For that purpose, the STM tunneling junction resistance must be reduced below $10\text{ M}\Omega$, that the end atom of the tip apex enters in a repulsive interaction.

Thus, I selected the herringbone reconstruction presented in Fig. 7.7 a. I chose this area because no defects were visible at the elbow sites. The successful manipulation of the molecules using the lateral manipulation mode is presented along the yellow arrows on Fig. 7.7 a and show that the machine has the capability and stability to manipulate molecules laterally step by step. Further manipulations to move molecules have been performed by scanning over the area of interest with a low tunneling resistance and resulting in most cases in the pushing of the molecules [238]. The result of the emptied herringbone reconstruction is presented in Fig. 7.7 b. As one can see enough space to manipulate windmills by voltage pulses along the reconstruction of Au(111) is now available.

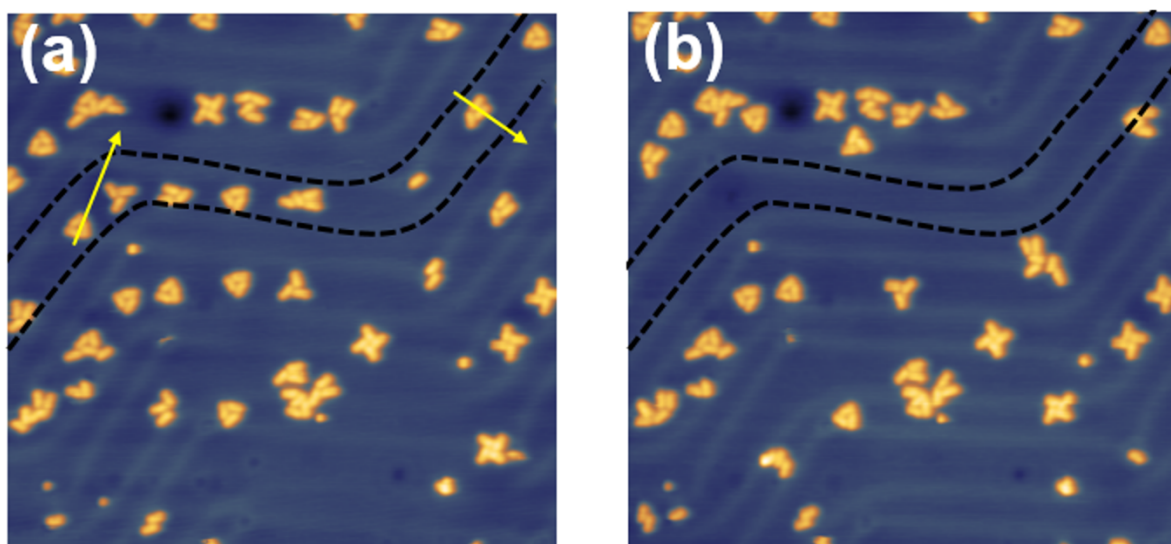


Figure 7.7 – Lateral manipulation of selected supramolecular assemblies. (a) LT-UHV STM image recorded with scanner 2 of the four-probe-STM. (a) STM image before cleaning and (b) after scanning twice over the marked area in a pushing molecular manipulation mode using $I=2\text{ nA}$, $V=50\text{ mV}$ and after manipulating two molecules, as marked with the yellow arrows (manipulation parameter: $I=1.0\text{ nA}$, $V=2.0\text{ V}$, $t=5\text{ s}$) (image sizes: $50\text{ nm} \times 50\text{ nm}$, $I=20\text{ pA}$, $V=500\text{ mV}$).

Single tip LT-UHV-STM images and inelastic tunneling current manipulation of the windmill tetramers have been already studied [34, 186]. As the wings of the windmill are not aligned with the fcc domain, an alternated zigzag motion is needed to move it in a defined direction. This motion can be triggered by applying voltage pulses on two different wings of the molecular assembly. To determine the values of the voltage pulses needed for translation or rotation, one needs to consider the electronic spectra of the molecular tetrameric assembly. At positive bias voltage, an electronic resonance at +2.3 V is observed [34]. It is necessary to tunnel into this molecular resonance to induce the movement. Due to the broadness of this resonance, a voltage of +1.8 V is already enough to tunnel into the resonance and to trigger the motion (as described in [34]). For higher voltage values exceeding +2.5 V, hydrogen-bonds break and the windmill is destroyed. In this case, a resonant tunneling phenomenon occurs through the excited states and the electrons are mainly transferred elastically through the excited ABP wing. However, only a small amount of those electrons are not transferred elastically. Since even for 10 pA of current, there are millions of electrons transferred per second through ABP, this leads to an increase of the vibrational energy of the excited state [239]. Normally, this energy excess is redistributed inside the molecular structure and then to the surface.

For the windmill structure and certainly due to the relative independence of the electronic structure of the four ABP molecules in the tetramer, part of this vibrational energy is consumed by the windmill to move from one minimum energy position on the surface to the next one without destruction of the assembly. For this purpose, one has also to wait long enough to accumulate the vibrational energy in the excited states. In Fig. 7.8 a successful manipulation over a distance of 5 nm is the result of cumulating 19 pulses of 8 s. Thereby, I could observe a rotation (from Fig. 7.8 a to Fig. 7.8 b), movement in the direction of the tip (from Fig. 7.8 c to Fig. 7.8 d) and the motion away from the tip (from Fig. 7.8 e to Fig. 7.8 f). This is in good agreement with the work presented in [34].

Further testing the four-probe STM, I was able to successfully manipulate molecules with one tip and image at the same time with another tip on another region of the gold surface without the tips influencing each other. Only at high voltages ($V > +3.0$ V) the tips interfered by a crosstalk, resulting in an increased noise level.

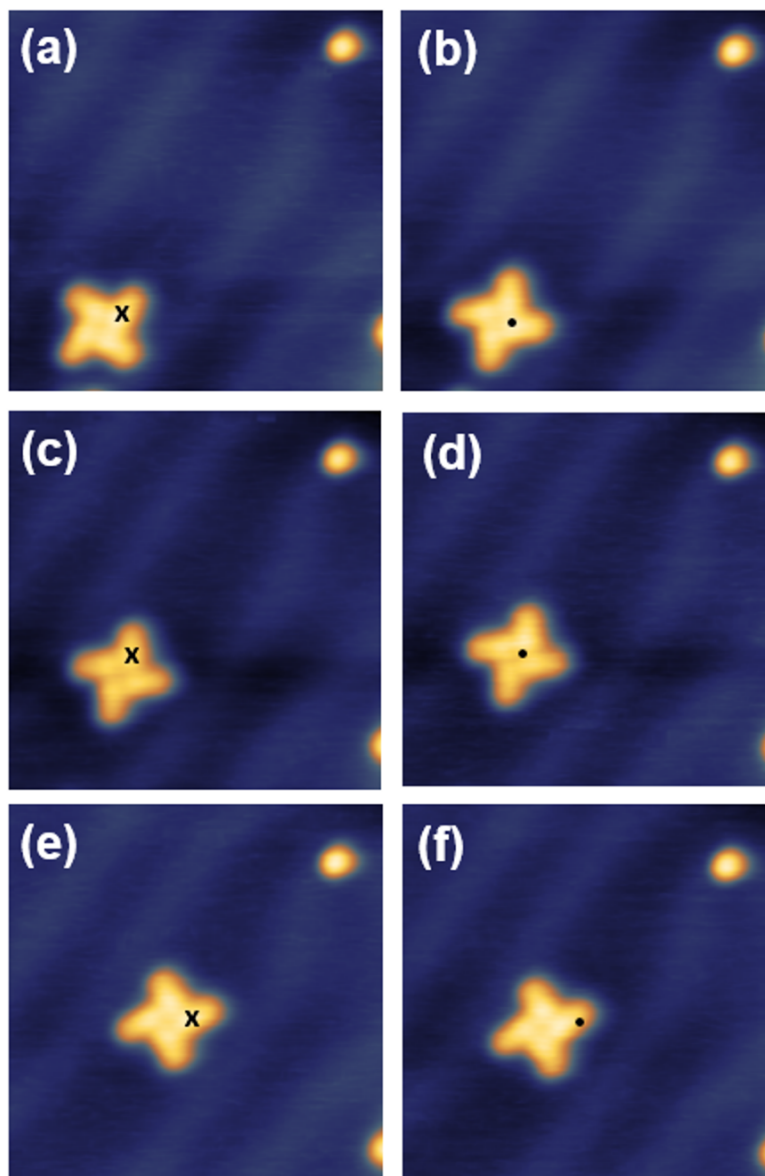


Figure 7.8 – Typical events of motion after voltage pulses are presented in figures from (a) to (f). The cross marks the position of the voltage pulse before and the dot is marking the position of the voltage pulse after the motion of the molecule. From (a) to (b) a rotation of the assembly took place. From (c) to (d), the molecule was moved in the direction to the STM tip. From (e) to (f) the molecule was moved away from the STM tip (image size 10.5 nm × 10.5 nm, $I=0.05$ nA, $V=500$ mV; manipulation parameter: $I=1.0$ nA, $V=2.3$ V, pulse time $t=8$ s).

However, on the four-probe STM not every voltage pulse lead to a controlled manipulation event. The most frequently observed uncontrolled event occurred when the voltage pulse was accidentally too large or when intentionally the pulse was larger to pass over a narrow turn. After one of these pulses, a trimer was formed as presented in Fig. 7.9 b and additionally the fourth ABP molecule was going in between two wings of this

newly formed trimer. After further applying voltage pulses, generally in the center of the molecule with a bias voltage of around 2.1 V, the assembly restructured to form again the windmill with four hydrogen-bonded ABP molecules (Fig. 7.9 c). This recovering was successful in more than 90 % of the cases.

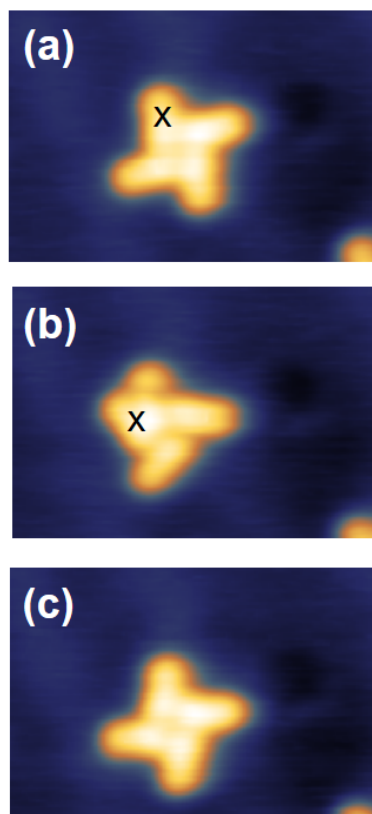


Figure 7.9 – Reorganization of a supramolecular assembly. (a) An intact molecule-vehicle attempted to be manipulated by applying a voltage at the position marked by the cross for moving the assembly (manipulation parameter: $I=1.1$ nA, $V=2.3$ V, $t=8$ s) and (b) the same molecule reorganized after this voltage pulse, another voltage pulse was applied on the molecular assembly, the position is marked with the cross (manipulation parameter: $I=0.5$ nA, $V=2.0$ V) (image sizes: 8.4 nm \times 5.4 nm, $I=0.05$ nA, $V=500$ mV). (c) The final conformation of the windmill molecule after the bias voltage pulse in (b). The only difference between (a) and (c) is a small rotation of the molecule of about 20° .

A further annoying event happened when the windmill molecule suddenly jumped to the tip and reappeared in the next STM image at another location on the surface. There is not yet an explanation of this phenomenon, which fortunately is quite rare. One possible interpretation is that after a large number of bias voltage pulses, the atomic structure at

the tip apex is re-organized. This creates a different inhomogeneous electric field pattern at the end of the tip, which can attract one windmill on the tip apex. Another possible explanation could be a changed set point during the trace back of the tip. Thus, the molecule is moved unintentional with the lateral manipulation tool of the STM.

Another interesting cumulative effect occurs when the windmill is stacked at a turn. In this case, it happens that a too large number of pulses destroys the supramolecular assembly. This is because the vibrational energy accumulates in the excited states and is passing over the reaction barrier for detachment of some wings from the windmill tetramer. Fortunately, this phenomenon never happened during a manipulation along the gold reconstruction, but only when stacked at the elbow site. However, at least 50 voltage pulses could be cumulated without any destruction of the windmill structure.

7.5 Conclusion

In this chapter, I described the experiments performed to test the performance of the LT-UHV four-probe STM head with SEM by the company ScientaOmicron. I described the setup of the machine with its specific characteristics. Firstly, I tested the SEM and the duration of the approach of two tips to each other to about 600 nm. This approach worked in a feasible time far under the cooled down time of the STM at 5 K that is 38 hours. The approach of several tips with the SEM to each other can be destructive for hydrogenated surface, as the electron beam has an energy of a few keV. At these conditions, a dehydrogenation of the passivated surface would occur. Possible solutions for a non-destructive approach would be to use an optical microscope that would however complicate the approach of the tips, as the resolution would be not high enough. Alternatively, one can use a shutter during the approach with the SEM. The approach of more than two tips must be tested and improved relating to the timing and the minimum distance between the tips must be further decreased and is now at 20 nm.

Secondly, I tested the STM capabilities of the machine. For that purposes, I prepared successfully an Au(111) surface in the preparation chamber and used the four different tips of the four-probe STM to image the herringbone reconstruction and subsequently imaged the surface with atomic resolution, which needs a stability of about 6 pm. This illustrates that this new instrument, containing four independent LT-UHV-STM has a high stability and a low noise level. After this stability test, I repeated some manipulation experiments on supramolecular assemblies of ABP molecules on Au(111). The

results obtained on the LT-UHV-STM in Dresden could be reproduced with every tip of the four-probe STM. Thereby, I could show that the machine has the capability of manipulating molecules and molecular assemblies by the lateral manipulation mode of an STM and to move the assemblies by voltage pulses along the herringbone reconstruction. Especially for the manipulation of assemblies by voltage pulses, the machine needs a high precision, as the pulse must be applied locally on the windmill. In addition, I could show that the tips do not influence each other during voltage pulses up to about 3.0 V and that measurements on other tips are simultaneously possible during these manipulations. Summarizing, I have performed imaging and could show that manipulation is possible on all of the four tips available on the four-probe STM. No difference in performances were noticed between the different tips.

8 Summary and outlook

Chemical synthesis of designed molecular species and atomic and molecular manipulation are of importance to investigate the application of single organic molecules as active electronic elements. The underlying surface can be considered as a part of the nanodevice that should have a small buffer layer ensuring the decoupling, but also the capability to build atomic wires on this surface. In my PhD thesis, I used low-temperature ultrahigh vacuum scanning tunneling microscopy, which provides a clean and noise-free environment for the different issues. Additionally, the experimental method has the capability to image molecular species with high resolution to identify chemical products after on-surface reactions. By STM it is also possible to precisely control and manipulate molecular and atomic structures.

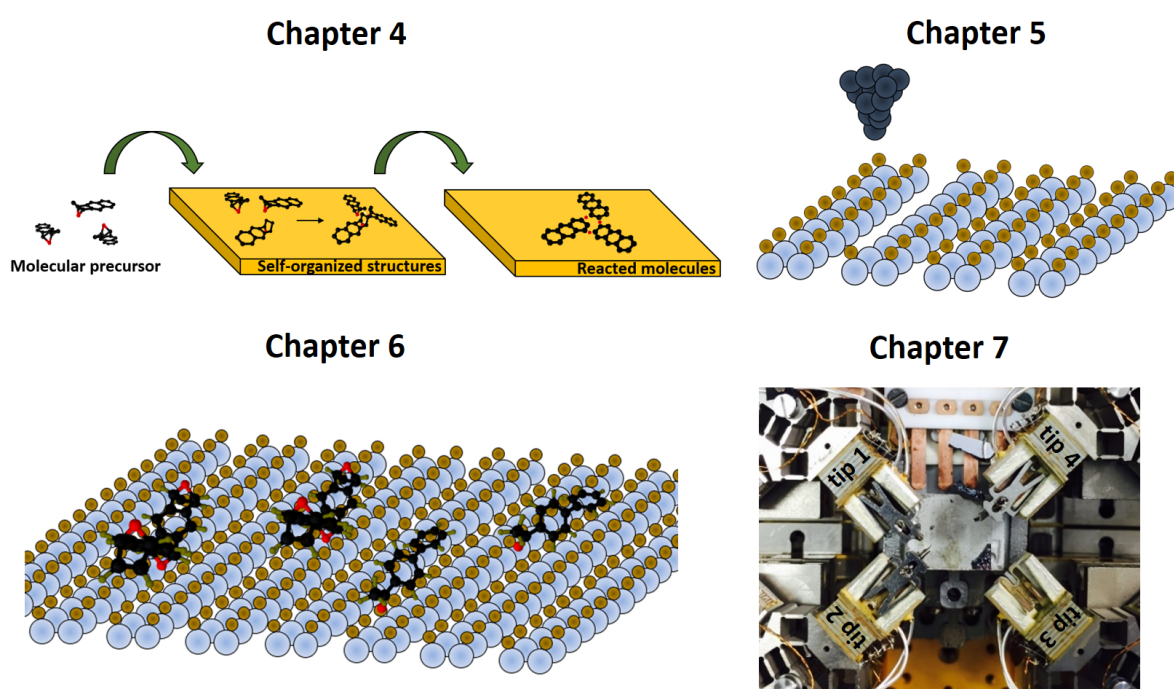


Figure 8.1 – Graphical summary of the experimental results subdivided into the four main experimental chapters.

The main results obtained in the dissertation are summarized graphically in Fig. 8.1. In chapter 4, two molecules are investigated on the Au(111) surface. Reaction products after on-surface synthesis have been obtained *via* annealing. In particular, I obtained bisanthrene molecules and the non-alternant polyaromatic hydrocarbon diindenopyrene on Au(111) and investigated their electronic properties.

The next chapter deals with the preparation of a semiconducting surface with a hydrogen layer as a small buffer layer, the Si(001)-(2x1):H surface and its characterization. The surface has a band gap, while electronic states of DB-defects have defined electronic states in the surface band gap. Furthermore, this substrate can be capped with a second passivated silicon surface, allowing to be transferred outside vacuum without an increasing of the defect density of the surface. Also, I could achieve DB defects controllably by applying voltage pulses using the tip of the STM and produced with this method atomic wires with DB defects.

Chapter 6 deals with molecules on the Si(001)-(2x1):H surface and the investigation of on-surface reactions to generate PAH's on less-reactive substrates. Thus, I have presented the on-surface generation of hexacene by a surface-assisted reduction. Secondly, I have shown that ABP molecules can form highly organized nanostructures on this surface. The formed one-dimensional molecular chains interact *via* its π -stacked phenyl rings that are considered as conducting channel. Also, I have shown that a single ABP molecule acts as a switch as one can reversibly passivate and depassivate a single DB by a hydrogen transfer.

The last experimental chapter deals with the realization of transport measurements of molecular scale devices. For that purpose, I had the chance to test the new low-temperature four-probe STM installed at CEMES-CNRS. I could show the possibility to approach two tips to each other by using the SEM of the four-probe STM. As the actuation needs an atomic precision for all the different tips at the same time, I could show the high stability of this scanning probe microscope. Therefore, assemblies of ABP molecules have been imaged and manipulated by any of the four tips using the lateral manipulation mode, as well as by voltage pulses. The stability of the system has been proven as all tips are working independently and in parallel.

The results of this thesis promote the development of molecular-based devices that can open new routes to applications at the nanoscale. The experimental results of the four chapters represent by themselves small steps towards the realization of atomic- and molecular-scale electronics, but need to be merged together in the future. As most of the successful chemical reactions are obtained on coinage metal surfaces (Chapter 4), transfer methods of molecular structures need to be investigated and further reactions

must be explored on other substrates. Hence, one could for example use these synthesized molecular structures on insulating or semiconducting surface. Furthermore, the molecules (Chapter 6) that have been investigated can be integrated into the obtained atomic wires on passivated silicon (Chapter 5) and their functionality tested. Hence, one needs to fulfill transport experiments and test the functionality of the different molecular species in these planar electronic scale devices. However, molecular scale devices are further afar and still several studies need to be done to better understand processes at the atomic and molecular scale.

The substitution of the efficient silicon-based technology that is a system elaborated over several decades is ambitious and will be possible only if molecular electronics exhibits clear advantages. A more realistic approach is the integration of the nanoscale devices into the existing technology, which would be called a hybrid technology. Thus, the use of the silicon surface is a smart choice, as the silicon-based technology also makes use of this substrate. The CMOS-technology would not be replaced, but only single components would be added additionally that make use of molecular scale electronics.

9 Appendix

9.1 Dibromo-dimethyl-naphthalene on Au(111)

For another reaction on surfaces, I tested a precursor molecule that has a naphthalene core with two bromine atoms and two methyl groups (see Fig. 9.2 b) [240]. After sublimation of the precursor molecule onto Au(111), the surface will be annealed to trigger a chemical reaction. The precursor molecules form a large honeycomb structure, as seen in Fig. 9.1 a. In this Figure also a fast-fourier transformation (FFT) of the position framed with the black rectangle is presented. I observe clearly six reflexes in the FFT and can conclude that the structure has a long-range order and the network is hexagonal. In the close-up STM image (Fig. 9.1 b), a single honeycomb is presented. By lateral manipulation, I could prove that such a structure contains 12 single molecules. The molecular structure is partially superimposed within the image and I propose that the molecules form these honeycomb structures by a halogen-hydrogen interaction.

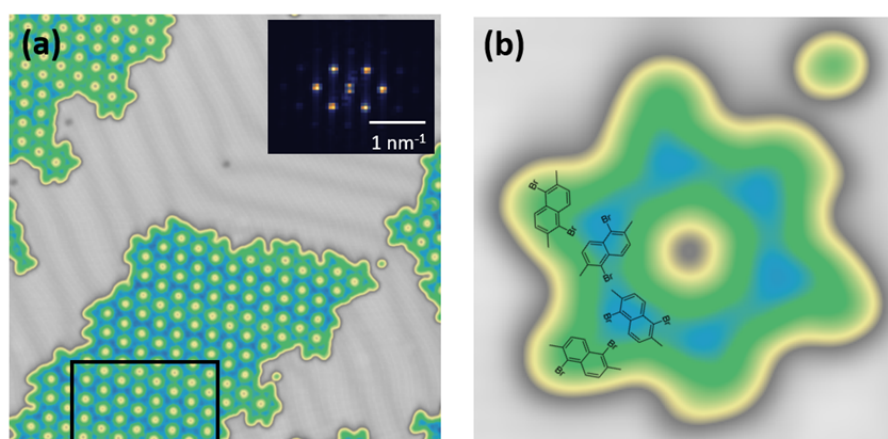


Figure 9.1 – Dibromo-dimethyl-naphthalene on Au(111) before annealing. (a) Overview STM-image. The molecules are forming a honeycomb network after deposition. As inset the FFT of the position marked with the rectangle can be seen. (Image: $V=0.5$ V, $I=50$ pA, size: 40 nm x 40 nm) (b) Close-up STM image of an isolated honeycomb. A part of the molecular structure is superimposed. (Image: $V=0.1$ V, $I=50$ pA, size: 5 nm x 5 nm)

The debromination is firstly observed after annealing the sample to a temperature of 120 °C. However, not all monomers are reacted after this annealing step. Thus, I still find regions with honeycomb networks that are formed by the precursor molecules. Indeed, no covalently coupled molecules are observed. Instead, additionally to the honeycomb network densely packed islands of molecules are present (see Fig. 9.2 a). In these islands, the formed molecules are debrominated. Again, I used lateral manipulation to test whether the molecules are covalently bonded. As I could easily separate the molecules (possible at a tunneling resistance of $R = 10 \text{ M}\Omega$), I can exclude covalent bonding between them. I assume that instead of the covalent coupling a passivation of the radical sites of the precursor molecules occurs. This passivation is due to residual hydrogen that is present in the vacuum chamber. From this, I can conclude that our densely packed molecular islands consists of dimethyl-naphthalene and I superimposed the molecular structure within one of these islands. For this molecule, the Ullmann-coupling is not working, but the radical sites are passivated with hydrogen as shown in Fig. 9.2 b. To validate that the formation of Ullmann-coupled structures is not possible, I also annealed the sample to 150 °C and 200 °C, subsequently. After annealing to 150 °C only densely packed islands can be observed and further annealing leads to a desorption of the molecules. Similar results are obtained by sublimating molecules on the hot surface.

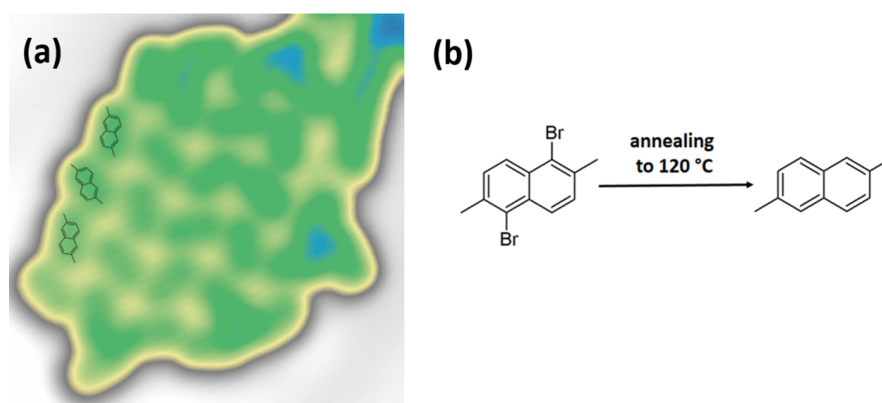


Figure 9.2 – Dibromo-dimethyl-naphthalene on Au(111) after annealing to 120 °C. (a) Close-up STM image of a densely packed structure and superimposed the molecular structure of dimethyl-naphthalene. (Image: $V=0.5 \text{ V}$, $I=50 \text{ pA}$, size: $7 \text{ nm} \times 7 \text{ nm}$) (c) Chemical reaction after debromination.

9.2 Epiminotetracene on Au(111)

In this experiment, I used a tetracene-precursor that has two epimino-groups within the molecular backbone as shown in Fig. 9.3 a. The corresponding STM image of these isolated precursor molecules features a dumbbell-shaped topography. The protruding parts of the molecules can be assigned to the epimino-groups. After annealing the Au(111) surface to 170 °C for five minutes, I observe different planarized molecular species on surface (Figs. 9.3 b-e, upper row).

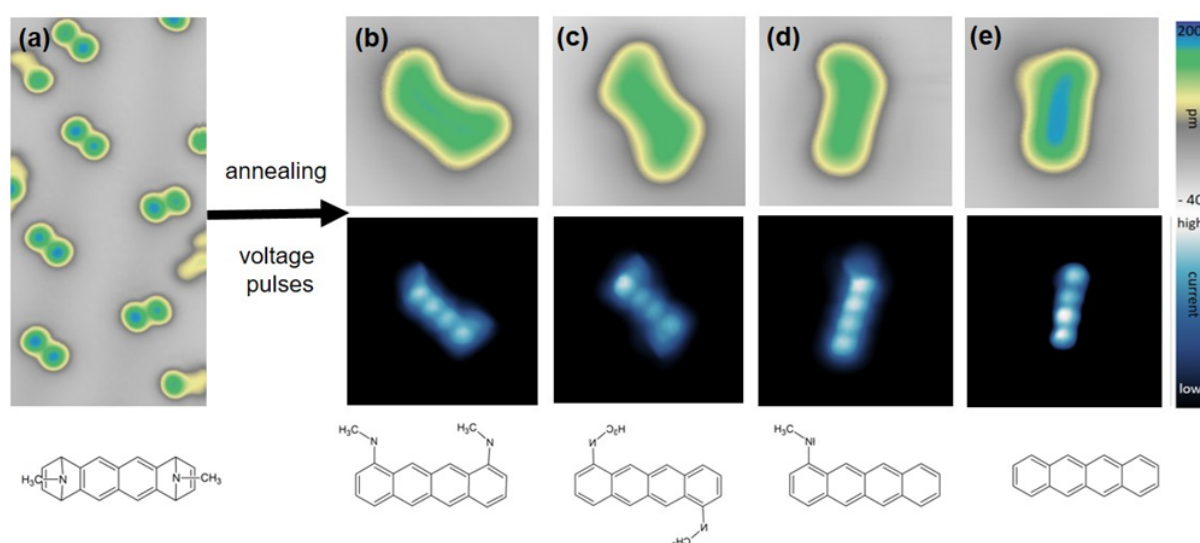


Figure 9.3 – The molecule Tn(NCH₃)₂. (a) Chemical structure of the precursor molecule and overview STM image of a submonolayer of precursor molecules on Au(111). (image size: 6.25 nm x 12.5 nm, V=-0.56 V, I=73 pA) (b)-(e) Top row: Constant-current STM images of the different species found after annealing to 170 °C. (V=0.5 V, I=100 pA, image sizes: 2.5 nm x 2.5 nm); Middle row: Constant-height STM images of the same molecules achieved with a CO-functionalized tip. (image sizes: 2.5 nm x 2.5 nm, V=10 mV); Bottom row: Proposed chemical structures of resulting molecules.

To understand the different reacted molecular species, I functionalized the tip with a single CO molecule, and enhanced the resolution of the STM images by measuring over the molecules in the constant-height mode (Figs. 9.3 b-e, middle row). From these images the benzene-rings of the tetracene unit can be nicely resolved. The molecules of Figs. 9.1 b-d have a site-group at the outer benzene-rings. It seems that within the planarized molecules the epimino-group can be either cleaved from one carbon atom leading to the formation of a benzene ring with an amide-group at the site or can be cleaved completely from the molecule leading to the formation of an acene. The pre-

sumed molecular structures of the reacted molecules are presented in the bottom row of Figs. 9.3 b-e. Furthermore, it was also possible to trigger this reaction by voltage pulses with voltages above 3.0 V.

Bibliography

- [1] G. E. Moore. Cramming more components onto integrated circuits, reprinted from electronics, volume 38, number 8, april 19, 1965, pp.114 ff. *IEEE Solid-State Circuits Society Newsletter*, 11(3):33–35, 2006.
- [2] H. Bu. 5 nanometer transistors inching their way into chips. <https://www.ibm.com/blogs/think/2017/06/5-nanometer-transistors/>, 5.June 2017.
- [3] F. Schwierz, H. Wong, and J. J. Liou. *Nanometer CMOS*. World Scientific Publishing Co., Inc., 2008.
- [4] R. M. Metzger. Quo vadis, unimolecular electronics? *Nanoscale*, 10(22):10316–10332, 2018.
- [5] A. Aviram and M. A. Ratner. Molecular rectifiers. *Chem. Phys. Lett.*, 29(2):277–283, 1974.
- [6] J. C. Cuevas and E. Scheer. *Molecular Electronics: An introduction to theory and experiment*. Molecular Electronics. 2010.
- [7] F. Moresco, G. Meyer, K.-H. Rieder, H. Tang, A. Gourdon, and C. Joachim. Conformational changes of single molecules induced by scanning tunneling microscopy manipulation: A route to molecular switching. *Phys. Rev. Lett.*, 86(4):672–675, 2001.
- [8] R. M. Metzger. Electrical rectification by a molecule: the advent of unimolecular electronic devices. *Acc. Chem. Res.*, 32(11):950–957, 1999.
- [9] M. Elbing, R. Ochs, M. Koentopp, M. Fischer, C. von Hänisch, F. Weigend, F. Evers, H. B. Weber, and M. Mayor. A single-molecule diode. *Proceedings of the National Academy of Sciences of the United States of America*, 102(25):8815–8820, 2005.

- [10] D. K. James and J. M. Tour. *Molecular Wires and Electronics*, pages 33–62. Springer Berlin Heidelberg, Berlin, Heidelberg, 2005.
- [11] C. Joachim, J. K. Gimzewski, and A. Aviram. Electronics using hybrid-molecular and mono-molecular devices. *Nature*, 408:541, 2000.
- [12] I. Duchemin and C. Joachim. A quantum digital half adder inside a single molecule. *Chem. Phys. Lett.*, 406:167–172, 2005.
- [13] L. Gao, Q. Liu, Y. Y. Zhang, N. Jiang, H. G. Zhang, Z. H. Cheng, W. F. Qiu, S. X. Du, Y. Q. Liu, W. A. Hofer, and H. J. Gao. Constructing an array of anchored single-molecule rotors on gold surfaces. *Phys. Rev. Lett.*, 101(19):197209, 2008.
- [14] G. Franc and A. Gourdon. Covalent networks through on-surface chemistry in ultra-high vacuum: state-of-the-art and recent developments. *Phys. Chem. Chem. Phys.*, 13(32):14283–14292, 2011.
- [15] R. Lindner and A. Kühnle. On-surface reactions. *ChemPhysChem*, 16(8):1582–1592, 2015.
- [16] J. Méndez, M. F. López, and J. A. Martín-Gago. On-surface synthesis of cyclic organic molecules. *Chem. Soc. Rev.*, 40(9):4578–4590, 2011.
- [17] W.-H. Soe, C. Manzano, N. Ranaud, P. D. Mendoza, A. D. Sarkar, F. Ample, M. Hliwa, A. M. Echavarren, N. Chandrasekhar, and C. Joachim. Manipulating molecular quantum states with classical metal atom inputs: Demonstration of a single molecule nor logic gate. *ACS Nano*, 5(2):1436–1440, 2011.
- [18] D. Skidin, O. Faizy, J. Krüger, F. Eisenhut, A. Jancarik, K.-H. Nguyen, G. Cuniberti, A. Gourdon, F. Moresco, and C. Joachim. Unimolecular logic gate with classical input by single gold atoms. *ACS Nano*, 12(2):1139–1146, 2011.
- [19] G. Binnig, H. Rohrer, C. Gerber, and E. Weibel. Surface studies by scanning tunneling microscopy. *Phys. Rev. Lett.*, 49(1):57–61, 1982.
- [20] G. Binnig, H. Rohrer, C. Gerber, and E. Weibel. 7 x 7 reconstruction on si(111) resolved in real space. *Phys. Rev. Lett.*, 50(2):120–123, 1983.
- [21] K. Morgenstern, N. Lorente, and K.-H. Rieder. Controlled manipulation of single atoms and small molecules using the scanning tunnelling microscope. *Phys. Status Solidi B*, 250(9):80, 2013.

- [22] G. Binnig, H. Rohrer, C. Gerber, and E. Weibel. Tunneling through a controllable vacuum gap. *Appl. Phys. Lett.*, 40(2):178–180, 1982.
- [23] R. Wiesendanger, editor. *Scanning tunneling microscopy (STM)*, pages 11–209. Cambridge University Press, Cambridge, 1994.
- [24] B. Voigtländer. *Scanning Probe Microscopy: Atomic Force Microscopy and Scanning Tunneling Microscopy*, pages 1–11. Springer Berlin Heidelberg, Berlin, Heidelberg, 2015.
- [25] J. Bardeen. Tunnelling from a many-particle point of view. *Phys. Rev. Lett.*, 6(2):57–59, 1961.
- [26] L. Gross, N. Moll, F. Mohn, A. Curioni, G. Meyer, F. Hanke, and M. Persson. High-resolution molecular orbital imaging using a p-wave stm tip. *Phys. Rev. Lett.*, 107(8):086101, 2011.
- [27] B. Voigtländer. *Scanning Probe Microscopy: Atomic Force Microscopy and Scanning Tunneling Microscopy*, pages 309–334. Springer Berlin Heidelberg, Berlin, Heidelberg, 2015.
- [28] N. Pavliček and L. Gross. Generation, manipulation and characterization of molecules by atomic force microscopy. *Nat. Rev. Chem.*, 1:0005, 2017.
- [29] J. Krüger, F. García, F. Eisenhut, D. Skidin, J. M. Alonso, E. Guitián, D. Pérez, G. Cuniberti, F. Moresco, and D. Peña. Decacene: On-surface generation. *Angew. Chem., Int. Ed.*, 129(39):12107–12110, 2017.
- [30] F. Moresco. Manipulation of large molecules by low-temperature stm: model systems for molecular electronics. *Phys. Rep.*, 399(4):175–225, 2004.
- [31] B. C. Stipe, M. A. Rezaei, and W. Ho. Inducing and viewing the rotational motion of a single molecule. *Science*, 279(5358):1907–1909, 1998.
- [32] J. Henzl, M. Mehlhorn, H. Gawronski, K.-H. Rieder, and K. Morgenstern. Reversible cis–trans isomerization of a single azobenzene molecule. *Angew. Chem., Int. Ed.*, 45(4):603–606, 2006.
- [33] T. Kudernac, N. Ruangsapapichat, M. Parschau, B. Maciá, N. Katsonis, S. R. Harutyunyan, K.-H. Ernst, and B. L. Feringa. Electrically driven directional motion of a four-wheeled molecule on a metal surface. *Nature*, 479:208, 2011.
- [34] A. Nickel, R. Ohmann, J. Meyer, M. Grisolia, C. Joachim, F. Moresco, and G. Cu-

- niberti. Moving nanostructures: Pulse-induced positioning of supramolecular assemblies. *ACS Nano*, 7(1):191–197, 2013.
- [35] H. L. Tierney, J. W. Han, A. D. Jewell, E. V. Iski, A. E. Baber, David S. Sholl, and E. C. H. Sykes. Chirality and rotation of asymmetric surface-bound thioethers. *J. Phys. Chem. C*, 115(4):897–901, 2011.
- [36] H. L. Tierney, C. J. Murphy, A. D. Jewell, A. E. Baber, E. V. Iski, H. Y. Khodavardian, A. F. McGuire, N. Klebanov, and E. C. H. Sykes. Experimental demonstration of a single-molecule electric motor. *Nat. Nanotechnol.*, 6:625, 2011.
- [37] M. Alemani, M. V. Peters, S. Hecht, K.-H. Rieder, F. Moresco, and L. Grill. Electric field-induced isomerization of azobenzene by stm. *J. Am. Chem. Soc.*, 128(45):14446–14447, 2006.
- [38] R. O. Jones and O. Gunnarsson. The density functional formalism, its applications and prospects. *Rev. Mod. Phys.*, 61(3):689–746, 1989.
- [39] P. Hohenberg and W. Kohn. Inhomogeneous electron gas. *Phys. Rev.*, 136(3B):B864–B871, 1964.
- [40] L. Kronik and J. B. Neaton. Excited-state properties of molecular solids from first principles. *Annu. Rev. Phys. Chem.*, 67(1):587–616, 2016.
- [41] W. Kohn and L. J. Sham. Self-consistent equations including exchange and correlation effects. *Phys. Rev.*, 140(4A):A1133–A1138, 1965.
- [42] J. VandeVondele, M. Krack, F. Mohamed, M. Parrinello, T. Chassaing, and J. Hutter. Quickstep: Fast and accurate density functional calculations using a mixed gaussian and plane waves approach. *Comput. Phys. Commun.*, 167(2):103–128, 2005.
- [43] J. P. Perdew, K. Burke, and M. Ernzerhof. Generalized gradient approximation made simple. *Phys. Rev. Lett.*, 77(18):3865–3868, 1996.
- [44] A. K. Rappe, C. J. Casewit, K. S. Colwell, W. A. Goddard, and W. M. Skiff. Uff, a full periodic table force field for molecular mechanics and molecular dynamics simulations. *J. Am. Chem. Soc.*, 114(25):10024–10035, 1992.
- [45] G. Meyer. A simple low-temperature ultrahigh-vacuum scanning tunneling microscope capable of atomic manipulation. *Rev. Sci. Instrum.*, 67(8):2960–2965, 1996.

- [46] V. M. Hallmark, S. Chiang, J. F. Rabolt, J. D. Swalen, and R. J. Wilson. Observation of atomic corrugation on au(111) by scanning tunneling microscopy. *Phys. Rev. Lett.*, 59(25):2879–2882, 1987.
- [47] C. Wöll, S. Chiang, R. J. Wilson, and P. H. Lippel. Determination of atom positions at stacking-fault dislocations on au(111) by scanning tunneling microscopy. *Phys. Rev. B*, 39(11):7988–7991, 1989.
- [48] E. I. Altman and R. J. Colton. Nucleation, growth, and structure of fullerene films on au(111). *Surf. Sci.*, 279(1):49–67, 1992.
- [49] J. Kliewer, R. Berndt, E. V. Chulkov, V. M. Silkin, P. M. Echenique, and S. Crampin. Dimensionality effects in the lifetime of surface states. *Science*, 288(5470):1399–1402, 2000.
- [50] D. Nečas and P. Klapetek. Gwyddion: an open-source software for spm data analysis. *Cent. Eur. J. Phys.*, 10(1):181–188, 2012.
- [51] L. Gross, F. Mohn, N. Moll, B. Schuler, A. Criado, E. Guitián, D. Peña, A. Gourdon, and G. Meyer. Bond-order discrimination by atomic force microscopy. *Science*, 337(6100):1326–1329, 2012.
- [52] L. Gross. Recent advances in submolecular resolution with scanning probe microscopy. *Nat. Chem.*, 3:273, 2011.
- [53] P. Hapala, G. Kichin, C. Wagner, F. S. Tautz, R. Temirov, and P. Jelínek. Mechanism of high-resolution stm/afm imaging with functionalized tips. *Phys. Rev. B*, 90(8):085421, 2014.
- [54] R. Temirov and F. S. Tautz. *Scanning Tunnelling Microscopy with Single Molecule Force Sensors*, pages 275–301. Springer International Publishing, Cham, 2015.
- [55] L. Bartels, G. Meyer, and K.-H. Rieder. Controlled vertical manipulation of single co molecules with the scanning tunneling microscope: A route to chemical contrast. *Appl. Phys. Lett.*, 71(2):213–215, 1997.
- [56] J. Krüger, F. Eisenhut, D. Skidin, T. Lehmann, D. A. Ryndyk, G. Cuniberti, F. Garcia, J. M. Alonso, E. Guitian, D. Perez, D. Pena, G. Trinquier, J.-P. Malrieu, F. Moresco, and C. Joachim. Electronic resonances and gap stabilization of higher acenes on a gold surface. *ACS Nano*, 12(8):8506–8511, 2018.

- [57] F. Eisenhut, T. Lehmann, A. Viertel, D. Skidin, J. Krüger, S. Nikipar, D. A. Ryndyk, C. Joachim, S. Hecht, F. Moresco, and G. Cuniberti. On-surface annulation reaction cascade for the selective synthesis of diindenopyrene. *ACS Nano*, 11(12):12419–12425, 2017.
- [58] A. Kühnle. Self-assembly of organic molecules at metal surfaces. *Curr. Opin. Colloid Interface Sci.*, 14(2):157–168, 2009.
- [59] J. V. Barth. Molecular architectonic on metal surfaces. *Annu. Rev. Phys. Chem.*, 58(1):375–407, 2007.
- [60] J. V. Barth, G. Costantini, and K. Kern. Engineering atomic and molecular nanostructures at surfaces. *Nature*, 437:671, 2005.
- [61] L. Sosa-Vargas, E. Kim, and A.-J. Attias. Beyond "decorative" 2d supramolecular self-assembly: strategies towards functional surfaces for nanotechnology. *Mater. Horiz.*, 4(4):570–583, 2017.
- [62] A. M. Sweetman, S. P. Jarvis, Hongqian Sang, I. Lekkas, P. Rahe, Y. Wang, J. Wang, N. R. Champness, L. Kantorovich, and P. Moriarty. Mapping the force field of a hydrogen-bonded assembly. *Nat. Commun.*, 5:3931, 2014.
- [63] P. Liljeroth, I. Swart, S. Paavilainen, J. Repp, and G. Meyer. Single-molecule synthesis and characterization of metalligand complexes by low-temperature stm. *Nano Lett.*, 10(7):2475–2479, 2010.
- [64] J. Meyer, A. Nickel, R. Ohmann, L. Lokamani, C. Toher, D. Ryndyk, Y. Garmshausen, S. Hecht, F. Moresco, and G. Cuniberti. Tuning the formation of discrete coordination nanostructures. *Chem. Commun.*, 51, 2015.
- [65] S. Kawai, A. S. Foster, T. Björkman, S. Nowakowska, J. Björk, F. F. Canova, L. H. Gade, T. A. Jung, and E. Meyer. Van der waals interactions and the limits of isolated atom models at interfaces. *Nat. Commun.*, 7:11559, 2016.
- [66] Q. Shen, H.-Y. Gao, and H. Fuchs. Frontiers of on-surface synthesis: From principles to applications. *Nano Today*, 13:77–96, 2017.
- [67] A. Gourdon. On-surface covalent coupling in ultrahigh vacuum. *Angew. Chem., Int. Ed.*, 47(37):6950–6953, 2008.
- [68] A. L. Pinaridi, G. Otero-Irurueta, I. Palacio, J. I. Martinez, C. Sanchez-Sanchez, M. Tello, C. Rogero, A. Cossaro, A. Preobrajenski, B. Gómez-Lor, A. Jancarik,

- I. G. Stará, I. Starý, M. F. Lopez, J. Méndez, and J. A. Martin-Gago. Tailored formation of n-doped nanoarchitectures by diffusion-controlled on-surface (cyclo)dehydrogenation of heteroaromatics. *ACS Nano*, 7(4):3676–3684, 2013.
- [69] M. Treier, C. A. Pignedoli, T. Laino, R. Rieger, K. Müllen, D. Passerone, and R. Fasel. Surface-assisted cyclodehydrogenation provides a synthetic route towards easily processable and chemically tailored nanographenes. *Nat. Chem.*, 3:61, 2010.
- [70] G. Otero, G. Biddau, C. Sánchez-Sánchez, R. Caillard, M. F. López, C. Rogero, F. J. Palomares, N. Cabello, M. A. Basanta, J. Ortega, J. Méndez, A. M. Echavarrén, R. Pérez, B. Gómez-Lor, and J. A. Martín-Gago. Fullerenes from aromatic precursors by surface-catalysed cyclodehydrogenation. *Nature*, 454:865, 2008.
- [71] S.-W. Hla, L. Bartels, G. Meyer, and K.-H. Rieder. Inducing all steps of a chemical reaction with the scanning tunneling microscope tip: Towards single molecule engineering. *Phys. Rev. Lett.*, 85(13):2777–2780, 2000.
- [72] L. Grill, M. Dyer, L. Lafferentz, M. Persson, M. V. Peters, and S. Hecht. Nanoarchitectures by covalent assembly of molecular building blocks. *Nat. Nanotechnol.*, 2(11):687–691, 2007.
- [73] M. Lackinger. Surface-assisted ullmann coupling. *Chem. Commun.*, 53(56):7872–7885, 2017.
- [74] C. Nacci, F. Ample, D. Bleger, S. Hecht, C. Joachim, and L. Grill. Conductance of a single flexible molecular wire composed of alternating donor and acceptor units. *Nat. Commun.*, 6:7397, 2015.
- [75] L. Lafferentz, F. Ample, H. Yu, S. Hecht, C. Joachim, and L. Grill. Conductance of a single conjugated polymer as a continuous function of its length. *Science*, 323(5918):1193–1197, 2009.
- [76] J. Cai, P. Ruffieux, R. Jaafar, M. Bieri, T. Braun, S. Blankenburg, M. Muoth, A. P. Seitsonen, M. Saleh, X. Feng, K. Mullen, and R. Fasel. Atomically precise bottom-up fabrication of graphene nanoribbons. *Nature*, 466(7305):470–473, 2010.
- [77] P. Ruffieux, S. Wang, B. Yang, C. Sánchez-Sánchez, J. Liu, T. Dienel, L. Talirz, P. Shinde, C. A. Pignedoli, D. Passerone, T. Dumslaff, X. Feng, K. Müllen, and

- R. Fasel. On-surface synthesis of graphene nanoribbons with zigzag edge topology. *Nature*, 531(7595):489–492, 2016.
- [78] J. Krüger, F. Eisenhut, T. Lehmann, J. M. Alonso, J. Meyer, D. Skidin, R. Ohmann, D. A. Ryndyk, D. Pérez, E. Guitián, D. Peña, F. Moresco, and G. Cuniberti. Molecular self-assembly driven by on-surface reduction: Anthracene and tetracene on au(111). *J. Phys. Chem. C*, 121(37):20353–20358, 2017.
- [79] B. Schuler, S. Fatayer, F. Mohn, N. Moll, N. Pavliček, G. Meyer, D. Peña, and L. Gross. Reversible bergman cyclization by atomic manipulation. *Nat. Chem.*, 8(3):220–224, 2016.
- [80] N. Pavliček, B. Schuler, S. Collazos, N. Moll, D. Pérez, E. Guitián, G. Meyer, D. Peña, and L. Gross. On-surface generation and imaging of arynes by atomic force microscopy. *Nat. Chem.*, 7(8):623–628, 2015.
- [81] S. Kawai, K. Takahashi, S. Ito, R. Pawlak, T. Meier, P. Spijker, F. F. Canova, J. Tracey, K. Nozaki, A. S. Foster, and E. Meyer. Competing annulene and radialene structures in a single anti-aromatic molecule studied by high-resolution atomic force microscopy. *ACS Nano*, 11(8):8122–8130, 2017.
- [82] J. Hieulle, E. Carbonell-Sanromà, M. Vilas-Varela, A. Garcia-Lekue, E. Guitián, D. Peña, and J. I. Pascual. On-surface route for producing planar nanographenes with azulene moieties. *Nano Lett.*, 18(1):418–423, 2018.
- [83] J. Krüger, N. Pavliček, J. M. Alonso, D. Pérez, E. Guitián, T. Lehmann, G. Cuniberti, A. Gourdon, G. Meyer, L. Gross, F. Moresco, and D. Peña. Tetracene formation by on-surface reduction. *ACS Nano*, 10(4):4538–4542, 2016.
- [84] J. Krüger, F. Eisenhut, J. M. Alonso, T. Lehmann, E. Guitian, D. Perez, D. Skidin, F. Gamaleja, D. A. Ryndyk, C. Joachim, D. Pena, F. Moresco, and G. Cuniberti. Imaging the electronic structure of on-surface generated hexacene. *Chem. Commun.*, 53(10):1583–1586, 2017.
- [85] J. Eichhorn. *Encyclopedia of Interfacial Chemistry*, pages 406–413. 2018.
- [86] D.-E. Jiang and S. Dai. Circumacenes versus periacenes: Homo–lumo gap and transition from nonmagnetic to magnetic ground state with size. *Chem. Phys. Lett.*, 466(1):72–75, 2008.
- [87] D.-E. Jiang, B. G. Sumpter, and S. Dai. First principles study of magnetism in nanographenes. *J. Chem. Phys.*, 127(12):124703, 2007.

- [88] Q. Ye and C. Chi. Recent highlights and perspectives on acene based molecules and materials. *Chem. Mater.*, 26(14):4046–4056, 2014.
- [89] S. Muhammad, H.-L. Xu, R.-L. Zhong, Z.-M. Su, A. G. Al-Sehemi, and A. Irfan. Quantum chemical design of nonlinear optical materials by sp²-hybridized carbon nanomaterials: issues and opportunities. *J. Mater. Chem. C*, 1(35):5439–5449, 2013.
- [90] E. H. Fort, P. M. Donovan, and L. T. Scott. Dielsalder reactivity of polycyclic aromatic hydrocarbon bay regions: Implications for metal-free growth of single-chirality carbon nanotubes. *J. Am. Chem. Soc.*, 131(44):16006–16007, 2009.
- [91] E.H. Fort and L.T. Scott. One-step conversion of aromatic hydrocarbon bay regions into unsubstituted benzene rings: A reagent for the low-temperature, metal-free growth of single-chirality carbon nanotubes. *Angew. Chem., Int. Ed.*, 49(37):6626–6628, 2010.
- [92] Z. Sun, Q. Ye, C. Chi, and J. Wu. Low band gap polycyclic hydrocarbons: from closed-shell near infrared dyes and semiconductors to open-shell radicals. *Chem. Soc. Rev.*, 41(23):7857–7889, 2012.
- [93] L. Zöphel, R. Berger, P. Gao, V. Enkelmann, M. Baumgarten, M. Wagner, and K. Müllen. Toward the peri-pentacene framework. *Chem. - Eur. J.*, 19(52):17821–17826, 2013.
- [94] C. Rogers, C. Chen, Z. Pedramrazi, A. A. Omrani, H.-Z. Tsai, H. S. Jung, S. Lin, M. F. Crommie, and F. R. Fischer. Closing the nanographene gap: Surface-assisted synthesis of peripentacene from 6,6-bipentacene precursors. *Angew. Chem., Int. Ed.*, 54(50):15143–15146, 2015.
- [95] X.-Y. Wang, T. Dienel, M. Di Giovannantonio, G. B. Barin, N. Kharche, O. Deniz, J. I. Urgel, R. Widmer, S. Stolz, L. H. De Lima, M. Muntwiler, M. Tommasini, V. Meunier, P. Ruffieux, X. Feng, R. Fasel, K. Müllen, and A. Narita. Heteroatom-doped perihexacene from a double helicene precursor: On-surface synthesis and properties. *J. Am. Chem. Soc.*, 139(13):4671–4674, 2017.
- [96] Y.-Q. Zhang, J. Björk, P. Weber, R. Hellwig, K. Diller, A. C. Papageorgiou, S. C. Oh, S. Fischer, F. Allegretti, S. Klyatskaya, M. Ruben, J. V. Barth, and F. Klappenberger. Unusual deprotonated alkynyl hydrogen bonding in metal-supported hydrocarbon assembly. *J. Phys. Chem. C*, 119(17):9669–9679, 2015.

- [97] R. W. A. Havenith, H. Jiao, L. W. Jenneskens, J. H. van Lenthe, M. Sarobe, P. v. R. Schleyer, M. Kataoka, A. Necula, and L. T. Scott. Stability and aromaticity of the cyclopenta-fused pyrene congeners. *J. Am. Chem. Soc.*, 124(10):2363–2370, 2002.
- [98] J. Liu, T. Dienel, J. Liu, O. Groening, J. Cai, X. Feng, K. Müllen, P. Ruffieux, and R. Fasel. Building pentagons into graphenic structures by on-surface polymerization and aromatic cyclodehydrogenation of phenyl-substituted polycyclic aromatic hydrocarbons. *J. Phys. Chem. C*, 120(31):17588–17593, 2016.
- [99] S. Tebi, M. Paszkiewicz, H. Aldahhak, F. Allegretti, S. Gonglach, M. Haas, M. Waser, P. S. Deimel, P. C. Aguilar, Y.-Q. Zhang, A. C. Papageorgiou, D. A. Duncan, J. V. Barth, W. G. Schmidt, R. Koch, U. Gerstmann, E. Rauls, F. Klappenberger, W. Schöfberger, and S. Müllegger. On-surface site-selective cyclization of corrole radicals. *ACS Nano*, 11(3):3383–3391, 2017.
- [100] D. G. de Oteyza, P. Gorman, Y.-C. Chen, S. Wickenburg, A. Riss, D. J. Mowbray, G. Etkin, Z. Pedramrazi, H.-Z. Tsai, A. Rubio, M. F. Crommie, and F. R. Fischer. Direct imaging of covalent bond structure in single-molecule chemical reactions. *Science*, 340(6139):1434, 2013.
- [101] D. G. de Oteyza, A. Pérez Paz, Y.-C. Chen, Z. Pedramrazi, A. Riss, S. Wickenburg, H.-Z. Tsai, F. R. Fischer, M. F. Crommie, and A. Rubio. Noncovalent dimerization after enediyne cyclization on au(111). *J. Am. Chem. Soc.*, 138(34):10963–10967, 2016.
- [102] S. Kawai, V. Haapasilta, B. D. Lindner, K. Tahara, P. Spijker, J. A. Buitendijk, R. Pawlak, T. Meier, Y. Tobe, A. S. Foster, and E. Meyer. Thermal control of sequential on-surface transformation of a hydrocarbon molecule on a copper surface. *Nat. Commun.*, 7:12711, 2016.
- [103] L. Wang, H. Kong, X. Chen, X. Du, F. Chen, X. Liu, and H. Wang. Conformation-induced self-assembly of rubrene on au(111) surface. *Appl. Phys. Lett.*, 95(9):093102, 2009.
- [104] R.-F. Dou, X.-C. Ma, L. Xi, H. L. Yip, K. Y. Wong, W. M. Lau, J.-F. Jia, Q.-K. Xue, W.-S. Yang, H. Ma, and A. K. Y. Jen. Self-assembled monolayers of aromatic thiols stabilized by parallel-displaced $\pi\pi$ stacking interactions. *Langmuir*, 22(7):3049–3056, 2006.

- [105] T. A. Pham, F. Song, M.-T. Nguyen, and M. Stohr. Self-assembly of pyrene derivatives on au(111): substituent effects on intermolecular interactions. *Chem. Commun.*, 50(91):14089–14092, 2014.
- [106] H. Walch, R. Gutzler, T. Sirtl, G. Eder, and M. Lackinger. Material- and orientation-dependent reactivity for heterogeneously catalyzed carbonbromine bond homolysis. *J. Phys. Chem. C*, 114(29):12604–12609, 2010.
- [107] M. H. Chang, W. J. Jang, M. W. Lee, U. S. Jeon, S. Han, and S.-J. Kahng. Networks of non-planar molecules with halogen bonds studied using scanning tunneling microscopy on au (111). *Appl. Surf. Sci.*, 432:110–114.
- [108] A. Batra, D. Cvetko, G. Kladnik, O. Adak, C. Cardoso, A. Ferretti, D. Prezzi, E. Molinari, A. Morgante, and L. Venkataraman. Probing the mechanism for graphene nanoribbon formation on gold surfaces through x-ray spectroscopy. *Chem. Sci.*, 5(11):4419–4423, 2014.
- [109] M. Bieri, M.-T. Nguyen, O. Gröning, J. Cai, M. Treier, K. Aït-Mansour, P. Ruffieux, C. A. Pignedoli, D. Passerone, M. Kastler, K. Müllen, and R. Fasel. Two-dimensional polymer formation on surfaces: Insight into the roles of precursor mobility and reactivity. *J. Am. Chem. Soc.*, 132(46):16669–16676, 2010.
- [110] C. Nacci, S. Hecht, and L. Grill. *On-Surface Synthesis: Proceedings of the International Workshop On-Surface Synthesis*, pages 1–21. Springer International Publishing, Cham, 2016.
- [111] L. Dong, S. Wang, W. Wang, C. Chen, T. Lin, J. Adisojoso, and N. Lin. *On-Surface Synthesis: Proceedings of the International Workshop On-Surface Synthesis*, pages 23–42. Springer International Publishing, Cham, 2016.
- [112] Jonas Björk, Felix Hanke, and Sven Stafström. Mechanisms of halogen-based covalent self-assembly on metal surfaces. *J. Am. Chem. Soc.*, 135(15):5768–5775, 2013. PMID: 23506285.
- [113] Lawrence T. Scott. Chemistry at the interior atoms of polycyclic aromatic hydrocarbons. *Chem. Soc. Rev.*, 44(18):6464–6471, 2015.
- [114] H. Alper. Catalysis at surfaces. *Can. J. Chem. Eng.*, 67(5):879–879, 1989.
- [115] E. Nardi, L. Chen, S. Clair, M. Koudia, L. Giovanelli, X. Feng, K. Müllen, and M. Abel. On-surface reaction between tetracarbonitrile-functionalized molecules and copper atoms. *J. Phys. Chem. C*, 118(47):27549–27553, 2014.

- [116] F. Chiaravalloti, G. Dujardin, D. Riedel, H. P. Pinto, and A. S. Foster. Atomic-scale study of the adsorption of calcium fluoride on si(100) at low-coverage regime. *Phys. Rev. B*, 84(15):155433, 2011.
- [117] M. Kittelmann, R. Lindner, and A. Kühnle. On-surfaces synthesis on insulating substrates. In *On-Surface Synthesis*, pages 181–197. Springer International Publishing.
- [118] V. G. Bordo and H. Rubahn. *Optics and Spectroscopy at Surfaces and Interfaces*, pages 201–220. 1998.
- [119] M. Kolmer, S. Godlewski, H. Kawai, B. Such, F. Krok, M. Saeys, C. Joachim, and M. Szymonski. Electronic properties of stm-constructed dangling-bond dimer lines on a ge(001)-(2×1):h surface. *Phys. Rev. B*, 86, 2012.
- [120] M. Kolmer, S. Godlewski, R. Zuzak, M. Wojtaszek, C. Rauer, A. Thuairé, J.-M. Hartmann, H. Moriceau, C. Joachim, and M. Szymonski. Atomic scale fabrication of dangling bond structures on hydrogen passivated si(0 0 1) wafers processed and nanopackaged in a clean room environment. *Appl. Surf. Sci.*, 288:83–89, 2014.
- [121] R. Robles, M. Kepenekian, C. Joachim, R. Rurali, and N. Lorente. On-surface atomic wires and logic gates. pages 83–93. Springer International Publishing.
- [122] M. Kepenekian, F. D. Novaes, R. Robles, S. Monturet, H. Kawai, C. Joachim, and N. Lorente. Electron transport through dangling-bond silicon wires on h-passivated si(100). *J. Phys.: Condens. Matter*, 25(2):025503, 2012.
- [123] T. Huff, H. Labidi, M. Rashidi, L. Livadaru, T. Dienel, R. Achal, W. Vine, J. Pitters, and R. A. Wolkow. Binary atomic silicon logic. *Nat. Electron.*, 1(12):636–643, 2018.
- [124] J. Wyrick, X. Wang, P. Namboodiri, S. W. Schmucker, R. V. Kashid, and R. M. Silver. Atom-by-atom construction of a cyclic artificial molecule in silicon. *Nano Lett.*, 18(12):7502–7508, 2018.
- [125] H. Kawai, F. Ample, Q. Wang, Y. K. Yeo, M. Saeys, and C. Joachim. Dangling-bond logic gates on a si(100)-(2 × 1)-h surface. *J. Phys.: Condens. Matter*, 24(9):095011, 2012.
- [126] J. J. Boland. Scanning tunnelling microscopy of the interaction of hydrogen with silicon surfaces. *Adv. Phys.*, 42(2):129–171, 1993.

- [127] M. C. Hersam, N. P. Guisinger, J. W. Lyding, D. S. Thompson, and J. S. Moore. Atomic-level study of the robustness of the $\text{si}(100)\text{-}2\times 1\text{:h}$ surface following exposure to ambient conditions. *Appl. Phys. Lett.*, 78(7):886–888, 2001.
- [128] P. Reynaud, A. Thuair, D. Sordes, C. Rauer, J. M. Hartmann, H. Moriceau, B. Bhartia, S. R. Puniredd, C. Troadec, M. P. Srinivasan, X. Baillin, and S. Chermamy. Nanopackaging solution from clean room to uhv environment: Hydrogen passivated $\text{si}(100)$ substrate fabrication and use for atomic scale investigations and self-assembled monolayer grafting. *Procedia Eng.*, 141:121–129, 2016.
- [129] J. E. Morris. *Nanopackaging: Nanotechnologies and Electronics Packaging*, pages 1–14. Springer US, Boston, MA, 2008.
- [130] D. Winau, H. Itoh, A. K. Schmid, and T. Ichinokawa. Reconstructions and growth of ag on $\text{si}(001)(2\times 1)$. *Surf. Sci.*, 303(1):139–145, 1994.
- [131] H. Kawai, O. Neucheva, T. L. Yap, C. Joachim, and M. Saeys. On-surface atomic wires and logic gates. pages 105–120. Springer International Publishing.
- [132] T. L. Yap, H. Kawai, O. A. Neucheva, A. T. S. Wee, C. Troadec, M. Saeys, and C. Joachim. $\text{Si}(100)\text{-}2\times 1\text{-h}$ dimer rows contrast inversion in low-temperature scanning tunneling microscope images. *Surf. Sci.*, 632:L13–L17, 2015.
- [133] H. Kawai, O. Neucheva, T. L. Yap, C. Joachim, and M. Saeys. Electronic characterization of a single dangling bond on $n\text{-}$ and $p\text{-type}$ $\text{si}(001)\text{-}(2\times 1)\text{:h}$. *Surf. Sci.*, 645:88–92, 2016.
- [134] H. Labidi, M. Taucer, M. Rashidi, M. Koleini, L. Livadaru, J. Pitters, M. Cloutier, M. Salomons, and R. A. Wolkow. Scanning tunneling spectroscopy reveals a silicon dangling bond charge state transition. *New J. Phys.*, 17(7):073023, 2015.
- [135] J. L. Pitters, L. Livadaru, M. B. Haider, and R. A. Wolkow. Tunnel coupled dangling bond structures on hydrogen terminated silicon surfaces. *J. Chem. Phys.*, 134(6):064712, 2011.
- [136] Y. Morita and H. Tokumoto. Ideal hydrogen termination of $\text{si}(001)$ surface by wet-chemical preparation. *Appl. Phys. Lett.*, 67(18):2654–2656, 1995.
- [137] Z. Xie, I. Bâldea, G. Haugstad, and C. Daniel F. Mechanical deformation distinguishes tunneling pathways in molecular junctions. *J. Am. Chem. Soc.*, 141(1):497–504, 2019.

- [138] Y. Selzer, A. Salomon, and D. Cahen. The importance of chemical bonding to the contact for tunneling through alkyl chains. *J. Phys. Chem. B*, 106(40):10432–10439, 2002.
- [139] M. McEllistrem, G. Haase, D. Chen, and R. J. Hamers. Electrostatic sample-tip interactions in the scanning tunneling microscope. *Phys. Rev. Lett.*, 70(16):2471–2474, 1993.
- [140] R. T. Tung. Schottky-barrier formation at single-crystal metal-semiconductor interfaces. *Phys. Rev. Lett.*, 52(6):461–464, 1984.
- [141] T. Hitosugi, T. Hashizume, S. Heike, H. Kajiyama, Y. Wada, S. Watanabe, T. Hasegawa, and K. Kitazawa. Scanning tunneling microscopy/spectroscopy of dangling-bond wires fabricated on the si(100)-2×1-h surface. *Appl. Surf. Sci.*, 130-132:340–345, 1998.
- [142] R. Achal, M. Rashidi, J. Croshaw, D. Churchill, M. Taucer, T. Huff, M. Cloutier, J. Pitters, and R. A. Wolkow. Lithography for robust and editable atomic-scale silicon devices and memories. *Nat. Commun.*, 9(1):2778, 2018.
- [143] M. Rashidi, W. Vine, T. Dienel, L. Livadaru, J. Retallick, T. Huff, K. Walus, and R. A. Wolkow. Initiating and monitoring the evolution of single electrons within atom-defined structures. *Phys. Rev. Lett.*, 121(16):166801, 2018.
- [144] M. Fuechsle, J. A. Miwa, S. Mahapatra, H. Ryu, S. Lee, O. Warschkow, L. C. L. Hollenberg, G. Klimeck, and M. Y. Simmons. A single-atom transistor. *Nat. Nanotechnol.*, 7:242, 2012.
- [145] M. B. Haider, J. L. Pitters, G. A. DiLabio, L. Livadaru, J. Y. Mutus, and R. A. Wolkow. Controlled coupling and occupation of silicon atomic quantum dots at room temperature. *Phys. Rev. Lett.*, 102(4):046805, 2009.
- [146] S. R. Schofield, P. Studer, C. F. Hirjibehedin, N. J. Curson, G. Aeppli, and D. R. Bowler. Quantum engineering at the silicon surface using dangling bonds. *Nat. Commun.*, 4:1649, 2013.
- [147] F. Ample, I. Duchemin, M. Hliwa, and C. Joachim. Single or molecule and or atomic circuit logic gates interconnected on a si(100)h surface. *J. Phys.: Condens. Matter*, 23(12):125303, 2011.
- [148] P. Avouris, R. E. Walkup, A. R. Rossi, H. C. Akpati, P. Nordlander, T. C. Shen,

- G. C. Abeln, and J. W. Lyding. Breaking individual chemical bonds via stm-induced excitations. *Surf. Sci.*, 363(1):368–377, 1996.
- [149] T. Hitosugi, S. Heike, T. Onogi, T. Hashizume, S. Watanabe, Z. Q. Li, K. Ohno, Y. Kawazoe, T. Hasegawa, and K. Kitazawa. Jahn-teller distortion in dangling-bond linear chains fabricated on a hydrogen-terminated si(100)- 2×1 surface. *Phys. Rev. Lett.*, 82(20):4034–4037, 1999.
- [150] J. L. Pitters, P. G. Piva, X. Tong, and R. A. Wolkow. Reversible passivation of silicon dangling bonds with the stable radical tempo. *Nano Lett.*, 3(10):1431–1435, 2003.
- [151] N. Pavliček, Z. Majzik, G. Meyer, and L. Gross. Tip-induced passivation of dangling bonds on hydrogenated si(100)- 2×1 . *Appl. Phys. Lett.*, 111(5):053104, 2017.
- [152] T. R. Huff, H. Labidi, M. Rashidi, M. Koleini, R. Achal, M. H. Salomons, and R. A. Wolkow. Atomic white-out: Enabling atomic circuitry through mechanically induced bonding of single hydrogen atoms to a silicon surface. *ACS Nano*, 11(9):8636–8642, 2017.
- [153] M. Engelund, R. Zuzak, S. Godlewski, M. Kolmer, T. Frederiksen, A. García-Lekue, D. Sánchez-Portal, and M. Szymonski. Tunneling spectroscopy of close-spaced dangling-bond pairs in si(001):h. *Sci. Rep.*, 5:14496, 2015.
- [154] G. Li, Y.-C. Chang, R. Tsu, and J. E. Greene. Electronic structure of the si(001) 2×1 :h surface and pathway for h₂ desorption. *Surf. Sci.*, 330(1):20–26, 1995.
- [155] F. Eisenhut, J. Krüger, D. Skidin, S. Nikipar, J. M. Alonso, E. Guitián, D. Pérez, D. A. Ryndyk, D. Peña, F. Moresco, and G. Cuniberti. Hexacene generated on passivated silicon. *Nanoscale*, 10(26):12582–12587, 2018.
- [156] M. Kittelmann, P. Rahe, M. Nimmrich, C. M. Hauke, A. Gourdon, and A. Kühnle. On-surface covalent linking of organic building blocks on a bulk insulator. *ACS Nano*, 5:8420–8425, 2011.
- [157] P. Olszowski, B. Zapotoczny, J. S. Prauzner-Bechcicki, M. Vilas-Varela, D. Pérez, E. Guitián, D. Peña, and M. Szymonski. Aryl halide c–c coupling on ge(001):h surfaces. *J. Phys. Chem. C*, 119:27478–27482, 2015.
- [158] A. Richter, V. Haapasilta, C. Venturini, R. Bechstein, A. Gourdon, A. S. Foster,

- and A. Kuhnle. Diacetylene polymerization on a bulk insulator surface. *Phys. Chem. Chem. Phys.*, 19:15172–15176, 2017.
- [159] M. C. Hersam, N. P. Guisinger, and J. W. Lyding. Isolating, imaging, and electrically characterizing individual organic molecules on the si(100) surface with the scanning tunneling microscope. *J. Vac. Sci. Technol., A*, 18:1349–1353, 2000.
- [160] S. Godlewski, H. Kawai, M. Kolmer, R. Zuzak, A. M. Echavarren, C. Joachim, M. Szymonski, and M. Saeys. Single-molecule rotational switch on a dangling bond dimer bearing. *ACS Nano*, 10:8499–8507, 2016.
- [161] S. Godlewski, M. Kolmer, H. Kawai, B. Such, R. Zuzak, M. Saeys, P. de Mendoza, A. M. Echavarren, C. Joachim, and M. Szymonski. Contacting a conjugated molecule with a surface dangling bond dimer on a hydrogenated ge(001) surface allows imaging of the hidden ground electronic state. *ACS Nano*, 7:10105–10111, 2013.
- [162] M. C. Hersam, N. P. Guisinger, and J. W. Lyding. Silicon-based molecular nanotechnology. *Nanotechnology*, 11:70, 2000.
- [163] F. Ample and C. Joachim. The chemisorption of polyaromatic hydrocarbons on si(100)h dangling bonds. *Surf. Sci.*, 602:1563–1571, 2008.
- [164] A. Bellec, F. Ample, D. Riedel, G. Dujardin, and C. Joachim. Imaging molecular orbitals by scanning tunneling microscopy on a passivated semiconductor. *Nano Lett.*, 9:144–147, 2009.
- [165] M. Gruyters, T. Pingel, T. G. Gopakumar, N. Néel, Ch Schütt, F. Köhler, R. Herges, and R. Berndt. Electronic ground-state and orbital ordering of iron phthalocyanine on h/si(111) unraveled by spatially resolved tunneling spectroscopy. *J. Phys. Chem. C*, 116:20882–20886, 2012.
- [166] S. Godlewski, M. Kolmer, M. Englund, H. Kawai, R. Zuzak, A. Garcia-Lekue, M. Saeys, A. M. Echavarren, C. Joachim, D. Sanchez-Portal, and M. Szymonski. Interaction of a conjugated polyaromatic molecule with a single dangling bond quantum dot on a hydrogenated semiconductor. *Phys. Chem. Chem. Phys.*, 18:3854–3861, 2016.
- [167] L. Gross, F. Mohn, N. Moll, P. Liljeroth, and G. Meyer. The chemical structure of a molecule resolved by atomic force microscopy. *Science*, 325:1110–1114, 2009.

- [168] T. L. Cocker, D. Peller, P. Yu, J. Repp, and R. Huber. Tracking the ultrafast motion of a single molecule by femtosecond orbital imaging. *Nature*, 539:263–267, 2016.
- [169] O. A. Neucheveva, F. Ample, and C. Joachim. Mechanical conformation switching of a single pentacene molecule on si(100)-(2 × 1). *J. Phys. Chem. C*, 117:26040–26047, 2013.
- [170] A. Nickel, T. Lehmann, J. Meyer, F. Eisenhut, R. Ohmann, D. A. Ryndyk, C. Joachim, F. Moresco, and G. Cuniberti. Electronically driven single-molecule switch on silicon dangling bonds. *J. Phys. Chem. C*, 120:27027–27032, 2016.
- [171] A. Nitzan and M. A. Ratner. Electron transport in molecular wire junctions. *Science*, 300:1384–1389, 2003.
- [172] N. J. Tao. Electron transport in molecular junctions. *Nat. Nanotechnol.*, 1:173–181, 2006.
- [173] W-H. Soe, C. Manzano, N. Renaud, P. de Mendoza, A. De Sarkar, F. Ample, M. Hliwa, A. M. Echavarren, N. Chandrasekhar, and C. Joachim. Manipulating molecular quantum states with classical metal atom inputs: Demonstration of a single molecule nor logic gate. *ACS Nano*, 5:1436–1440, 2011.
- [174] J.E. Anthony. The larger acenes: Versatile organic semiconductors. *Angew. Chem. Int. Ed.*, 47:452–483, 2008.
- [175] J. I. Urgel, H. Hayashi, M. Di Giovannantonio, C. A. Pignedoli, S. Mishra, O. Deniz, M. Yamashita, T. Dienel, P. Ruffieux, H. Yamada, and R. Fasel. On-surface synthesis of heptacene organometallic complexes. *J. Am. Chem. Soc.*, 139:11658–11661, 2017.
- [176] M. Zugermeier, M. Gruber, M. Schmid, B. P. Klein, L. Ruppenthal, P. Muller, R. Einholz, W. Hieringer, R. Berndt, H. F. Bettinger, and J. M. Gottfried. On-surface synthesis of heptacene and its interaction with a metal surface. *Nanoscale*, 9:12461–12469, 2017.
- [177] R. Zuzak, R. Dorel, M. Kolmer, M. Szymonski, S Godlewski, and M. E. Antonio. Higher acenes by on-surface dehydrogenation: From heptacene to undecacene. *Angew. Chem., Int. Ed.*, 57(33):10500–10505, 2018.
- [178] M. Bendikov, H. M. Duong, K. Starkey, K. N. Houk, E. A. Carter, and F. Wudl. Oligoacenes: theoretical prediction of open-shell singlet diradical ground states. *J. Am. Chem. Soc.*, 126:7416–7417, 2004.

- [179] S. S. Zade and M. Bendikov. Heptacene and beyond: The longest characterized acenes. *Angew. Chem. Int. Ed.*, 49:4012–4015, 2010.
- [180] P. Gupta, V. L. Colvin, and S. M. George. Hydrogen desorption kinetics from monohydride and dihydride species on silicon surfaces. *Phys. Rev. B*, 37(14):8234–8243, 1988.
- [181] J. J. Boland. Structure of the h-saturated si(100) surface. *Phys. Rev. Lett.*, 65(26):3325–3328, 1990.
- [182] G. L. Larson and J. L. Fry. *Ionic and Organometallic-Catalyzed Organosilane Reductions*, volume 71, pages 1–737. John Wiley Sons, Inc., 2008.
- [183] D. D. M. Wayner and R. A. Wolkow. Organic modification of hydrogen terminated silicon surfaces. *J. Chem. Soc., Perkin Trans. 2*, pages 23–34, 2002.
- [184] M. Z. Hossain, H. S. Kato, and M. Kawai. Self-directed chain reaction by small ketones with the dangling bond site on the si(100)-(2 × 1)-h surface: Acetophenone, a unique example. *J. Am. Chem. Soc.*, 130:11518–11523, 2008.
- [185] S. R. Schofield, S. A. Sarairoh, P. V. Smith, M. W. Radny, and B. V. King. Organic bonding to silicon via a carbonyl group: new insights from atomic-scale images. *J. Am. Chem. Soc.*, 129:11402–11407, 2007.
- [186] R. Ohmann, J. Meyer, A. Nickel, J. Echeverria, M. Grisolia, C. Joachim, F. Moresco, and G. Cuniberti. Supramolecular rotor and translator at work: On-surface movement of single atoms. *ACS Nano*, 9(8):8394–8400, 2015.
- [187] F. Eisenhut, C. Durand, F. Moresco, J.-P. Launay, and C. Joachim. Training for the 1st international nano-car race: the dresden molecule-vehicle. *Eur. Phys. J. Appl. Phys.*, 76(1):10001, 2016.
- [188] S. R. Schofield, O. Warschkow, D. R. Belcher, K. A. Rahnejat, M. W. Radny, and P. V. Smith. Phenyl attachment to si(001) via stm manipulation of acetophenone. *J. Phys. Chem. C*, 117(11):5736–5741, 2013.
- [189] H. Mehdipour. Single-hydrogen dissociation paths for upright and flat acetophenone adsorbates on the si(001) surface. *J. Phys. Chem. C*, 118(41):23682–23689, 2014.
- [190] P. G. Piva, G. A. DiLabio, J. L. Pitters, J. Zikovsky, M. Rezeq, S. Dogel, W. A.

- Hofer, and R. A. Wolkow. Field regulation of single-molecule conductivity by a charged surface atom. *Nature*, 435:658, 2005.
- [191] G. P. Lopinski, D. D. M. Wayner, and R. A. Wolkow. Self-directed growth of molecular nanostructures on silicon. *Nature*, 406:48–51, 2000.
- [192] J. L. Pitters, I. Dogel, G. A. DiLabio, and R. A. Wolkow. Linear nanostructure formation of aldehydes by self-directed growth on hydrogen-terminated silicon(100). *J. Phys. Chem. B*, 110(5):2159–2163, 2006.
- [193] G. Kirczenow, P. G. Piva, and R. A. Wolkow. Linear chains of styrene and methylstyrene molecules and their heterojunctions on silicon: Theory and experiment. *Phys. Rev. B*, 72(24):245306, 2005.
- [194] M. Z. Hossain, H. S. Kato, and M. Kawai. Selective chain reaction of acetone leading to the successive growth of mutually perpendicular molecular lines on the si(100)-(2×1)-h surface. *J. Am. Chem. Soc.*, 129:12304–12309, 2007.
- [195] A. Rochefort and A. Beausoleil. Formation of π -coupled organic wire on the si(001)[2×1] surface. *Chem. Phys. Lett.*, 400(4):347–352, 2004.
- [196] P. G. Piva, R. A. Wolkow, and G. Kirczenow. Nonlocal conductance modulation by molecules: Scanning tunneling microscopy of substituted styrene heterostructures on h-terminated si(100). *Phys. Rev. Lett.*, 101(10):106801, 2008.
- [197] M. Z. Hossain, H. S. Kato, and M. Kawai. Controlled fabrication of 1d molecular lines across the dimer rows on the si(100)(2 × 1)h surface through the radical chain reaction. *J. Am. Chem. Soc.*, 127:15030–15031, 2005.
- [198] A. Rochefort, R. Martel, and P. Avouris. Electrical switching in π -resonant 1d intermolecular channels. *Nano Lett.*, 2(8):877–880, 2002.
- [199] A. Rochefort and P. Boyer. Tailoring electronic and charge transport properties of molecular π -stacked heterojunctions. *Appl. Phys. Lett.*, 89(9):092115, 2006.
- [200] A. Rochefort, P. Boyer, and B. Nacer. Resonant tunneling transport in highly organized oligoacene assemblies. *Org. Electron.*, 8(1):1–7, 2007.
- [201] M. Smeu, R. A. Wolkow, and H. Guo. Conduction modulation of π -stacked ethylbenzene wires on si(100) with substituent groups. *Theor. Chem. Acc.*, 131(1):1085, 2012.
- [202] M. Z. Hossain, H. S. Kato, J. Jung, Y. Kim, and M. Kawai. Molecular assembly

- through the chain reaction of substituted acenes on the $\text{si}(100)-(2 \times 1)-h$ surface. *J. Phys. Chem. C*, 117(38):19436–19441, 2013.
- [203] A. J. Mayne, L. Soukiassian, N. Commaux, G. Comtet, and G. Dujardin. Molecular molds. *Appl. Phys. Lett.*, 85(22):5379–5381, 2004.
- [204] P. Liljeroth, J. Repp, and G. Meyer. Current-induced hydrogen tautomerization and conductance switching of naphthalocyanine molecules. *Science*, 317(5842):1203–1206, 2007.
- [205] J. N. Ladenthin, L. Grill, S. Gawinkowski, S. Liu, J. Waluk, and T. Kumagai. Hot carrier-induced tautomerization within a single porphycene molecule on $\text{cu}(111)$. *ACS Nano*, 9(7):7287–7295, 2015.
- [206] J. S. Prauzner-Bechcicki, S. Godlewski, and M. Szymonski. Atomic- and molecular-scale devices and systems for single-molecule electronics. *Phys. Status Solidi A*, 209(4):603–613, 2012.
- [207] H. Ohnishi, Y. Kondo, and K. Takayanagi. Quantized conductance through individual rows of suspended gold atoms. *Nature*, 395:780, 1998.
- [208] C. L. Petersen, F. Grey, I. Shiraki, and S. Hasegawa. Microfour-point probe for studying electronic transport through surface states. *Appl. Phys. Lett.*, 77(23):3782–3784, 2000.
- [209] T. Kanagawa, R. Hobarra, I. Matsuda, T. Tanikawa, A. Natori, and S. Hasegawa. Anisotropy in conductance of a quasi-one-dimensional metallic surface state measured by a square micro-four-point probe method. *Phys. Rev. Lett.*, 91(3):036805, 2003.
- [210] J. Homoth, M. Wenderoth, T. Druga, L. Winking, R. G. Ulbrich, C. A. Bobisch, B. Weyers, A. Bannani, E. Zubkov, A. M. Bernhart, M. R. Kaspers, and R. Möller. Electronic transport on the nanoscale: Ballistic transmission and ohm’s law. *Nano Lett.*, 9(4):1588–1592, 2009.
- [211] F. Song, J. W. Wells, K. Handrup, Z. S. Li, S. N. Bao, K. Schulte, M. Ahola-Tuomi, L. C. Mayor, J. C. Swarbrick, E. W. Perkins, L. Gammelgaard, and Ph Hofmann. Direct measurement of electrical conductance through a self-assembled molecular layer. *Nat. Nanotechnol.*, 4:373, 2009.
- [212] G. Schull, T. Frederiksen, A. Arnau, D. Sánchez-Portal, and R. Berndt. Atomic-

- scale engineering of electrodes for single-molecule contacts. *Nat. Nanotechnol.*, 6:23, 2010.
- [213] M. Koch, F. Ample, C. Joachim, and L. Grill. Voltage-dependent conductance of a single graphene nanoribbon. *Nat. Nanotechnol.*, 7:713, 2012.
- [214] C. Schirm, M. Matt, F. Pauly, J. C. Cuevas, P. Nielaba, and E. Scheer. A current-driven single-atom memory. *Nat. Nanotechnol.*, 8:645, 2013.
- [215] M. Wojtaszek, J. Lis, R. Zuzak, B. Such, and M. Szymonski. Inversion layer on the ge(001) surface from the four-probe conductance measurements. *Appl. Phys. Lett.*, 105(4):042111, 2014.
- [216] J. Baringhaus, M. Ruan, F. Edler, A. Tejada, M. Sicot, A. Taleb-Ibrahimi, A.-P. Li, Z. Jiang, E. H. Conrad, C. Berger, C. Tegenkamp, and W. A. de Heer. Exceptional ballistic transport in epitaxial graphene nanoribbons. *Nature*, 506:349, 2014.
- [217] J. Lis, M. Wojtaszek, R. Zuzak, B. Such, and M. Szymonski. Appearance of effective surface conductivity: An experimental and analytic study. *Phys. Rev. B*, 92(3):035309, 2015.
- [218] J. Baringhaus, M. Settnes, J. Aprojanz, S. R. Power, A.-P. Jauho, and C. Tegenkamp. Electron interference in ballistic graphene nanoconstrictions. *Phys. Rev. Lett.*, 116(18):186602, 2016.
- [219] A. Bannani, C. A. Bobisch, and R. Möller. Local potentiometry using a multi-probe scanning tunneling microscope. *Rev. Sci. Instrum.*, 79(8):083704, 2008.
- [220] S. V. Aradhya and L. Venkataraman. Single-molecule junctions beyond electronic transport. *Nat. Nanotechnol.*, 8:399, 2013.
- [221] A. Aviram, C. Joachim, and M. Pomerantz. Evidence of switching and rectification by a single molecule effected with a scanning tunneling microscope. *Chem. Phys. Lett.*, 146(6):490–495, 1988.
- [222] C. Joachim, J. K. Gimzewski, R. R. Schlittler, and C. Chavy. Electronic transparency of a single c60 molecule. *Phys. Rev. Lett.*, 74(11):2102–2105, 1995.
- [223] T. Frederiksen, G. Foti, F. Scheurer, V. Speisser, and G. Schull. Chemical control of electrical contact to sp² carbon atoms. *Nat. Commun.*, 5:3659, 2014.
- [224] R. H. M. Smit, Y. Noat, C. Untiedt, N. D. Lang, M. C. van Hemert, and J. M. van

- Ruitenbeek. Measurement of the conductance of a hydrogen molecule. *Nature*, 419:906, 2002.
- [225] B. Xu and N. J. Tao. Measurement of single-molecule resistance by repeated formation of molecular junctions. *Science*, 301(5637):1221–1223, 2003.
- [226] D. Skidin, T. Erdmann, S. Nikipar, F. Eisenhut, J. Krüger, F. Günther, S. Gemming, A. Kiriya, B. Voit, D. A. Ryndyk, C. Joachim, F. Moresco, and G. Cuniberti. Tuning the conductance of a molecular wire by the interplay of donor and acceptor units. *Nanoscale*, 10(36):17131–17139, 2018.
- [227] T. Nakagama, O. Kubo, Y. Shingaya, S. Higuchi, T. Hasegawa, C.-S. Jiang, T. Okuda, Y. Kuwahara, K. Takami, and M. Aono. Development and application of multiple-probe scanning probe microscopes. *Adv. Mater.*, 24(13):1675–1692, 2012.
- [228] A.-P. Li, K. W. Clark, X.-G. Zhang, and A. P. Baddorf. Electron transport at the nanometer-scale spatially revealed by four-probe scanning tunneling microscopy. *Adv. Funct. Mater.*, 23(20):2509–2524, 2013.
- [229] F. Eisenhut, C. Durand, F. Moresco, J.-P. Launay, and C. Joachim. Training for the 1st international nano-car race: the dresden molecule-vehicle. *Eur. Phys. J. Appl. Phys.*, 76(1):10001, 2016.
- [230] J. Yang, D. Sordes, M. Kolmer, D. Martrou, and C. Joachim. Imaging, single atom contact and single atom manipulations at low temperature using the new scientaomicron lt-uhv-4 stm. *Eur. Phys. J. Appl. Phys.*, 73(1):10702, 2016.
- [231] M. Kolmer, P. Olszowski, R. Zuzak, S. Godlewski, C. Joachim, and M. Szymon-ski. Two-probe stm experiments at the atomic level. *J. Phys.: Condens. Matter*, 29(44):444004, 2017.
- [232] M. Kolmer, P. Brandimarte, J. Lis, R. Zuzak, S. Godlewski, H. Kawai, A. Garcia-Lekue, N. Lorente, T. Frederiksen, C. Joachim, D. Sanchez-Portal, and M. Szymon-ski. Electronic transport in planar atomic-scale structures measured by two-probe scanning tunneling spectroscopy. *Nat. Commun.*, 10:1573, 2019.
- [233] B. V. C. Martins, M. Smeu, L. Livadaru, H. Guo, and R. A. Wolkow. Conductivity of si(111)-(7x7): The role of a single atomic step. *Phys. Rev. Lett.*, 112(24):246802, 2014.
- [234] F. Krok, M. R. Kaspers, A. M. Bernhart, M. Nikiel, B. R. Jany, P. Indyka, M. Wo-

- jtaszek, R. Möller, and C. A. Bobisch. Probing the electronic transport on the reconstructed au/ge(001) surface. *Beilstein J. Nanotechnol.*, 5:1463–1471, 2014.
- [235] M. Kolmer, S. Godlewski, J. Lis, B. Such, L. Kantorovich, and M. Szymonski. Construction of atomic-scale logic gates on a surface of hydrogen passivated germanium. *Microelectron. Eng.*, 109:262–265, 2013.
- [236] J. Yang, J. Deng, N. Chandrasekhar, and C. Joachim. Ultrahigh vacuum scanning tunneling microscope manipulation of single gold nanoislands on mos2 for constructing planar nanointerconnects. *J. Vac. Sci. Technol. B*, 25(5):13001–13008, 2007.
- [237] G. Rapenne and C. Joachim. The first nanocar race. *Nat. Rev. Mat.*, 2:17040, 2017.
- [238] T. A. Jung, R. R. Schlittler, J. K. Gimzewski, H. Tang, and C. Joachim. Controlled room-temperature positioning of individual molecules: Molecular flexure and motion. *Science*, 271(5246):181–184, 1996.
- [239] S. Monturet, M. Kepenekian, R. Robles, N. Lorente, and C. Joachim. Vibrational transition rule during a through-bond electron transfer process. *Chem. Phys. Lett.*, 567:1–5, 2013.
- [240] J. Liu, B. Xia, H. Xu, and N. Lin. Controlling the reaction steps of bifunctional molecules 1,5-dibromo-2,6-dimethylnaphthalene on different substrates. *J. Phys. Chem. C*, 122(24):13001–13008, 2018.

Curriculum vitae

Personal information

Name: Frank Eisenhut
Day of birth: 19. May 1989
Place of birth: Stendal

PhD-studies

July 2019 Defended PhD thesis
Title: *STM investigation of model systems for atomic and molecular scale electronics*

Nov. 2013 - June 2019 PhD student
Chair of Materials Science and Nanotechnology
Technische Universität Dresden

Education

Sep. 2013 Master of Science
Thesis: *Phase transformation of graphene under field assisted sintering*

Sep. 2011 Bachelor of Science
Thesis: *Dielektrisches Verhalten von CaTiO_3*

Oct. 2008 - Sep. 2013 Studies of physics
Universität Rostock

June 2007 Abitur
Diesterweg-Gymnasium, Tangermünde

Scientific contributions

Articles

1. F. Eisenhut, C. Durand, F. Moresco, J.-P. Launay, C. Joachim, *Eur. Phys. J. Appl. Phys.* **2016**, *76*, 10001.
2. F. Eisenhut, T. Lehmann, A. Viertel, D. Skidin, J. Krüger, S. Nikipar, D. A. Ryndyk, C. Joachim, S. Hecht, F. Moresco, G. Cuniberti, *ACS Nano* **2017**, *11*, 12419-12425.
3. F. Eisenhut, J. Krüger, D. Skidin, S. Nikipar, J. M. Alonso, E. Guitián, D. Pérez, D. A. Ryndyk, D. Peña, F. Moresco, G. Cuniberti, *Nanoscale* **2018**, *10*, 12582-12587.
4. F. Eisenhut, J. Meyer, J. Krüger, R. Ohmann, G. Cuniberti, F. Moresco, *Surf. Sci.* **2018**, *678*, 177-182.
5. F. Zhang, F. Eisenhut, E. Burkel, *Appl. Phys. Lett.* **2014**, *104*, 253108.
6. A. Nickel, T. Lehmann, J. Meyer, F. Eisenhut, R. Ohmann, D. A. Ryndyk, C. Joachim, F. Moresco, G. Cuniberti, *J. Phys. Chem. C* **2016**, *120*, 27027-27032.
7. J. Krüger, F. Eisenhut, J. M. Alonso, T. Lehmann, E. Guitián, D. Pérez, D. Skidin, F. Gamaleja, D. A. Ryndyk, C. Joachim, D. Peña, F. Moresco, G. Cuniberti, *Chem. Commun.* **2017**, *53*, 1583-1586.
8. J. Krüger, F. Eisenhut, T. Lehmann, J. M. Alonso, J. Meyer, D. Skidin, R. Ohmann, D. A. Ryndyk, D. Pérez, E. Guitián, D. Peña, F. Moresco, G. Cuniberti, *J. Phys. Chem. C* **2017**, *121*, 20353-20358.
9. J. Krüger, F. García, F. Eisenhut, D. Skidin, J. M. Alonso, E. Guitián, D. Pérez, G. Cuniberti, F. Moresco, D. Peña, *Angew. Chem. Int. Ed.* **2017**, *129*, 11945-11948.
10. D. Skidin, O. Faizy, J. Krüger, F. Eisenhut, A. Jancarik, K.-H. Nguyen, G. Cuniberti, F. Moresco, C. Joachim, *ACS Nano* **2018**, *12*, 1139-1145.

11. J. Krüger, F. Eisenhut, D. Skidin, T. Lehmann, D. A. Ryndyk, G. Cuniberti, F. Garcia, J. M. Alonso, E. Guitián, D. Pérez, D. Peña, G. Trinquier, J.-P. Malrieu, F. Moresco, C. Joachim, *ACS Nano* **2018**, *12*, 8506-8511.
12. D. Skidin, T. Erdmann, S. Nikipar, F. Eisenhut, J. Krüger, F. Günther, S. Gemming, A. Kiriya, B. Voit, D. A. Ryndyk, C. Joachim, F. Moresco, G. Cuniberti, *Nanoscale* **2018**, *10*, 17131-17139.

Talks

1. *A chrysene derivative as a promising candidate for an on-surface chemical reaction studied by LT-STM/STS*,
given at the DPG Frühjahrstagung,
Berlin, Germany (March 2015).
2. *Switches and wires for an atomic-scale technology*,
given at the E-MRS Fall Meeting,
Warsaw, Poland (September 2016).
3. *On-surface indene-formation by methyl bromide cleavage*,
given at the DPG Frühjahrstagung,
Dresden, Germany (March 2017).
4. *Dresden and the first Nanocar Race*,
given at the international conference "Trends in Nanotechnology",
Dresden, Germany (June 2017).
5. *On-surface synthesis of nitrogen-doped 5-7-membered nanographenes*,
given at the DPG Frühjahrstagung,
Berlin, Germany (March 2018).
6. *On-surface synthesis of non-alternant polyaromatic hydrocarbons*,
given at the international workshop "On-surface synthesis",
Sant Feliu de Guixols, Spain (September 2018).
7. *Inducing the controlled rotation of single o-MeO-DMBI molecules on Au(111)*,
presented at the DPG Frühjahrstagung,
Regensburg, Germany (April 2019).

Posters

1. *Growing mechanism and tip-induced switching of acetylbiphenyl on Si(100)-(2x1):H*, presented at the DPG Frühjahrstagung, Regensburg, Germany (March 2016).
2. *Molecular manipulation of acetylbiphenyl with a four-probe-STM*, presented at the DPG Frühjahrstagung, Dresden, Germany (March 2017).
3. *Imaging and manipulating different supramolecular assemblies of acetylbiphenyl with a four-probe scanning tunneling microscope*, presented at the international conference "Trends in nanotechnology", Dresden, Germany (June 2017).
4. *Ullmann-coupling suppressed by an intramolecular reaction: Synthesis and characterization of diindenopyrene on Au(111)*, presented at the European Conference on Molecular Electronics, Dresden, Germany (August 2017).
5. *Hexacene generated on passivated silicon*, presented at the DPG Frühjahrstagung, Berlin, Germany (March 2018).
6. *Epiminotetracenes on Au(111)*, presented at the conference "Building and probing small", Brüssel, Belgium (March 2019).
7. *Epiminotetracenes on Au(111)*, presented at the DPG Frühjahrstagung, Regensburg, Germany (April 2019).

Outreach

1. Participation in the video (November 2015):
Nanocar race, the first-ever race of molecule cars.
2. Participation in the video (May 2016):
The smallest car race in the world.
3. Interview for scienceblogs.de (May 2017):
Das Rennen der Nanomaschinen.
4. Participation in the video of Beilstein TV (May 2017):
The Nanocar of the TU Dresden: The windmill.
5. Participation in the video of Beilstein TV (May 2017):
Building atomic wires.
6. Participation in the video of Beilstein TV (May 2017):
Molecules as gears and switches.
7. Participation in the video of Beilstein TV (May 2017):
Acenes - On-surface generation of molecular wires.
8. Interview for the magazine "Stadtgeflüster" (May 2017):
Das Rennen der Nanomaschinen.

Acknowledgement

This thesis would not have been possible without the support of many people during the last years that I would like to acknowledge here. Firstly, I want to thank Prof. Gianuario Cuniberti. He gave me the chance to become a member of the Chair of Materials Science and Nanotechnology, where a great spirit prevails. Many different disciplines are addressed in his chair and by that I got the opportunity to see science from various perspectives. Furthermore, I am grateful on Prof. Kühnle's interest in my work, so that she was willing to be the second referee of this thesis.

I would like to express my special appreciation and thanks to my supervisor Dr. Francesca Moresco. You have been a tremendous mentor for me. I would like to thank you for allowing me to grow as a research scientist. Your advices on my career have been priceless. It was a pleasure to work with all the people that were part of the STM group starting with Jörg Meyer, Anja Nickel and Dr. Robin Ohmann, who introduced me to the different aspects of working with an STM until Tim Kühne, with whom I shared the lab within the last months. Special thanks goes to Justus Krüger and Dmitry Skidin, with whom I spent most of the time of my doctoral studies. I really enjoyed the time in the office and lab with all of you.

Furthermore, I would like to thank all the people with whom I have been able to collaborate within the recent years. Especially, I would like to thank the teams around Prof. Stefan Hecht (FU Berlin) and Prof. Diego Peña (CIQUS, Universidade de Santiago de Compostela) for their synthesis of precursor molecules, as well as their helpful comments to understand the experimental observations. Thanks also to Seddigeh Nikipar, Thomas Lehmann and Dr. Dmitry A. Ryndyk, who modeled our molecular systems, which led to a better understanding of the obtained results.

In addition, I am very grateful to the fruitful collaborations and inspiring meetings with excellent scientists within the university at the Center for Advancing Electronics Dresden (cfaed), within the European projects AtMol, PAMS and MEMO and during the first international Nanocar Race.

Furthermore, I am grateful that I got the ability to work with Dr. Christian Joachim. With his unique way of explaining complicated things at the molecular level, he was an

important contact for me. In addition, I am happy that you invited me into your group to a research stay at the CEMES in Toulouse and let me work at your four-probe STM. It was a great experience to work with you.

Finally, I would like to appreciate my family and friends, especially my wife Anna and my daughters Emilia and Rosalie, who supported me in the moments, when I needed them most. Words cannot express how grateful I am to you.

Statement of authorship

Folgende Erklärung gebe ich hiermit ab:

1. Ich versichere, dass ich die vorliegende Arbeit ohne unzulässige Hilfe Dritter und ohne Benutzung anderer als der angegebenen Hilfsmittel angefertigt habe; die aus fremden Quellen direkt oder indirekt übernommenen Gedanken sind als solche kenntlich gemacht.
2. Bei der Auswahl und Auswertung des Materials sowie bei der Herstellung des Manuskripts habe ich Unterstützung von folgenden Personen erhalten:
 - a) Prof. G. Cuniberti
 - b) Dr. F. Moresco
 - c) Prof. Dr. C. Joachim
 - d) Prof. D. Peña
 - e) Prof. S. Hecht
 - f) Dr. D. A. Ryndyk
 - g) Dr. X. Bouju

Weitere Personen waren an der geistigen Herstellung der vorliegenden Arbeit nicht beteiligt. Insbesondere habe ich nicht die Hilfe eines kommerziellen Promotionsberaters in Anspruch genommen. Dritte haben von mir keine geldwerten Leistungen für Arbeiten erhalten, die in Zusammenhang mit dem Inhalt der vorgelegten Dissertation stehen.

3. Die Arbeit wurde bisher weder im Inland noch im Ausland in gleicher oder ähnlicher Form einer anderen Prüfungsbehörde vorgelegt und ist auch noch nicht veröffentlicht worden.
4. Die Promotionsordnung der Fakultät Maschinenwesen an der TU Dresden vom 01.07.2001 wird anerkannt.

